LARS Information Note 042373

Computer-Aided Processing of Remotely Sensed Data for Temperature Mapping of Surface Water from Aircraft Altitudes

by
L. A. Bartolucci-Castedo
R. M. Hoffer
T. R. West

The Laboratory for Applications of Remote Sensing

Purdue University, West Lafayette, Indiana

1973

LARS Information Note 042373

COMPUTER-AIDED PROCESSING OF REMOTELY SENSED DATA FOR TEMPERATURE MAPPING OF SURFACE WATER FROM AIRCRAFT ALTITUDES

by

Luis A. Bartolucci-Castedo,
Roger M. Hoffer and
Terry R. West

August 1973

TABLE OF CONTENTS

TABLE OF CONTENTS
(Continued)

TABLE OF CONTENTS
(Continued)

LIST OF TABLES

LIST OF TABLES
(Continued)

LIST OF FIGURES

LIST OF FIGURES
(Continued)

LIST OF FIGURES
(Continued)

xi

LIST OF FIGURES
(Continued)

LIST OF FIGURES
(Continued)

ABSTRACT

A necessary aspect of any adequate water quality regulating procedure (one which can cope with large quantities of information) is a rapid and accurate data acquisition and processing system. Currently, computer-aided processing of remotely sensed data offers a satisfactiry method for accurate determination of certain water quality parameters, a significant one being surface water temperature.

This study was primarily concerned with water resources applications of techniques developed at the Laboratory for Applications of Remote Sensing (LARS) for computer-aided processing and analysis of digitized thermal scanner data. Quantitative determinations of water temperature and thermal mapping of streams and water bodies over extended areas were accomplished through the use of the "internal calibration

technique" and computerized data processing. This calibration technique allows absolute temperatures to be determined directly from the scanner data, as no surface observations (ground-truth) are necessary. In this way, water-temperature maps were produced with accuracies of ± 0.2° C from infrared scanner data collected at an altitude of 1,500 meters (5,000 feet).

The data utilized in this research were gathered over two segments of the Wabash River in Indiana--the Tippecanoe and Wabash river junction, and the Cayuga power plant (near the city of Cayuga in Vermillion county).

The effects of the non-linear relationship between emitted energy by a blackbody and its temperature were analyzed through the integration of Planck's Equation over selected wavelength bands and for temperatures normally encountered on the surface of the earth. The results showed that the "non-linearity effect" may introduce errors of the order of several degrees Centigrade on radiant temperatures as measured by means of the 4.5-5.5 μm band. However, these errors may be reduced by using either the 8.0-13.5 or the 9.3-11.7 μm waveband.

The influence of the atmosphere (flight altitude) on the accuracy of radiant temperature measurements was determined for a 608-meter (2,000-foot) and for a 3,040-meter (10,000-foot) flight. The results showed that radiant temperatures as measured through the 4.5-5.5 μm band are

influenced to a greater extent than those measured through either the 9.3-11.7 or 8.0-13.5 μm bands.

A "scan-line averaging" technique was developed and evaluated which produces a pictorial amelioration of the thermal maps without affecting the accuracy of radiant temperature measurements. In addition to that image enhancement, this technique was found to improve the separability between spectral classes of water.

The utilization of a special technique, the "Layered Classifier", has proved to be of considerable help in the thermal mapping of water for those times of the year when water radiant temperatures were the same as the temperature of the adjacent soils and vegetation.

Finally, a proposed procedural sequence of analysis is recommended for the effective application of remote sensing and computer-aided data processing techniques to thermal mapping of surface water for use on an operation basis.

CHAPTER I

INTRODUCTION

Introductory Statement

Many of the problems created by water pollution are those which have been brought about by the indiscriminate use of the streams as waste disposal systems without consideration of the possibility that eventually they would become too contaminated.

In order to establish an adequate criterion for water quality norms, rapid and accurate means of evaluating water pollution levels must be readily available. At the present time, remote sensing* and computer-aided data processing offer a satisfactory method for the determination of certain water quality parameters, one of which is temperature, in a quantitative manner and over large geographic areas employing relatively small amounts of time and effort.

---

*Hoffer (1971) defines remote sensing as "the science involved with the gathering of data about the earth's surface or near-surface environment through the use of a variety of sensor systems that are usually borne by aircraft and spacecraft, and the processing of these data into managing of man's environment".

Within the past few years, airborne radiation thermometer (ART) and multispectral thermal scanner systems have been used to detect, from aircraft altitudes, the onset of volcanic eruptions in Hawaii and Coast Rica (Parker and Wolfe, 1966), sea ice and crevasses in Artic regions (McLerran, 1964), geothermal activities in Yellowstone National Park (McLerran and Morgan, 1966; Smedes, 1968; and Pierce, 1968), forest fires in the western United States (Hirsch, 1962; Hirsch 1964; and Hirsch, 1968), subsurface fires in coal mining districts (Slavecki, 1964), and circulation patterns in the oceans (McLeish, 1964).

For more than a decade, thermal infrared radiation meters have also been used in orbiting space platforms, primarily as vehicle attitude control systems (Horizon Sensors). However, in the second flight of Project Mercury, Mission MA-5 (1961), the automatic stabilization and control system of the space capsule was employed in an alternate mode as an infrared radiation thermometer (IRT). Thus, radiant temperatures of the earth surface and clouds were measured (Ehler, 1962).

Since the early 60's, the TIROS Operational Satellites (TOS) and the NIMBUS meterological satellites have been equipped with high resolution infrared radiometers (HRIR). The TIROS VII thermal infrared data have been used to determine sea surface temperatures over large geographical areas (Greaves, 1966). The NIMBUS infrared scanning

radiometer has gathered data for temperature mapping of night-time cloud-cover and earth surface features (Goldberg et al., 1964).

In the near future, thermal infrared (IR) systems will be collecting considerable amounts of earth resources data from orbiting space platforms, such as SKYLAB, ERTS-B, and perhaps SPACE SHUTTLE. The large amount of data gathered by these systems will require computer-aided techniques for fast handling and processing of the raw data into useful information. Such information would permit a better understanding of our environment and serve as a basis for an adequate and intelligent management of our natural resources.

In short, thermal infrared sensors have been widely used in the past few years from aircraft and spacecraft' altitudes. However, in most cases the analysis and interpretation of the data has been done in a qualitative or semiquantitative manner. Therefore, accurate and reliable methods of processing and analyzing large quantities of thermal radiation data in a rapid and more quantitative fashion are needed.

The objectives of this investigation were:

1. To determine the accuracy and reliability of the internal calibration technique and of the LARSYS linear calibration function.

2. To compare the 4.5-5.5 μm, 8.0-13.5 μm, and 9.3-11.7 μm thermal data in an attempt to determine the optimum

emissive wavelength band for measurements of surface water temperatures from remote locations.

3. To determine the atmospheric effects caused by differences in flight altitude on remotely measured surface water temperatures.

4. To evaluate the use of scan-line overlap redundancy in its enhancement of multispectral aircraft scanner data as applied to measurements of water surface temperature.

5. To demonstrate the effectiveness of using pattern recognition algorithms in conjunction with the internal calibration technique for thermal mapping of water bodies only.

6. To study the thermal gradient and patterns in the Wabash River caused by a waste heat effluent from a fossil fuel power plant.

Definition of Terms

One of the fundamental physical quantities that describes the state of matter is temperature. Temperature, as all primary physical quantities*, has to be defined operationally, that is, through the operations and instruments used in its measurement. To date, two basic

---

*Worthing (1940) has stated that "At present we know of no purely mechanical quantity--that is, one expressible in terms of mass, length and time only--which can be used, however inconveniently, in place of temperature. We are inclined to conclude that temperature is probably itself a basic concept."

methods for measuring the thermal energy content of a body are known. The first is by physical contact of the measuring device with the target, and the second, by measuring its thermal emission from a remote location. Thus, in the scientific literature, the physical quantity measured by the first method is usually referred to as real temperature, true temperature, actual temperature, contact temperature, and in the case of measuring water temperatures, bucket temperature. Temperatures determined by the second method are generally referred to as radiometric temperature, apparent temperature, color temperature and brightness temperature.

For the sake of consistency and in order to avoid confusion caused by the variety of terms used (and sometimes misused) as technical "jargon" in describing measurements of temperature, in the present study the author shall use the term "kinetic temperature" to denote the quantity measured with the conventional contact thermometers. "Radiant temperature" shall be used to describe the thermal state of water as measured with radiation meters. The adjectives "kinetic" and "radiant" that modify the term "temperature" refer to the forms of energies being measured, that is, kinetic energy (average translational energy of molecules) and radiant energy (emitted by accelerated charged particles).

Atmospheric Windows-Portions of the electromagnetic spectrum where radiation passing through the atmosphere is not significantly altered by absorption, reflection or scattering by the atmospheric constituents.

Seven primary atmospheric windows are used for remote sensing purposes (Hoffer, 1972).

1.	0.3 - 1.35 μm	(U.V., Visible, Reflective IR)
2.	1.5 - 1.8 μm	(Reflective IR)
3.	2.0 - 2.4 μm	(Reflective IR)
4.	2.9 - 4.2 μm	(Mixed Reflective and Emissive IR)
5.	4.5 - 5.5 μm	(Thermal or Emissive IR)
6.	8.0 - 14.0 μm	(Thermal or Emissive IR)
7.	Over 1 mm	(Microwave and Radio Regions)

Spatial Resolution (of Scanner)-Minimum separation between two objects for which they appear distinct when viewed by the scanner.

Spectral Resolution (of Scanner)-Minimum separation between two wavelength for which they appear distinct when viewed by the scanner.

Radiance-The radiant energy emitted by a body in a specific direction per unit time, per unit projected area of surface, per unit solid angle. (Watts per square centimeter per steradian).

Emissivity-The ratio of the rate of radiant energy emission from a body, as a consequence of its temperature and the intrinsic properties of the material, to the corresponding rate of emission from a blackbody at the same temperature. (Pure number, less than or equal to 1).

Blackbody-An object which emits or absorbs all radiation in all wavelengths of the electromagnetic spectrum. Often called "Perfect Radiator". Its emissivity is 1. (See Figure 1.1)

Graybody-An object which emits with a constant emissivity less than 1. The shape of the energy distribution curve of a graybody is similar in form but different in magnitude from that of a blackbody. (See Figure 1.1)

Non-Graybody-An object which emits with an emissivity less than 1, but the emissivity is a function of wavelength. (In nature most objects are non-gray bodies. For example, snow is almost a perfect radiator in the thermal IR region, but reflects almost 100% the radiation falling on it in the visible.) (See Figure 1.1)

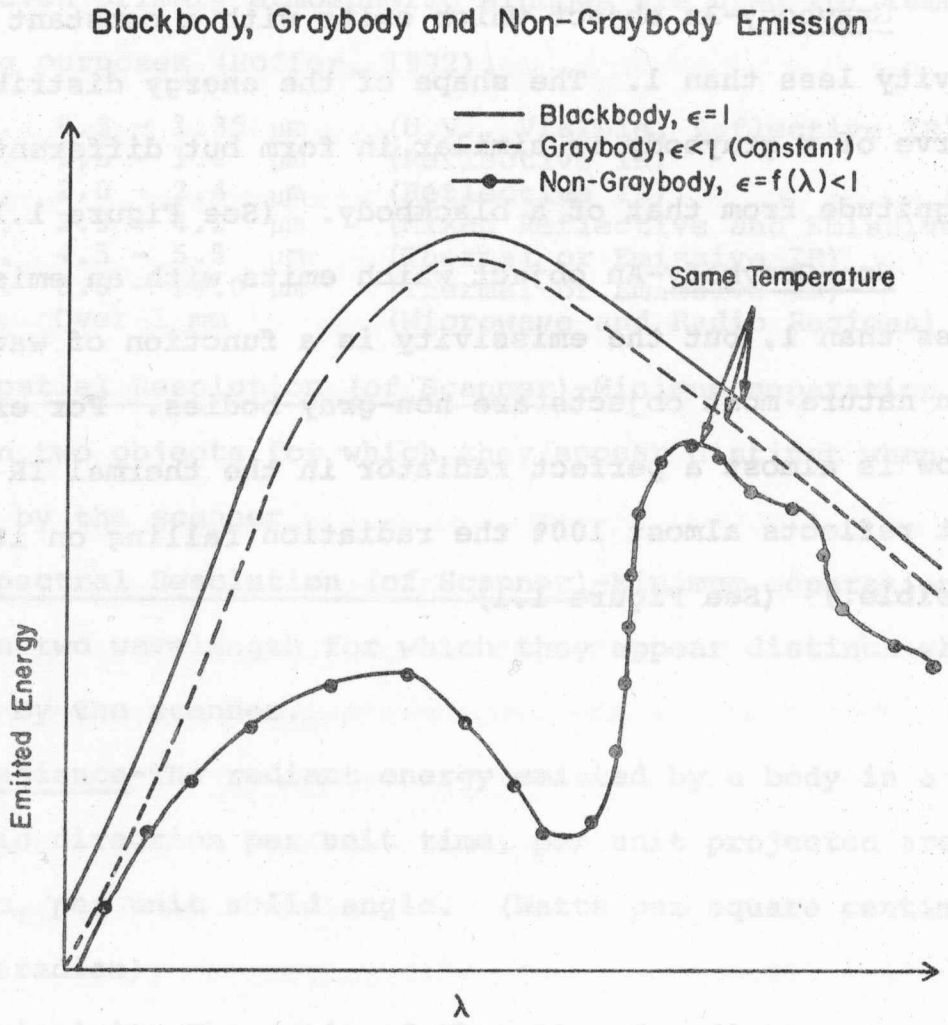

Figure 1.1. Comparison of the emissive characteristics of a blackbody, graybody and non-graybody over a range of wavelengths.

CHAPTER II

REVIEW OF THE LITERATURE

Introductory Statement

Since the advent of quantum physics, the laws describing the physical phenomenon of electromagnetic radiation have been mathematically formulated and their interrelationships describing the energy-matter interactions have been developed. A great deal of information on the theoretical basis of radiation is available in numerous Physics textbooks. However, most of this theory is beyond the scope of this work. We shall only review the fundamentals of thermal infrared (IR) radiation and its relation to the kinetic temperature of the emitting target.

Heisenberg's Uncertainty Principle describes an inherent problem encountered in any kind of measurement. It states that it is impossible to measure a physical quantity without disturbing the quantity itself. This is particularly true in measuring temperatures with conventional contact thermometer in which the measuring device comes

into physical contact with the target, causing an appreciable disturbance in its thermal state. Remote sensing determinations of temperature offer an alternative -- a method of measuring temperatures without disturbing the thermal state of the target. However, several environmental factors may introduce substantial errors in radiation measurements; consequently, a great deal of investigation has been conducted in order to determine these sources of error and to evaluate quantitatively their influence on radiation measurements. The most pertinent results in this area of research and the principles of thermal IR radiation are summarized in the following sections.

Radiation Principles

Radiation Laws

When a charged particle is forced to change its state of motion, or in other words to change its energy level as it is accelerated, it emits electromagnetic radiation that is transmitted through space. Such radiation is transmitted in the form of an electromagnetic wave, if thought of in terms of classical physics, or in discrete bundles of energy -- quanta if explained by quantum physics. The basic mechanisms by which electromagnetic radiation is generated are given by Morse and Feshback (1953) in terms of quantum mechanics. Rossi (1957) describes the same phenomenon from a classical-mechanics point of view and explains the processes of radiation by drawing analogies to familiar

problems of statics and dynamics encountered in Newtonian mechanics. Planck (1932), Fleagle and Businger (1963) and Morse (1965) have given a complete account of Planck's radiation law, which states that for a blackbody, the radiation intensity increases markedly with temperature and the wavelength of maximum radiation decreases with increasing temperature.

In mathematical terms, the electromagnetic energy radiated by a blackbody is characterized by Planck's equation:

$W_\lambda = 2\pi C^2 h^{-5} (e^{hc/\lambda kT} - 1)^{-1}$ (Planck's equation) Eq. 2.1

where c = speed of light in vacuum ($2.997925 \pm 0.000003 \times 10^8$ m. $sec.^{-1}$)

h = Planck's constant ($6.6251 \pm 0.0002 \times 10^{-27}$ erg. sec.)

λ = wavelength (in micrometers)

T = temperature (in degrees Kelvin)

k = Boltzmann constant ($1.38046 \pm 0.00005 \times 10^{-16}$ erg. $deg.^{-1}$)

e = 2.71828 (pure number)

Figure 2.1 illustrates a family of Planck's radiation curves for a blackbody emitting in the thermal infrared region (4.0-16.0 μm) at different temperatures. The range of temperatures shown are those normally encountered on the earth's surface.

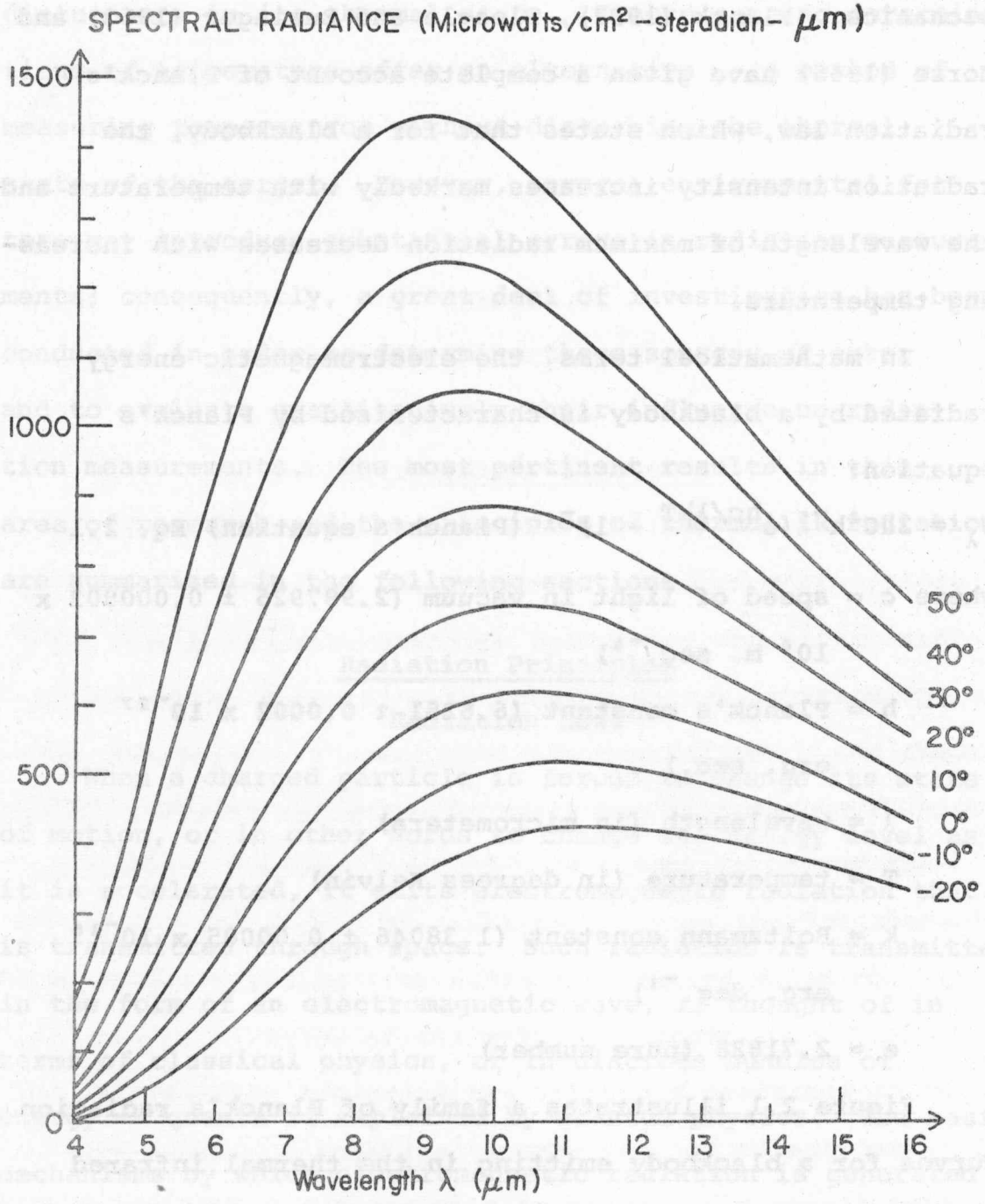

Figure 2.1 Planck's radiation curves for thermal emission from a blackbody at typical terrestrial temperatures.

Integration and differentiation of Planck's equation with respect to wavelength yields other fundamental radiation laws. For example, by integrating Planck's equation over all wavelengths, the Stefan-Boltzmann law can be deduced.

$$\int_0^\infty W_\lambda d\lambda = \int_0^\infty 2\Pi c^2 h\lambda^{-5}(e^{hc/\lambda kT} - 1)^{-1}\, d\lambda = \sigma T^4 = E$$

(Stefan-Boltzmann Law) Eq. 2.2

where E = total amount of radiant energy emitted by a blackbody over the entire spectrum

σ = Stefan-Boltzmann constant (5.67×10^{-5} erg. cm^{-2} $sec.^{-1}$ $°K^{-4}$)

Thus, according to this law, the total amount of radiation emitted by a blackbody varies as the fourth power of its temperature.

Wien's displacement law is also derived from Planck's equation. It is the result of differentiating Planck's equation with respect to wavelength, equating to zero, and solving for the wavelength of maximum intensity.

$$\frac{dI_\lambda}{d\lambda} = 0$$

$$\lambda_{max.} = \frac{\alpha}{T} \text{ (Wien's Displacement Law) Eq. 2.3}$$

where α = 2897 μm °K

T = absolute temperature (in degrees Kelvin).

Equation 2.3 indicates that the peak emissive power of a radiating blackbody shifts toward shorter wavelengths in inverse proportion to T, a phenomenon that can be observed in the curves shown in Figure 2.1.

Emissivity

The theoretical radiation laws have been formulated for radiation emitted by an ideal perfect radiatior (blackbody). However, they may be modified in order to account for the "non-blackness" of natural materials, since there are no true blackbodies found in nature. Siegel and Howell (1968) give an extensive and detailed summary on the emitting ability of natural bodies. This "emitting ability" of natural bodies is largely controlled by the emissivity of the material, which can be defined as a measure of how well a body can radiate energy as compared to a blackbody. Canaway and Van Bavel (1969) have stated that at present the Quantum Theory cannot account quantitatively for the non-blackness of natural materials except for very special cases such as polished pure metal surfaces. Therefore, emissivity values have to be empirically determined.

Measurements of Emissivity

Two distinct measurement techniques are employed for obtaining emissivity values -- the spectral reflection technique and the thermal technique. Wolfe et al. (1965) have described the methods and materials used for measuring

emissivities over desired wavelength and temperature intervals. In general, emissivity values increase with surface roughness and, for metals, increase with addition of impurities, or formation of contaminating surface films such as oxides.

It must be noted that emissivities experimentally determined are functions of wavelength, temperature and the direction of measurements. Thus, the emissivity may be expressed in the following manner:

$$\varepsilon = f(\lambda, T, \phi, \theta)$$

where λ = wavelength

T = temperature

ϕ and θ = angles describing the direction of measurements

The types of emissivity values empirically determined and reported in the literature are listed in Table 2.1.

Table 2.1. Types of empirically determined emissivities.

Directional spectral emissivity	$\varepsilon_{D\lambda} = f(\lambda, T, \phi, \theta)$
Total directional emissivity	$\varepsilon_{TD} = f(T, \phi, \theta)$
Hemispherical spectral emissivity	$\varepsilon_{H\lambda} = f(T, \lambda)$
Total hemispherical emissivity	$\varepsilon_{TH} = f(t)$

Laboratory measurements of emissivity are usually performed at a direction normal to the radiating surface and as a function of wavelength and temperature. However, for most

practical purposes the emissive power of natural surfaces is generally described by a single number -- the total hemispherical emissivity (ε_{TH}), which is formally defined by Siegel and Howell (1968) as "the integrated value of the directional spectral emissivity over all directions of a hemispherical envelope covering the emitting surface, and over all wavelengths". Thus, the emissivity value is left as a function of temperature only [$\varepsilon_{TH} = f(T)$]. In practice, though, because the emissive characteristics of most natural substances do not change considerably over small intervals of temperatures, such as the ones encountered on the surface of the earth, constant mean values of emissivity for different materials are reported by Wolfe (1965), Kondratyev (1969), and Buettner (1964), for specific wavelength and temperature intervals.

Utilization of the 3.0-5.5 and 8.0-14.0 μm Spectral Bands for Remote Sensing Purposes

Because of the selective transmission characteristics of the atmosphere, there are only two infrared spectral bands useful for remote measurements of temperature. That is, the 3.0-5.5 and 8.0-14.0 μm atmospheric windows.

To date, thermal mapping of earth surface features (soils, vegetation and water) from airborne infrared radiametric data has been accomplished using either one of the two IR atmospheric windows.

Adams et al. (1970) have stated that "thermal anomalies were easily identifiable" along many miles of coastline in Hawaii, utilizing the 3.0-5.5 μm wavelength band infrared imagery.

Lyon and Lee (1968) and Lee (1969) have reported that fresh water springs along the shores of Lake Mono, California, can be delineated on infrared imagery collected by a scanner operating in the 3.76-5.16 μm portion of the spectrum. The same investigators have stated that "Correlative use of a PRT-5 radiometer (8.0-14.0 μm) with the 3.76-5.16 μm imagery, produced isothermal maps with absolute temperature values within 0.5°C. of ground control measurements". This was accomplished by a reduction process of film density to temperature by means of an incremental densitometer. Lee (1969) concludes that "qualitatively and quantitatively, there seems to be no difference between the thermal imagery gathered in the 3.0-5.5 and 8.0-14.0 μm band passes."

Friedman (1968) has utilized infrared imagery gathered in the 4.5-5.5 and 8.0-14.0 μm wavelength bands to study the thermal anomalies of the Mono-Crater area in an attempt to correlate them with differences in surface lithology. However, he found that the 8.0-14.0 μm band was "more useful" than the 4.5-5.5 μm band.

Moore et al. (1972) have stated that "successful remote mapping of local springs and flowing wells was accomplished using thermal infrared imagery collected in the 4.5-5.5 μm band."

Rib and Miles (1969) state that "most of the tonal contrasts seen in the 8.0-14.0 micrometer band (imagery) is also evident, but not as distinct, on the 4.5-5.5 micrometer band." They also found that "considering all infrared bands where soils were analyzed, the maximum information was obtained in the 8.0-14.0 μm band." Furthermore, Tanguay and Miles (1970) found that "the thermal infrared data (8.0-13.5 μm) was particularly useful in detecting surfaces that were relatively hot or relatively cold," in contrast to thermal infrared data in the 4.5-5.5 μm band.

From the preceeding review, it is evident that a more quantitative comparison is needed, between the advantages and disadvantages of using either the 4.5-5.5, or the 8.0-14.0 μm spectral regions for accurate determinations of radiant temperatures. In the present study, thermal data from these two spectral bands are compared in an attempt to answer questions such as, (a) Which is the most appropriate thermal band for accurate remote sensing of water surface temperatures?, and (b) Which of the two bands is less subject to atmospheric effects?

Water Surface Temperature Measurements from Airborne IR Radiometric Data

The use of thermal IR instruments to determine water surface temperature is not a particularly recent development.

Hood and Ward (1969) stated that "airborne radiation thermometers (ART) were first used in 1953 in order to measure water surface temperatures over large areas of ocean".

However, the development and testing of suitable, reliable and accurate instruments and techniques has been a constantly developing situation. Only in the last two years or so have reliable thermal infrared scanner systems become available, and have accurate computer-aided data processing techniques been developed.

In order to make thermal IR radiation data meaningful, it is necessary to relate the relative radiance values (as measured by the instruments) to the temperature of the area being sensed. Hoffer and Bartolucci (1972) stated that "two quite different calibration techniques have been utilized to date. (1) The correlation method, and (2) the internal source calibration approach."

The correlation method is relatively simple and it is the most widely used, but does have some serious drawbacks. Variations in tone in the thermal IR imagery correspond to differences in temperatures of the scene imaged. Therefore, if temperature measurements using conventional contact thermometers are obtained for a number of locations on the river or water body at approximately the time the aircraft passes overhead, it is possible to correlate these temperatures with the density values on the imagery that correspond to the same locations, In this way, instead

of having the variations in gray tone on the image represent only relative differences in temperature, one can establish a correlation between the actual temperature of the water at a few points and the film density at those same points, and interpolate for intermediate density values. The major drawbacks of this technique are that (a) it takes only a few minutes to obtain the thermal IR data via airplane, but may take several hours to obtain surface temperatures measurements via conventional contact thermometers, during which time the water temperature may have changed considerably, and (b) the development of the film on which the data are recorded is subject to many possible variations in the processing sequence which can sometimes cause tonal differences to have a non-linear relationship or to vary from one place to another on the film.

The internal calibration technique, whereby the actual water surface temperature can be determined directly from the thermal infrared data without the necessity of surface measurements with contact thermometers, will be discussed in detail in Chapter III.

Emissivity of Water

One of the assumptions made in the internal source calibration technique is that the radiation characteristics of water in the thermal IR region approximates those of a perfect radiator or blackbody. Lee (1969) has stated that

one of the earliest measurements of water emissivities was made by Falckenberg (1928). Falckenberg found that the emissivity of water for "infrared waves" (without specifying the exact wavelength band) was 0.956. Anderson (1952) reported the results of the Lake Hefner heat budget studies in which measurements of emissivities from several types of water were conducted. These results are shown in Table 2.2.

Table 2.2. Emissivity of distilled, sea and lake water.

Water Type (Dissolved Solids)	Emissivity
Distilled water	0.970 ± 0.005
Sea water (33,420ppm)	0.970 ± 0.005
Lake Hefner water (347ppm)	0.970 ± 0.005
Lake Mead water (592ppm)	0.970 ± 0.005

The conclusion drawn from these measurements was that the emissivity of water is 0.970 ± 0.005, and the emissivity is independent of the amount of dissolved solids.

In order to test Anderson's conclusion that salinity does not affect the emissivity of water, Lee (1969) performed a laboratory experiment using two samples of distilled water and two samples of Mono Lake water (76,000ppm solids). The samples were maintained at a constant temperature and a series of radiant temperature measurements were made on each sample with a Barnes IT-3 radiometer, which integrates radiance over the 8.0-13.0 μm region. The results indicated that there was no difference between the emissivity of distilled water and that of the Mono Lake water (very high salinity).

It is interesting to note that from measurements also made by Anderson (1952) of the emissivity of muddy water, it seems that the amount of suspended sediments (turbidity) has no effects on the water emissivity either.

Holter et al. (1962) found that the emissivity of the ocean surface, for infrared wavelengths from 4.0 to 12.5 μm, is 0.98.

From experimental results, McAlister (1964) gives a value of 0.978 for the emissivity (total hemispherical emissivity) of water in the thermal infrared portion of the spectrum.

Weiss (1962) pointed out that "the emissivity of water is almost 1.0 for infrared wavelengths."

Buettner et al. (1964) and Buettner and Kern (1965) have reported the following emissivity values for water (Table 2.3), measured at approximately zero degrees centigrade using the 8-12 micrometer window:

Table 2.3. Emissivity of water.

	ε_v
Water, (fresh)	0.993
Water, plus thin film of petroleum	0.972
Water, plus thin film of corn oil	0.966

The above emissivity data (ε_v) refers to measurements of near vertical emission. At other angles the emissivity of water is smaller, which explains why these values are higher than those reported by other investigators that have determined the total hemispherical emissivity.

Centeno (1941) has also observed that the emissivity of fresh water near 10 micrometers is "almost unity," but above 12 micrometers it decreases continuously.

Thus, the above literature survey indicates that the emissive characteristics of water do not depart more than 2 to 3% from those of a perfect radiator.

Atmospheric Effects

When electromagnetic radiation traverses the atmosphere, it may interact with the atmospheric constituents in several ways. It may be reflected, scattered, or absorbed and re-emitted. Chandrasekhar (1960) has formulated the radiative transfer equations for electromagnetic radiation traveling through the terrestrial atmosphere which acts as a selective reflector, scatterer, absorber and radiator. The effects of the atmosphere on thermal IR radiation play an important role; first, in the selection of the optimum wavelength bands for measuring temperatures from remote locations, that is, bands coinciding with atmospheric windows; and second, in the calculation of correction factors to account for the attenuation or emission of energy by the intervening atmosphere. Figure 2.2 shows the transmission characteristics of the "atmospheric windows" in the thermal infrared portion of the spectrum, that is, the 3.0-5.5 and 8.0-14.0 micrometer spectral bands.

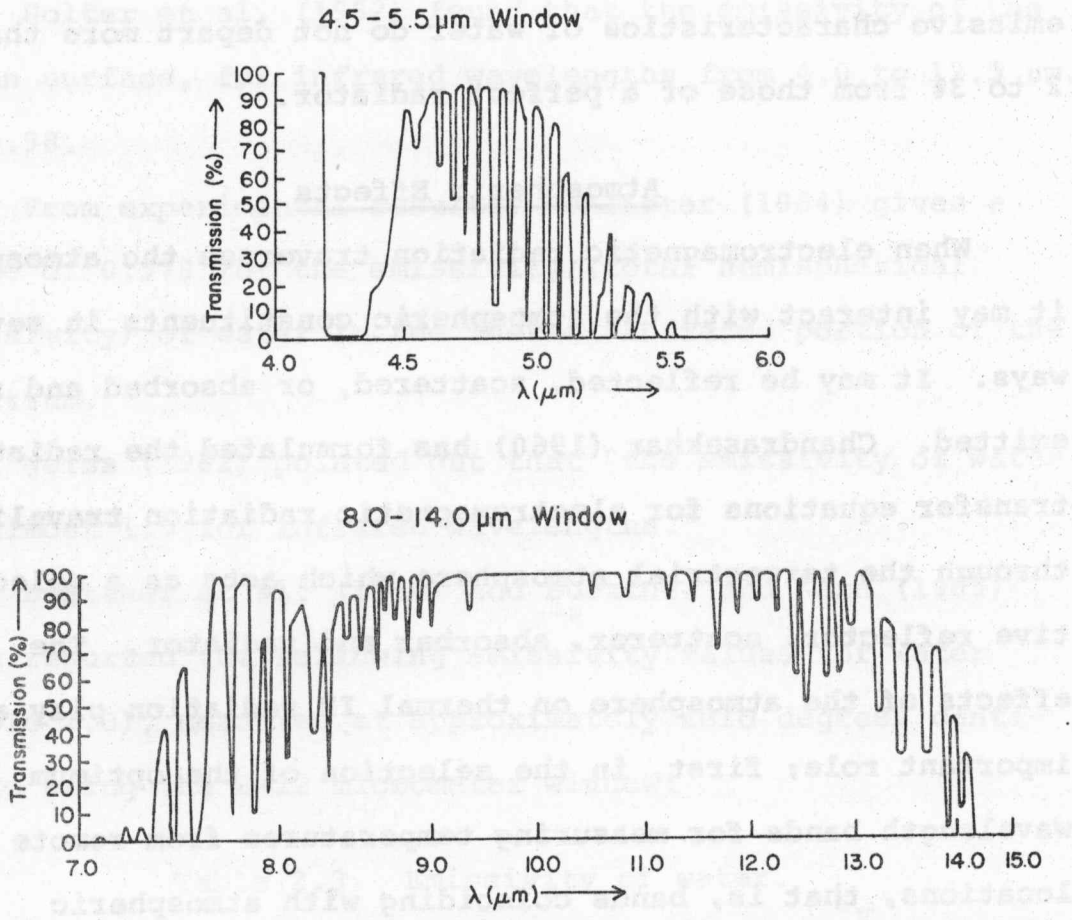

Figure 2.2. Transmission spectra of the atmosphere for 304 m. (1,000 ft.) path-length at sea level. Atmospheric windows in the thermal IR region of the spectrum. [Prepared by Santa Barbara Research Center, Goleta, California]

Saunders and Wilkins (1966) have reported that thermal scanner data gathered by low flying aircraft (about 1,000 ft.) will be biased by up to 1°C by the atmospheric effects. Saunders (1967) states that the radiant energy determined at flight level differs considerably from that measured near the surface. The flight level radiant energy is larger than, equal to, or less than the surface values, depending on whether the temperature of the atmosphere is greater than, equal to, or less than the surface temperature.

Pickett (1966) described an empirical method to correct infrared radiation measurements for environmental factors. It was found that flight altitude (thickness of intervening atmosphere) and air temperature were the most important factors introducing errors in the remotely measured surface temperatures. The correction formula is a linear function of these two factors:

$$C = 1.54 + 0.00046A - 0.043T$$

where C = environmental correction

A = altitude of flight (in feet), and

T = air temperature at 1,000 feet (in °C).

Pickett concludes that the errors introduced by the atmospheric effects can be reduced by applying this empirical correction so that the mean of the distribution of radiant temperatures is adjusted to zero and the standard deviation reduced by one-half. Table 2.4 contains a number of

correction factors in degrees centigrade, for a series of different air temperatures at flight level and for different flight altitudes. These corrections should be added to the radiant temperature readings.

Shaw (1966) has developed an atmospheric model and a computer program that would evaluate theoretically the relative importance of the environmental effects under given meteorological conditions on measurements of surface water radiant temperatures. It becomes evident from Shaw's theoretical studies that not only the two environmental factors accounted for by Pickett can considerably influence radiant temperature measurements, but also concentration of CO_2 and percentage of water vapor in the atmosphere may introduce errors large in magnitude.

An evaluation was made by Shaw and Irbe (1972) of the effects of the thermal infrared emission from water vapor and carbon dioxide in the optical path between the target and the detector on airborne radiation thermometer (ART) readings. They found that re-emission from these two atmospheric constituents contributed 10-15% of the measured radiation. However, using a simple graphical method based on their theoretical model, they were able to obtain an estimate of water surface temperature that was adjusted for the above environmental factors.

Results by Carlon (1971) indicate that water aerosols can also account for major changes in IR radiance, even

Table 2.4. Picketts' environmental corrections for radiant temperature readings[1].

Flight Altitude (Feet)	Air Temperature at Flight Level (C°)								
	-5	0	5	10	15	20	25	30	35
200	2.0	1.7	1.5	1.3	1.1	0.9	0.7	0.4	0.2
400	2.0	1.8	1.6	1.4	1.2	0.9	0.7	0.5	0.3
600	2.1	1.9	1.7	1.4	1.2	1.0	0.8	0.6	0.4
800	2.2	1.9	1.7	1.5	1.3	1.1	0.8	0.6	0.4
1000	2.2	2.0	1.8	1.6	1.4	1.1	0.9	0.7	0.5
1200	2.3	2.1	1.8	1.6	1.4	1.2	1.0	0.8	0.6
1400	2.3	2.1	1.9	1.7	1.5	1.3	1.0	0.8	0.6
1600	2.4	2.2	2.0	1.8	1.6	1.3	1.1	0.9	0.7
1800	2.5	2.3	2.0	1.8	1.6	1.4	1.2	1.0	0.8

[1]In degrees Centigrade to be added to the radiant temperature readings.

through an apparently clear atmosphere in the 8.0-13.5 μm band. Carlon had previously predicted in (1965) and (1966) the errors to be expected in readings of thermal radiation in the 8.0-14.0 atmospheric window that are caused by absorption and scattering by water droplets in an atmosphere with relative humidity in excess of 80%.

Weiss (1962) pointed out that atmospheric effects can be eliminated if viewing is restricted to approximately the 9 to 11 μm band. This narrower spectral region, however, would reduce the amount of energy available for the instrument to measure, and therefore could cause a degradation in the accuracy of the measurements because of increased noise.

Meteorological conditions, such as relative humidity at ground level, may also influence the surface water temperature readings as measured with radiation thermometers in a different way, that is, by affecting the rate of surface water evaporation.

Ewing and McAlister (1960) found that surface water temperatures as measured by an infrared radiometer dropped rapidly when evaporation was taking place. Their measurements of the long-wave infrared radiation from the top 0.1 mm of the evaporating ocean surface demonstrates the existence of a cool surface layer characterized by departures of as much as 0.6°C from the "surface temperature" found by conventional methods.

Investigations in this field were conducted by Marlott and Grossman (1968) in order to determine, among others, the effect of evaporation on water surface temperature measurements. They found that open waters are approximately 0.3°C cooler than waters covered with a mono-molecular film of cetyl alcohol that was employed to retard evaporation.

In summary, it is evident that the atmospheric effects on radiant temperature measurements may not be neglected; however, in most cases it is possible to apply correction factors that would considerably improve the readings.

CHAPTER III

MATERIALS AND METHODS

Location of Test Sites and Data Utilized

This study utilized multispectral scanner data collected over two segments of the Wabash River, Indiana. One test site is located near Lafayette, Indiana, and the other was Cayuga, Indiana.

Two data collection missions on different dates over the Lafayette area were flown. The flight paths were designated as Flightlines #36, starting at approximately one mile upstream from River Junction (junction of the Tippecanoe and Wabash Rivers) and following the Wabash River for approximately 25 miles downstream. The date, time of flight, altitude, flightline number, run number*, and type of scanner utilized for the two flight missions over the Lafayette test site are listed in Table 3.1.

The Cayuga test site is located in Vermillion County, about 8 km (5 miles) east of the Illinois-Indiana state

---

*At LARS, every set of multispectral data is identified by a number which is referred to as "run number".

Table 3.1. Available multispectral scanner data for the Lafayette and Cayuga test sites.

Lafayette - Wabash River Test Site Data

Date	Time (EST)	Altitude (meters)	FLT.LN.#	Run#	Scanner Type
6/30/70	10:45	912	36	70002500	"Old" scanner
8/13/70	15:47	608	36	70006801	"Old" scanner

Cayuga - Wabash River Test Site Data

7/01/70	09:44	3,040	50	70003100	"Old" scanner
7/01/70	09:46	608	50	70003200	"Old" scanner
8/09/72	16:31	1,520	4-A	72001800	"New" scanner
10/17/72	12:22	1,520	4-A	72046600	"New" scanner

line. Three data gathering missions were flown over a 15 mile long segment of the Wabash River near a fossil fuel power plant. At this point, the Wabash River is approximately 170 meters wide and makes a sharp "u" turn, thus offering an ideal natural site for the location of the power plant. Pertinent information concerning the multispectral scanner data collected over the Cayuga test site is illustrated in Table 3.1. Note that one of the three sets of data was collected with the "old" Michigan scanner and the other two were gathered with the "new" Michigan scanner. The two types of scanner and their configurations will be discussed in the next section of this chapter.

Data Collection - Instrumentation

Two major types of data were utilized in this research, a) airborne multispectral scanner data and b) ground control measurements of water temperatures.

Multispectral Scanner Data

The principal multispectral data source for the present investigation was an optical-mechanical scanner system owned by the University of Michigan and operated by Willow Run Laboratories*, Ann Arbor, Michigan.

Holter and Wolfe (1959) have extensively discussed the principles and opeartions of optical-mechanical line scanners.

---

*Presently chartered as the Environmental Research Institute of Michigan (ERIM).

The University of Michigan data collection system has undergone two major modifications during the period of this study. First, the original instrument ("old" Michigan scanner) was modified to accomodate two temperature reference plates for thermal data calibration purposes. Secondly, a coincident line of site for all the detector was implemented ("new" Michigan scanner). Since, data gathered by both systems will be analyzed in the present investigation, the configuration of both scanners will be discussed.

"Old" Michigan Scanner. The configuration of the "old" Michigan scanner system has been thoroughly described by Hasell and Larsen (1968) and by LARS staff, LARS (1967, 1968 and 1970).

A schematic representation of the scanner is shown in Figure 3.1. As the scan mirror rotates around an axis parallel to the flight direction, it sequentially sweeps adjacent strips of ground below the aircraft as well as a number of reference radiation sources within the scanner that are used for calibration purposes.

Until May, 1971 the Michigan data collection system was essentially composed of two individual dual-channel scanners mounted in a C-47 aircraft, that were capable of collecting radiation data through four separate apertures. Consequently, the output was not time synchronous and thus, spatial registration or overlaying problems resulted from

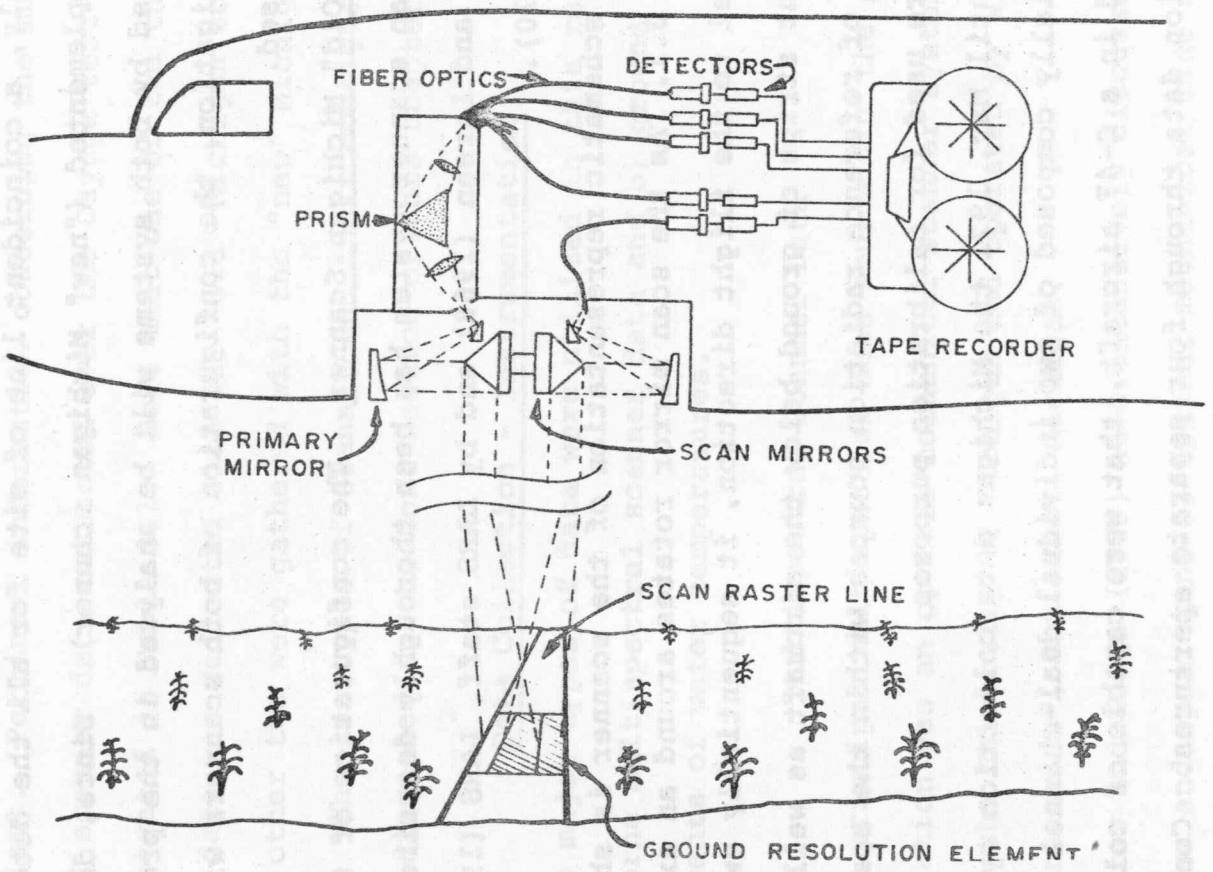

Figure 3.1. Schematic configuration of the "old" Michigan multispectral data collection system. [Illustration credit--R.A.Holmes]

this type of instrument configuration. However, solutions and techniques used in order to overcome the misregistration problems have been developed at LARS and reported by Anuta (1969 and 1970). Table 3.2 shows the types of detectors and their location with respect to the two scanners.

Table 3.2. Detector types and bands utilized in the "old" Michigan scanner system (prior to 1971).

	Aperture	Type of Detector	Bands
Scanner 1	A	Ge:Hg (4.2°K)	8.0-14.0 μm
	B	InSb (77°K)	4.5-5.5 μm
Scanner 2	A	Photomultipliers	0.4-1.0 μm
	B	InAs (77°K)	1.0-2.6 μm

The Michigan scanner system utilized in these studies has been modified from the original to accomodate two thermal reference sources. These temperature references consisted of two 0.63 cm (1/4 inch) copper plates which had been grooved and painted black to provide a non-reflective surface with high emissivity. The thermal scanner configuration is shown in Figure 3.2. The two temperature-controlled plates extended into the field of view of scanner 1. The normal field of view (FOV) of the scanner was 80°; with the plates, however, the external FOV was limited to 37°.

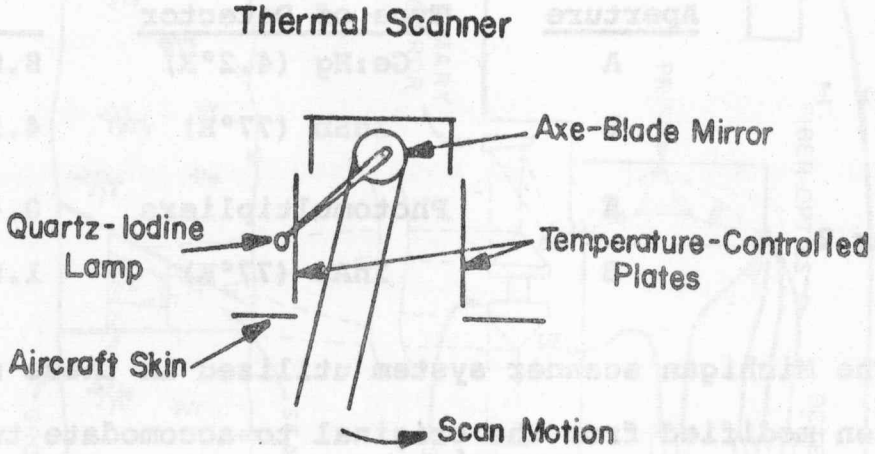

Figure 3.2. Schematic configuration of the Michigan thermal IR scanner. [From technical report ECOM-00013-137; Figure 17]

The geometry of the instantaneous FOV was different for the visible, near infrared and thermal regions, depending on the actual shape of the detectors used. Table 3.3 shows some of the performance parameters of the "old" Michigan scanner.

Table 3.3. Performance parameters of the "old" Michigan scanner system (prior to 1971).

Wavelength Range	Instantaneous FOV
0.4-1.0 μm	2 mr. ○ diam.
1.0-5.5 μm	2 x 4 mr. ▭ rect.
8.0-13.5 μm	4 x 4 mr. □ square
Scan Rate	3600 rpm or 60 scans/sec.
Total ground scan FOV	80° and 37°

This instrument had the capability of gathering spectral data in 15 discrete wavelength bands. The spectral bands and their corresponding channel number are shown in Table 3.4. However, thermal data were collected in only two channels, that is, the 4.5-5.5 and the 8.0-14.0 μm wavelength spectral bands.

"New" Michigan Scanner (M-7). The present configuration of the Michigan data collection system ("new" Michigan scanner) consists of a 12 channel single aperture scanner, which allows a coincident line of site for all the detectors. Figure 3.3 illustrates schematically the single aperture scanner. Total ground scan FOV has been increased

Table 3.4. Channel numbers and corresponding wavelength bands of the "old" Michigan scanner system.

	Channel No.	Spectral Band (μm)
Visible	1	0.40 - 0.44
	2	0.46 - 0.48
	3	0.50 - 0.52
	4	0.52 - 0.55
	5	0.55 - 0.58
	6	0.58 - 0.62
	7	0.62 - 0.66
	8	0.66 - 0.72
Reflective IR	9	0.72 - 0.80
	10	0.80 - 1.00
	11	1.00 - 1.40
	12	1.50 - 1.80
	13	2.00 - 2.60
Emissive IR	14	4.50 - 5.50
	15	8.00 - 14.00

to 90° for all portions of the spectrum. And the scan rate has been changed from 3600 rpm to 6000 rpm or an equivalent of 100 scans per second, thus allowing satisfactory operations at lower altitudes. Table 3.5 illustrates some of the performance parameters of the "new" Michigan scanner system (1971 to date).

Note that the shape of the instantaneous FOV (Table 3.5) in the visible region has been changed from a circular element for the "old" scanner of two milliradians in diameter to a square 2 x 2 mr., and the spatial resolution of the thermal channel has been increased (improved) to 3 x 3 milliradians in contrast to the 4 x 4 mr. used before May, 1971. Also, the thermal infrared detector used in the "new"

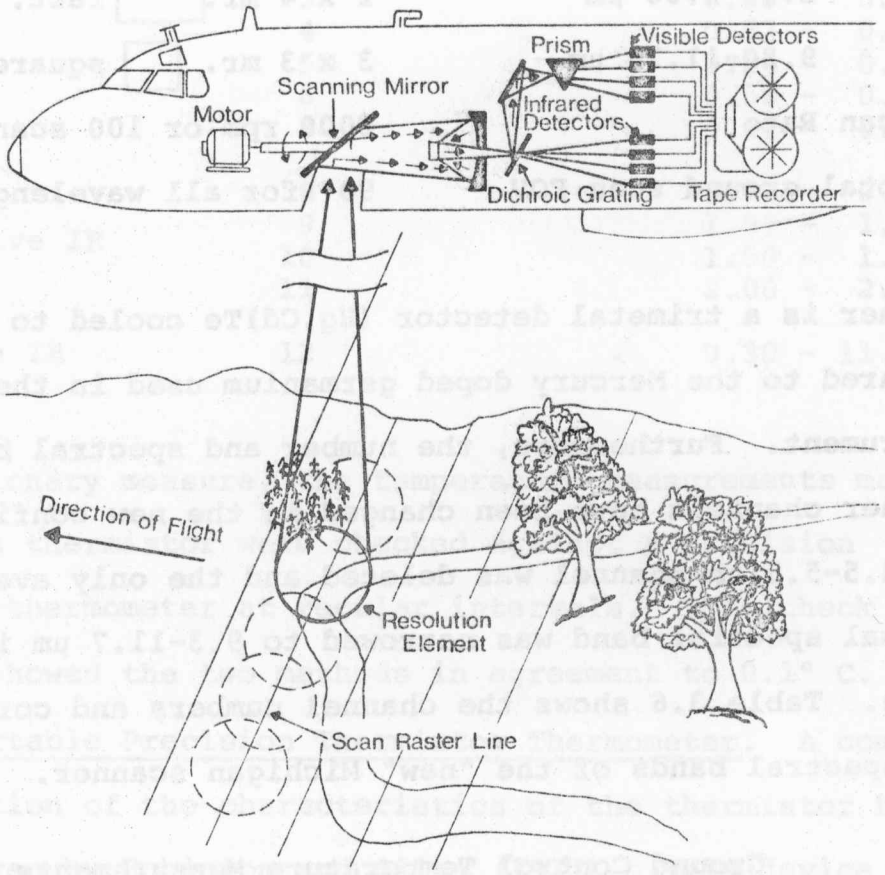

Figure 3.3. Schematic configuration of the "new" Michigan multispectral data collection system.

Table 3.5. Performance parameters of the "new" Michigan scanner system (1971 to date).

Wavelength Range	Instantaneous FOV
0.46-0.92 μm	2 x 2 mr. □ square
1.00-2.60 μm	2 x 4 mr. ▭ rect.
9.30-11.70 μm	3 x 3 mr. □ square
Scan Rate	6000 rpm or 100 scans/sec.
Total ground scan FOV	90° for all wavelength bands

scanner is a trimetal detector (Hg,Cd)Te cooled to 77°K as compared to the Mercury doped germanium used in the "old" instrument. Furthermore, the number and spectral bands or scanner channels have been changed in the new configuration. The 4.5-5.5 μm channel was deleted and the only available thermal spectral band was narrowed to 9.3-11.7 μm in band width. Table 3.6 shows the channel numbers and corresponding spectral bands of the "new" Michigan scanner.

Ground Control Temperature Measurements

In order to test the accuracy and dependability of the scanner and of the LARSYS processing systems for remote measurements of water surface temperatures, surface measurements were conducted at approximately the same time of the overflights. These kinetic temperature measurements were conducted at several different locations in the river, using a portable precision thermistor thermometer. As a

Table 3.6. Channel numbers and corresponding wavelength bands of the "new" Michigan scanner system.

	Channel No.	Spectral Band (μm)
Visible	1	0.46 - 0.49
	2	0.48 - 0.51
	3	0.50 - 0.54
	4	0.52 - 0.57
	5	0.54 - 0.60
	6	0.58 - 0.65
	7	0.61 - 0.70
Reflective IR	8	0.72 - 0.92
	9	1.00 - 1.40
	10	1.50 - 1.80
	11	2.00 - 2.60
Emissive IR	12	9.30 - 11.70

precautionary measure, the temperature measurements made with the thermistor were checked against a precision mercury thermometer at regular intervals. This check always showed the two methods in agreement to 0.1° C.

Portable Precision Thermistor Thermometer. A complete description of the characteristics of the thermistor has been given by Robinson and Silva (1970). This device has an accuracy of ± 0.1° C and it may be referenced to more precise standards to yield accuracies of the order to 0.04° C. The thermistor probe has a water time-constant of 1.7 seconds and has been carefully calibrated against a Taylor Permafused thermometer (Kumar, 1973). The temperatures can be read directly from a digital voltmeter. These qualities permit fast and accurate measurements of near

surface water temperatures. Figure 3.4 shows the portable precision thermistor thermometer and the digital voltmeter.

Data Handling

Introductory Statement

Some of the methods of data handling and data analysis utilized in this research are standard procedures used at LARS. However, parts of this investigation required special processing of the scanner data, such as the digitization of every available scan line for use in the "line averaging study." Also, a non-standard procedure of data analysis was employed and tested, that is, the "layered classifier." In the present chapter, the LARS standard methods of data handling and analysis will be briefly described, and the special (non-standard) procedures utilized in this study will be discussed in more detail. At LARS, the term "data handling" refers to any type of data manipulation (LARS, 1968) which is required in order to convert the raw data into a format compatible with the existing hardware and software.

LARS Standard Data Handling Procedures

The aircraft multispectral scanner output is recorded on an analog magnetic tape. Before the scanner data are suitable to be displayed or analyzed by the user (researcher) at LARS, it has to undergo a certain amount of data preprocessing (data handling). At LARS, some data

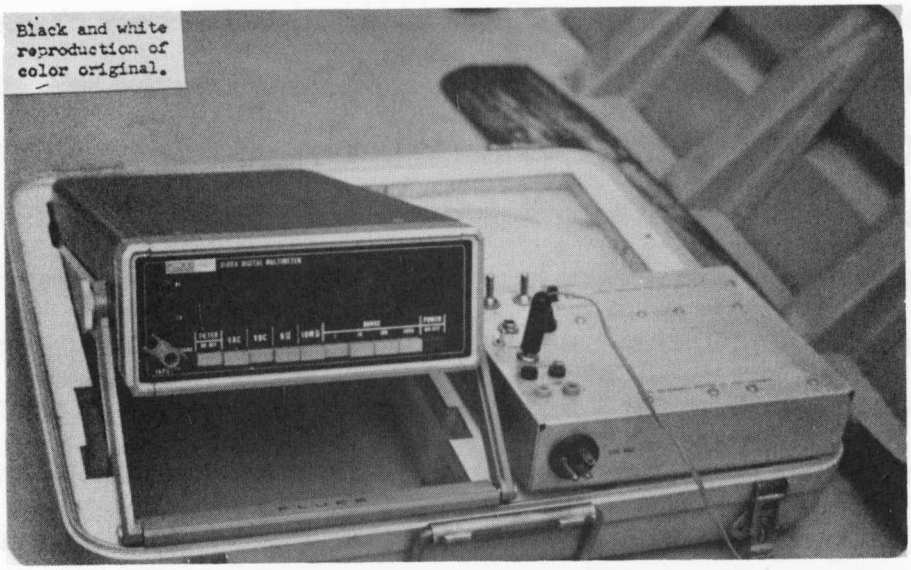

Figure 3.4. Portable precision thermistor thermometer and digital voltmeter.

handling procedures are followed on a routine basis, as is the case with the conversion of the data from analog to digital form (A/D conversion) by which the continuous signal is sampled periodically (digitization) at a convenient rate. Thus, the two dimensional spatial signal representing the scene being sensed is sampled along two perpendicular axes, that is, by the scanner raster in a direction normal to the scan lines, and by the A/D sampling in a direction parallel to the scan lines. The result is an X-Y grid reference system. Another LARS standard data handling procedure is to assign a "line number" and a "column number" to every point in the X-Y reference grid for later location and addressing of features on the imagery. This stage of the data handling is referred to as reformatting. Furthermore, during the reformatting process, calibration and identification information is written on the tape.

Finally, the end product of the data handling is a digital data tape ready to be used by the researcher and it is referred to as the LARS Aircraft Data Storage Tape.

Scan Line Averaging

General. In reality, all measurements are distorted to some extent by extraneous effects. In the particular case of measuring radiation emitted by an object, the quantity recorded by the instrument is in general the

resultant of two components; (1) the actual "signal" or desired information, and (2) a certain amount of unwanted features superimposed on the signal, which is usually referred to as "noise." The noise affecting thermal radiation measurements from airborne platforms, may originate from different parts of the "system," with the "system" consisting of the intervening atmosphere and all the different mechanical and electronical components that make up the instrument (scanner). If the noise introduced by the system is randomly distributed with respect to time, it is possible to improve the quality of the data, that is, to increase the signal to noise ratio (S/N) by means of an averaging operation. Thus, a number "n" of measurements of the same quantity is required. This requirement is "partially" met by the Michigan data collection system, in which a number "n" of successive scan line partially cover the same area on the ground. This is known as "overscanned data" or "scan line overlapping."

The amount of scan line overlapping depends on several factors, such as, (1) the ground speed of the aircraft, (2) its altitude above the ground, (3) the angular velocity of the scanner mirror, and (4) the size of the instantaneous field of view.

It is the purpose of this study to make use of the additional information contained in all the overlapping scan lines, by means of a line averaging procedure, in

order to enhance the quality of the thermal scanner data for temperature mapping of water bodies.

Procedures. At LARS, most of the aircraft scanner data is processed in such a way that only one out of a number "n" of overlapping scan lines is digitized, provided that every successive digitized scan line is contiguous to each other in order to preserve the geometry and spatial relationships of the targets on the ground. Thus, (n-1) of the available scan lines are not digitized. However, to utilize the scan overlap redundancy for enhancing thermal scanner data, each scan line available in the original analog tape must be digitized.

For purposes of assessing the advantages and disadvantages of averaging a number of scan lines, thermal scanner data gathered on June 30th, 1970 over the Wabash River near Lafayette, Indiana were redigitized and reformatted.

The data utilized in this study were gathered at 900 meters (3,000 feet) of altitude, at a ground speed of 120 knots (120 nautical miles per hour), with a scan mirror angular velocity of 3600 rpm (60 scans per second) and an instantaneous field of view of approximately 4 milliradians in diameter. From the above parameters, the number "n" of overlapping scan lines can be calculated. The calculations show that for this particular case there are eight overlapping scan lines "partially" covering the same area

on the ground. Therefore, only one out of eight available lines is necessary to maintain the geometric and spatial fidelity of the ground area being sensed.

However, the redigitized data employed in this study contained every available scan line. Once the data were reformatted into a format compatible with the LARSYS software package, a computer program called LINAVE (Simmons, 1971) was used to average a series of scan lines, ranging from two to a total of eight lines. The original computer program was later modified to offer the option of inserting weighting coefficients that would allow the researcher to weigh more or less heavily certain scan lines so as to produce a trade-off between loss of spatial resolution and improvement of the signal to noise ratio. Lindenlaub and Keat (1973) have proposed a criterion for choosing the optimum number of lines and the best weighting coefficients for a particular set of data. They have reported that two approaches to optimizing the resolution/signal-to-noise-ratio trade-off may be used:

> "In the first approach equal weighting coefficients are used and the number of lines averaged is chosen so that the resolution error equals the noise error. In other words, the number of lines averaged is increased until the point is reached where the resolution error just equals the noise error. In the second approach the weighting coefficients are chosen so as to minimize the sum of the resolution error and the noise error."

In order to be able to use the above mentioned approaches to determine the best number of lines to be

averaged and the weighting coefficients, Lindenlaub and Keat (1973) first had to devise a measure of the spatial resolution error and a method of computing it.

In the present investigation, the author has utilized a different approach to determine the optimum number of scan lines to be averaged and the best set of weighting coefficients to be used.

Thermal scanner data over the Wabash and Tippecanoe River junction, where reliable ground measurements of temperature were available, were averaged in the following systematic manner.

a. averaging two lines and skipping six
b. averaging three lines and skipping five
c. averaging four lines and skipping four
d. averaging five lines and skipping three
e. averaging six lines and skipping two
f. averaging seven lines and skipping one
g. averaging all the eight available overlapping lines

All of the above averaging sequences were first calculated with equally weighted scan lines. In a second series, the center lines were more heavily weighted. The resulting averaged scanner data were then compared to the non-averaged data in two different ways. First, from a pictorial or image oriented viewpoint (see Figure 4.9 for an example), and second, the separability of several pairs

of water spectral classes and other cover types were computed for the different averaged sets of data and non-averaged data. Table 4.3 shows the results of the separability measurements.

Measurement of Spectral Class Separability. The measurement of the separability of the different water spectral classes and different cover types was accomplished by using the $DIVERG program of the LARSYS software package. This program provided the capability of measuring the degree of separability of Gaussianly distributed classes and determining the optimum combination of channels (wavelength bands) for obtaining the highest average separability among the classes considered (LARS, 1970). The divergence value for a pair of spectral classes is in a sense proportional to the distance between their means and inversely proportional to the sum of their standard deviations (spread). This definition of the divergence measuring program $DIVERG or $SEP used at LARS, is of course a simplification of the actual algorithm. Swain et al. (1971) stated that higher values of divergence in general imply greater separation between classes and therefore the percent correct classification should be higher. Swain (1973) has shown that indeed, a higher divergence value implies a higher percent classification (see Figure 3.5).

Therefore, calculation of the divergence between pairs of line averaged and non-averaged spectral classes should

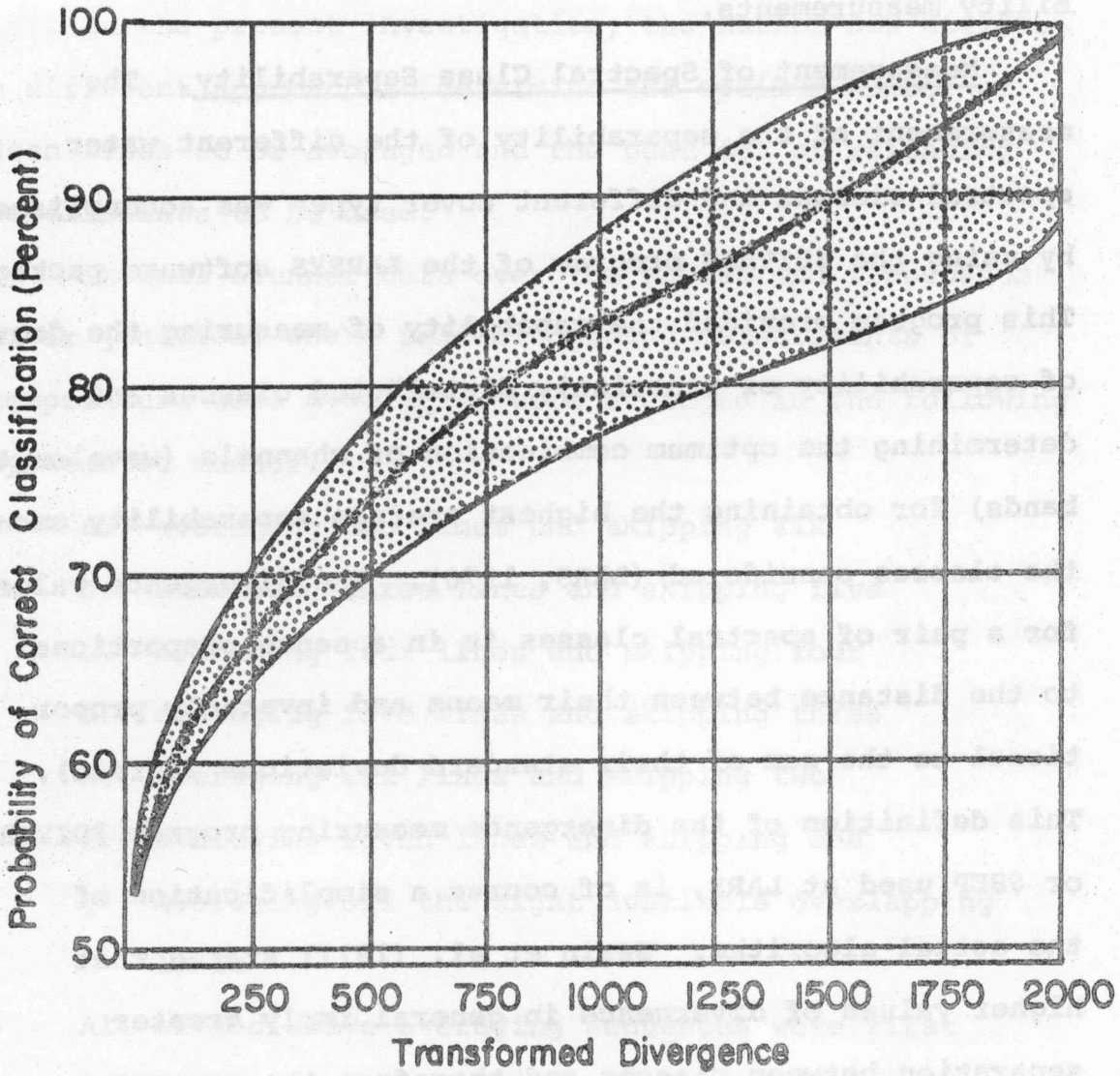

Figure 3.5. Empirical relation between transformed divergence and correct recognition (1-6 features). [Swain, 1973]

be an adequate measure of the advantages or disadvantages resulting from averaging overlapping scan lines.

Thermal IR Scanner Data Calibration

Assumptions - Their Validity. As stated in Chapter II, in order to determine the temperature of a body from remote measurements of thermal radiation, it is necessary to assume that the emissive characteristics of the target approximate those of a perfect radiator (blackbody), and also that there is a linear relationship between the emitted energy and the actual (kinetic) temperature of the body. In the case of a water target, the first assumption is satisfactorily met. That is, the emissivity of water in the thermal region of the spectrum is very close to unity, as pointed out by McAlister (1964); Holter et al. (1962); Weiss (1962); Buettner (1964) and others. The second assumption is needed because the calibration function implemented in the LARSYS software has the characteristics of a straight line, and it is represented by a function of the following form,

$$T = aD + b \qquad \text{Eq. 3.1}$$

where,

T = temperature (to be determined from the scanner data)

D = digitized scanner output (relative values ranging from 0 to 255)

a and b = constants to be determined from known reference temperatures).

Besides the requirement of having a linear relationship between radiation and temperature, it is also necessary that all transformations on the original measured radiance should be linear. In other words, the behavior of the preamplifiers, postamplifiers, and all of the preprocessing operations performed during the "data handling stage" should be linear.

The validity of the assumption that the emitted radiation of a blackbody is a linear function of its temperature is not evident at first sight, because the Stefan-Boltzmann Law states that the total energy radiated by a blackbody is proportional to the fourth power of its temperature, Eq. 2.2. Clearly, this is not a linear relation! Therefore, in order to examine the "linearity" assumption, the author has integrated Planck's equation (Martin and Bartolucci, 1973) for a series of temperatures ranging from -20 to 60 degrees Centigrade (typical terrestrial temperatures), and over selected bandwidths (4.5-5.5, 8.0-13.5 and 9.3-11.7 μm). These wavelength bands correspond to the thermal channels of the Michigan scanner system. Furthermore, the resulting values of radiated energy in the three different bandwidths were plotted versus temperature. Figures 3.6, 3.7, 3.8, 3.9, 3.10 and 3.11 illustrate the resulting curves.

Figure 3.6. Computer-plotted curve (asterisks) showing the relationship between the amount of emitted energy by a blackbody (vertical axis) and its temperature (horizontal axis) in the 4.5-5.5 micrometer spectral band. Integration between -20 and 60° C.

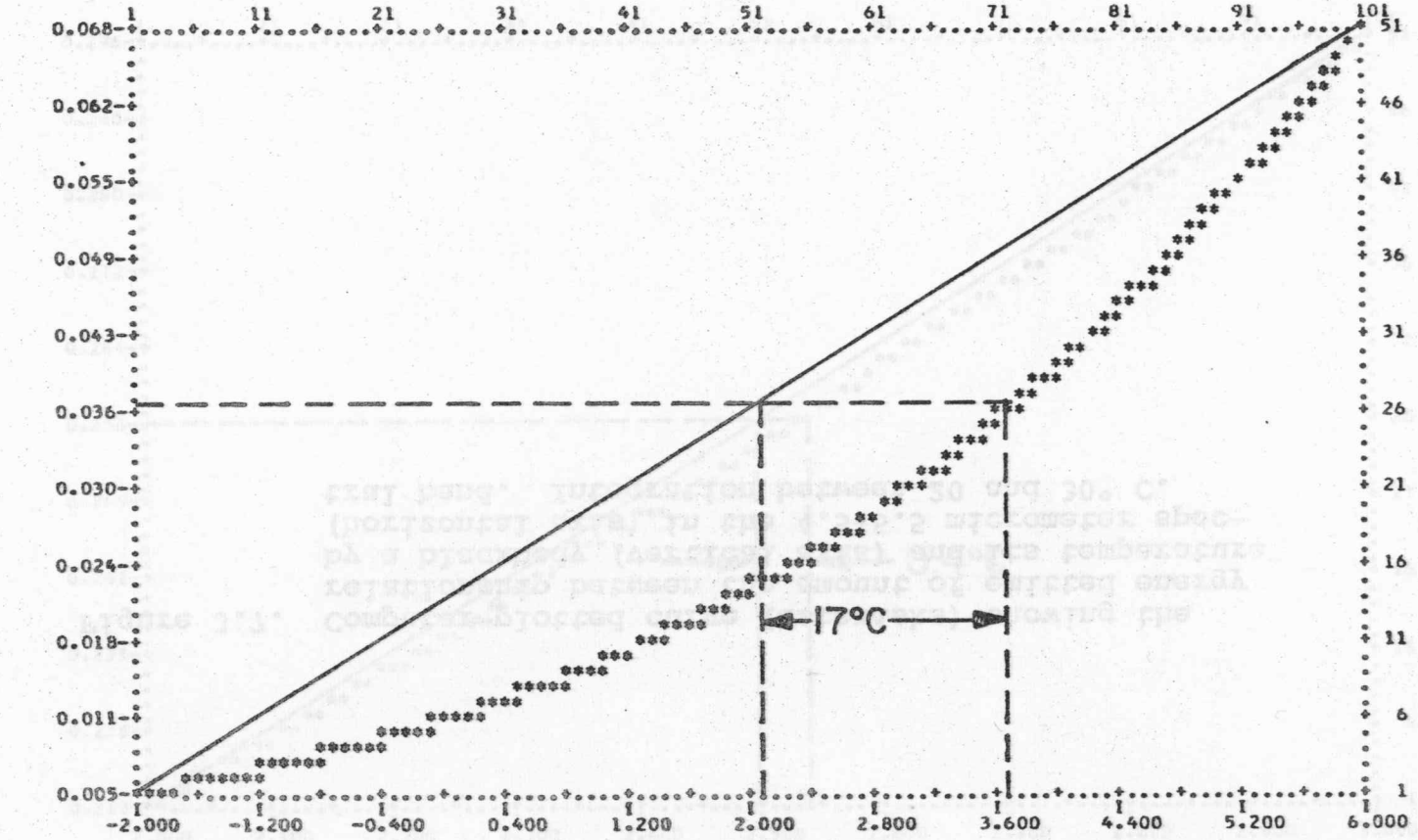

VERTICAL SCALE FACTOR = 10^{-2} HORTIZONTAL SCALE FACTOR = 10^{1} NUMBER POINTS PLOTTED = 801

RESOLUTION IS.... ONE UNIT ON Y-AXIS = 0.126E-04 ONE UNIT ON X-AXIS = 0.800E 00

PLOTTING ERROR IS PLUS OR MINUS 1/2 SCALE UNIT

Figure 3.6.

Figure 3.7. Computer-plotted curve (asterisks) showing the relationship between the amount of emitted energy by a blackbody (vertical axis) and its temperature (horizontal axis) in the 4.5-5.5 micrometer spectral band. Integration between 20 and 30° C.

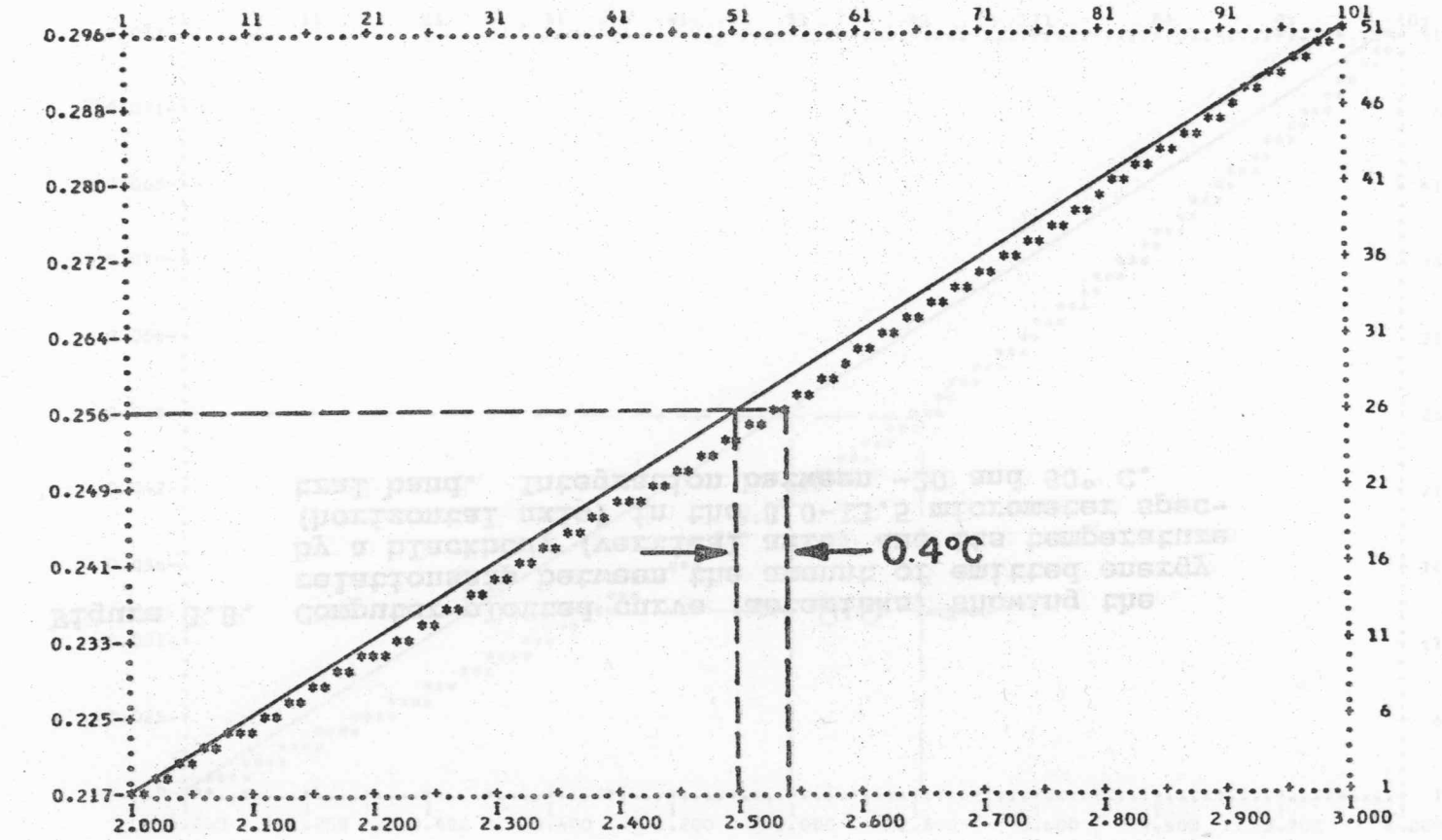

VERTICAL SCALE FACTOR = 10^{-3} HORTIZONTAL SCALE FACTOR = 10^{1} NUMBER POINTS PLOTTED = 101

RESOLUTION IS.... ONE UNIT ON Y-AXIS = 0.159E-05 ONE UNIT ON X-AXIS = 0.100E 00

PLOTTING ERROR IS PLUS OR MINUS 1/2 SCALE UNIT

Figure 3.7.

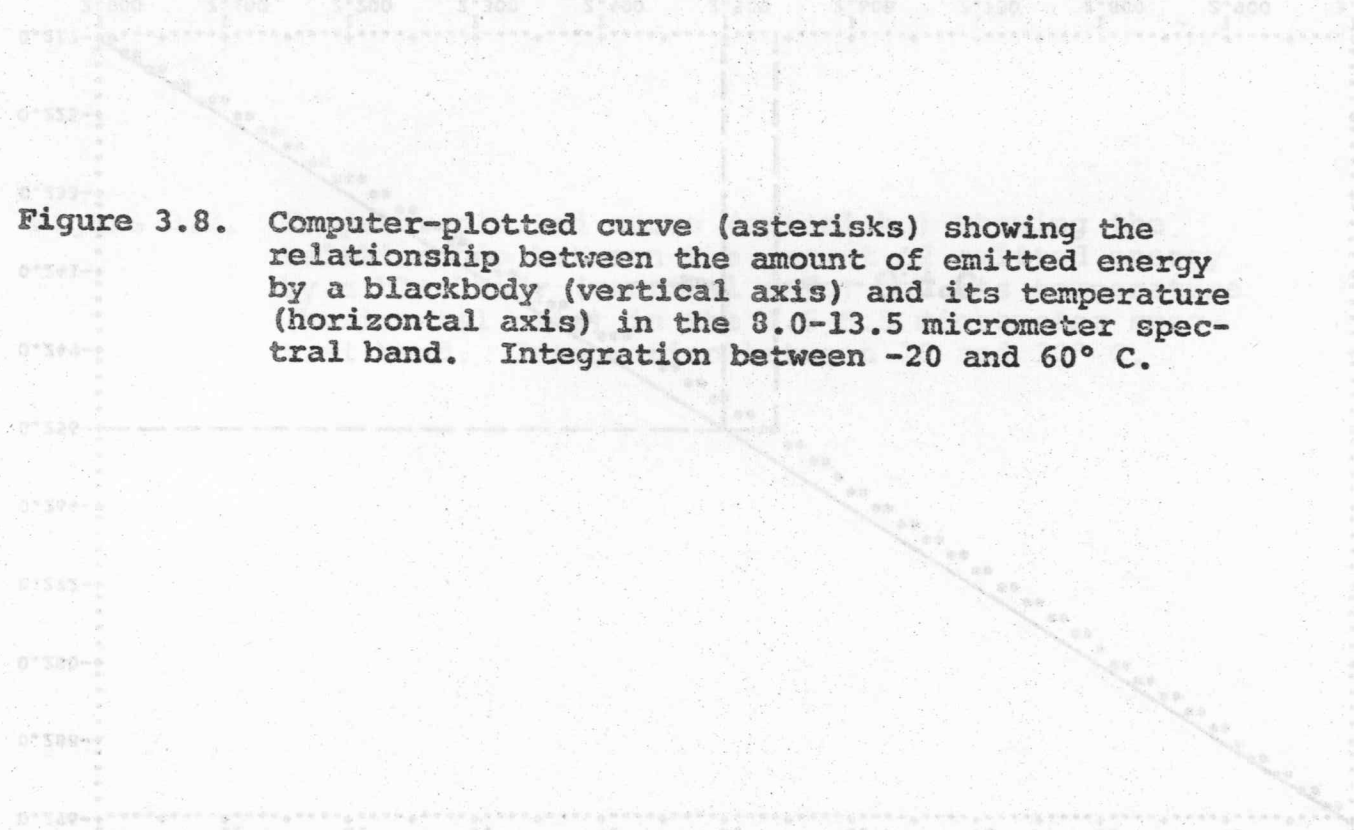

Figure 3.8. Computer-plotted curve (asterisks) showing the relationship between the amount of emitted energy by a blackbody (vertical axis) and its temperature (horizontal axis) in the 8.0-13.5 micrometer spectral band. Integration between -20 and 60° C.

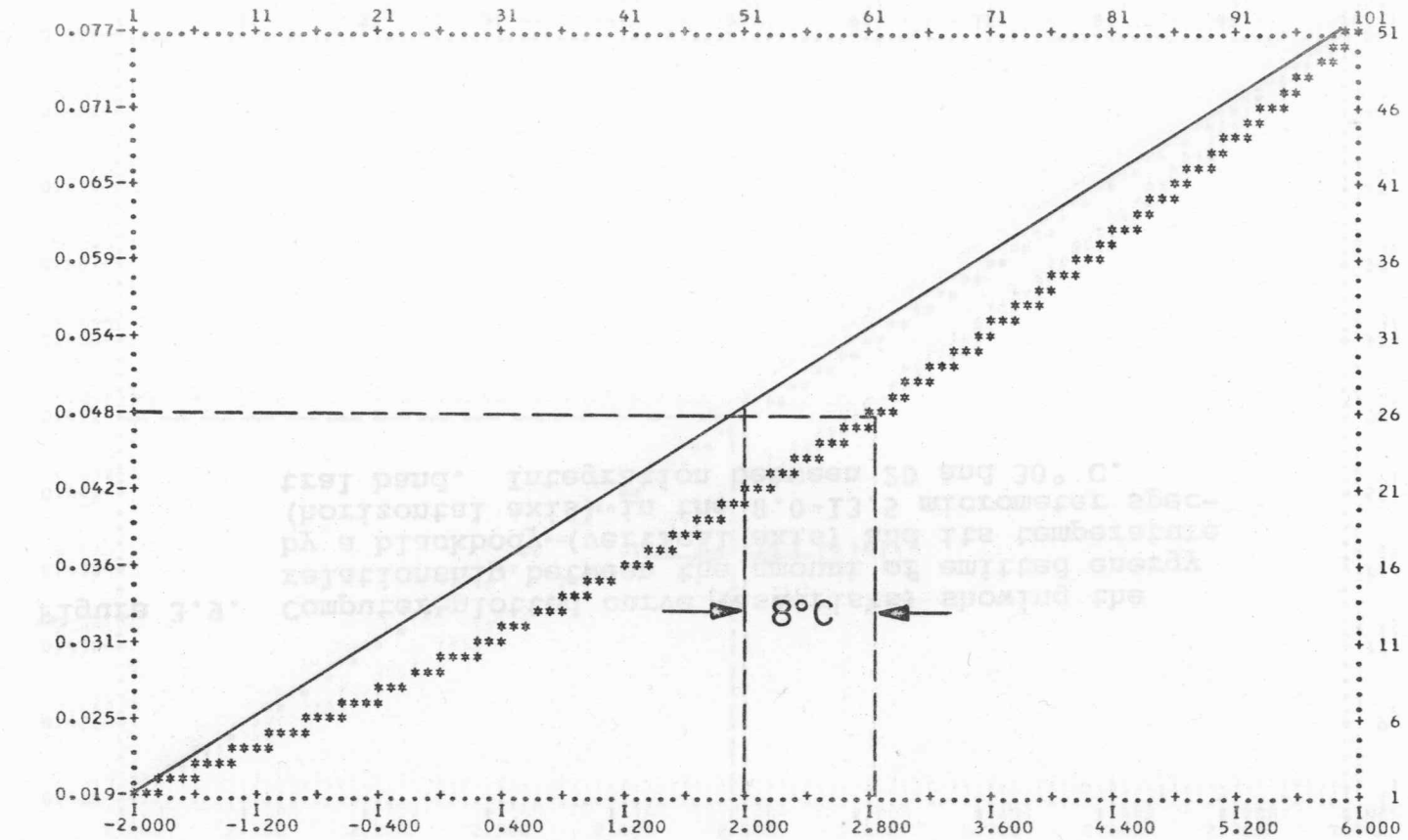

VERTICAL SCALE FACTOR = 10^{-1} HORTIZONTAL SCALE FACTOR = 10^{1} NUMBER POINTS PLOTTED = 801

RESOLUTION IS.... ONE UNIT ON Y-AXIS = 0.115E-03 ONE UNIT ON X-AXIS = 0.800E 00

PLOTTING ERROR IS PLUS OR MINUS 1/2 SCALE UNIT

Figure 3.8.

Figure 3.9. Computer-plotted curve (asterisks) showing the relationship between the amount of emitted energy by a blackbody (vertical axis) and its temperature (horizontal axis) in the 8.0-13.5 micrometer spectral band. Integration between 20 and 30° C.

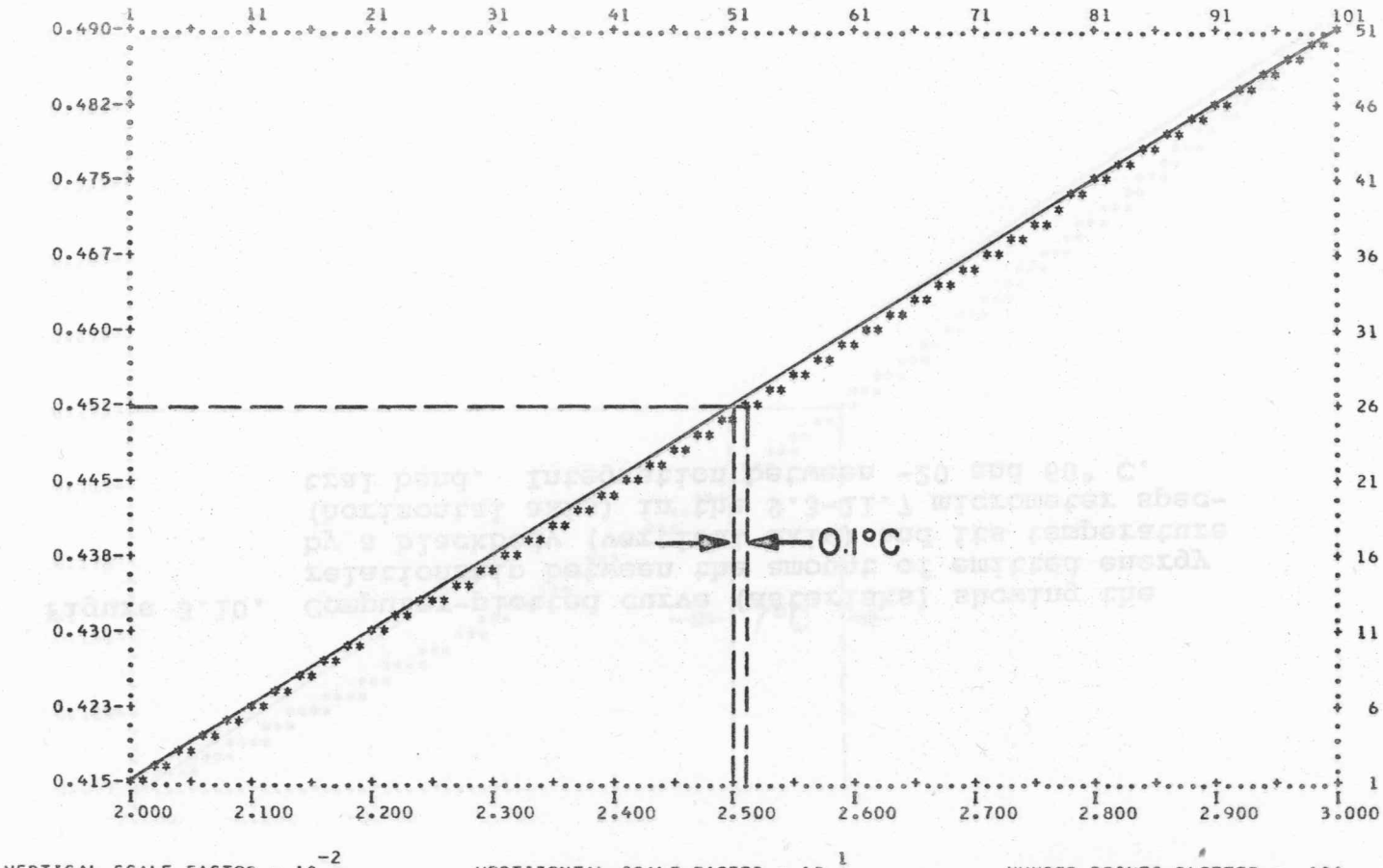

VERTICAL SCALE FACTOR = 10^{-2} HORTIZONTAL SCALE FACTOR = 10^{1} NUMBER POINTS PLOTTED = 101

RESOLUTION IS.... ONE UNIT ON Y-AXIS = 0.150E-04 ONE UNIT ON X-AXIS = 0.100E 00

PLOTTING ERROR IS PLUS OR MINUS 1/2 SCALE UNIT

Figure 3.9.

Figure 3.10. Computer-plotted curve (asterisks) showing the relationship between the amount of emitted energy by a blackbody (vertical axis) and its temperature (horizontal axis) in the 9.3-11.7 micrometer spectral band. Integration between -20 and 60° C.

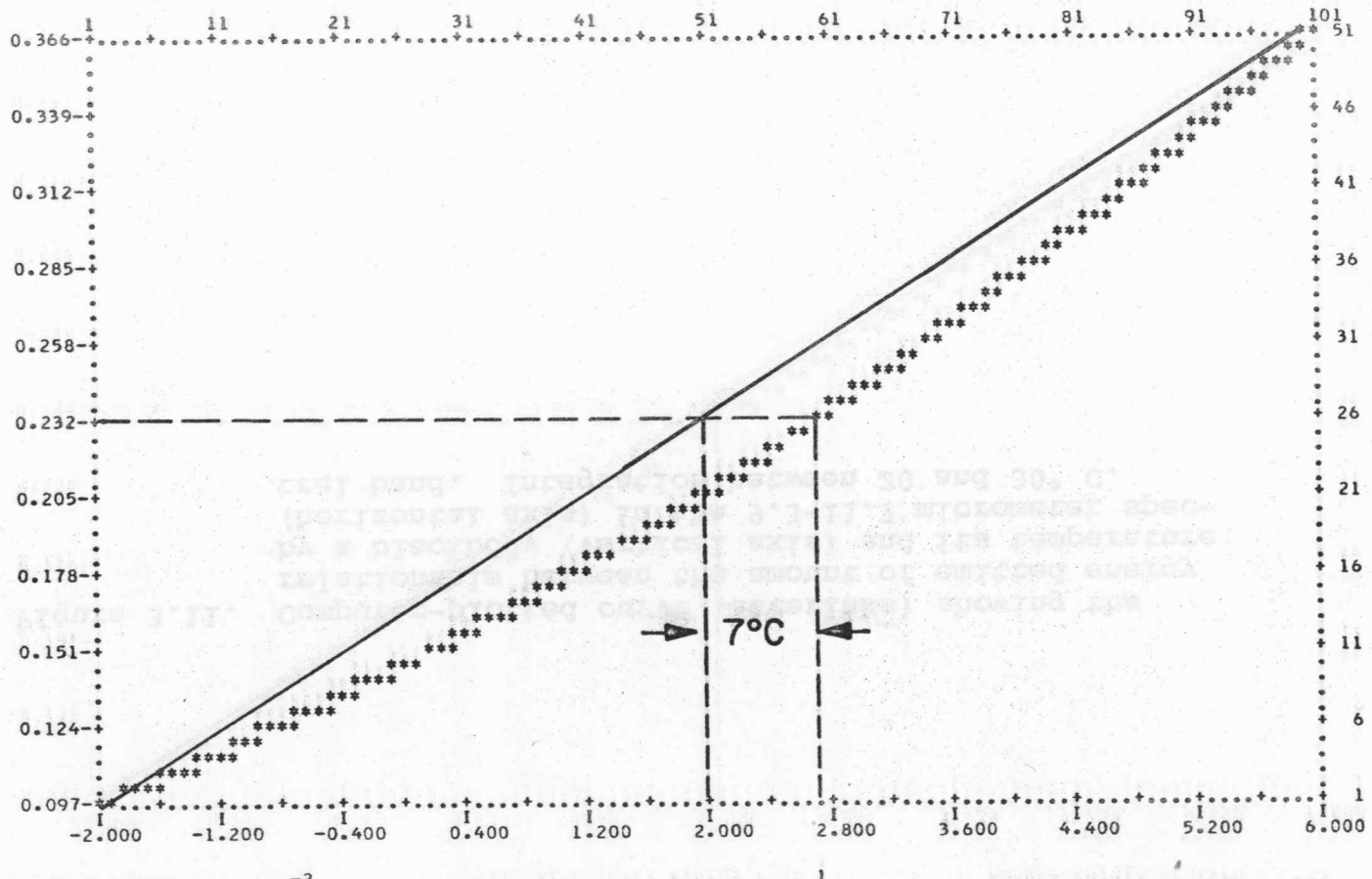

VERTICAL SCALE FACTOR = 10^{-2} HORTIZONTAL SCALE FACTOR = 10^{1} NUMBER POINTS PLOTTED = 801

RESOLUTION IS.... ONE UNIT ON Y-AXIS = 0.539E-04 ONE UNIT ON X-AXIS = 0.800E 00

PLOTTING ERROR IS PLUS OR MINUS 1/2 SCALE UNIT

/E

Figure 3.10.

Figure 3.11. Computer-plotted curve (asterisks) showing the relationship between the amount of emitted energy by a blackbody (vertical axis) and its temperature (horizontal axis) in the 9.3-11.7 micrometer spectral band. Integration between 20 and 30° C.

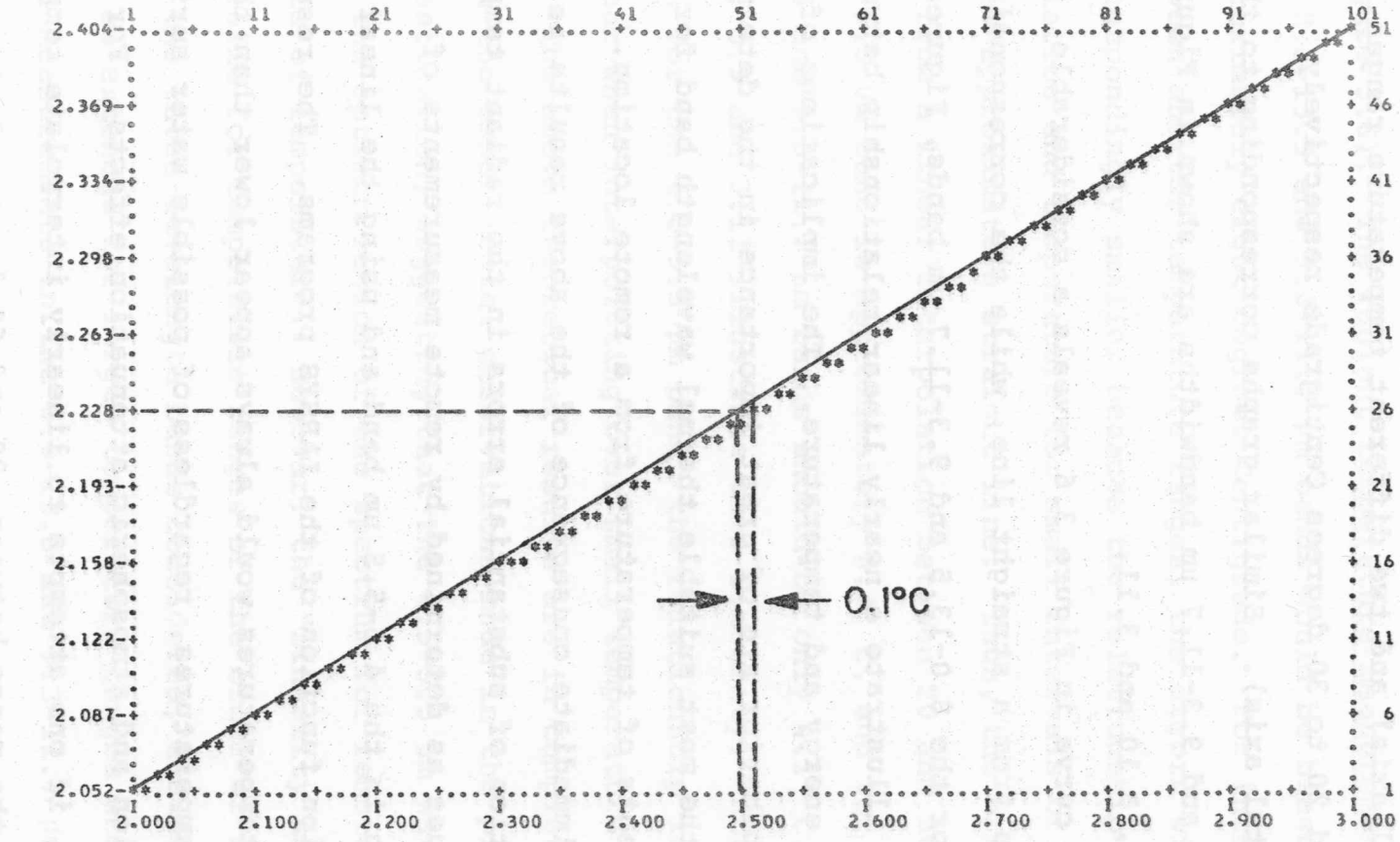

VERTICAL SCALE FACTOR = 10^{-3} HORTIZONTAL SCALE FACTOR = 10^{1} NUMBER POINTS PLOTTED = 101

RESOLUTION IS.... ONE UNIT ON Y-AXIS = 0.705E-05 ONE UNIT ON X-AXIS = 0.100E 00

PLOTTING ERROR IS PLUS OR MINUS 1/2 SCALE UNIT

Figure 3.11.

Figures 3.6 and 3.7 show the relationship between the energy emitted by a blackbody in the 4.5-5.5 μm waveband (vertical axis) and two different temperature ranges, -20 to 60 and 20 to 30 degrees Centigrade respectively (horizontal axis). Similar graphs corresponding to the 8.0-13.5 and 9.3-11.7 μm bandwidths are shown in Figures 3.8, 3.9, 3.10 and 3.11.

The curve in Figure 3.6 reveals a considerable departure from a straight line, while the corresponding curves for the 8.0-13.5 and 9.3-11.7 μm bands, Figures 3.8 and 3.10 illustrate a nearly linear relationship between radiated energy and temperature. The implications of this type of behavior are of great importance in the determination of the most suitable thermal wavelength band for measurements of temperature from a remote location.

An immediate consequence of the above results is the introduction of substantial errors in the radiant temperature values as determined by remote measurements of radiation in the 4.5-5.5 μm band and using the linear calibration function of the LARSYS programs. The resulting radiant temperatures would always appear lower than the actual temperatures, regardless of possible water surface evaporation and atmospheric attenuation effects. For instance, if one attempts to linearly interpolate temperatures in the range between -20 and 60 degrees Centigrade from measurements of radiation in the 4.5-5.5 μm band, the

resultant radiant temperatures will be biased by approximately 17° C lower than would actually be the case, (Figure 3.6). The radiant temperature measurements using the 8.0-13.5 and 9.3-11.7 μm bands would be biased by approximately eight degrees Centigrade. For interpolations between shorter temperature ranges, the errors will be correspondingly smaller because the relationship between radiation and temperature for small intervals of temperatures approximate a straight line. Thus, the error resulting from a linear interpolation between 20 and 30° C for the 4.5-5.5 μm band is approximately 0.4° C, and for the 8.0-13.5 and 9.3-11.7 μm bands should be only 0.1° C. Figures 3.7, 3.9 and 3.11 illustrate this linearity. Note that even for the 4.5-5.5 μm band, the relationship is nearly linear when interpolating over small temperature ranges.

The above theoretical results are in complete agreement with the experimental observations made in the present investigation, suggesting that the 4.5-5.5 μm waveband is not the optimum region of the spectrum for remote measurements of temperature. However, the "Linearity Assumption" is valid for temperature ranges of the order of 10° C for all the three wavelength bands considered, and its validity may be extended for larger temperature ranges when dealing with measurements in the 8.0-13.5 and 9.3-11.7 μm bands. In summary, the relationship between the amount of energy emitted by a blackbody and its temperature (provided the

range of temperatures in question is small--of the order of 10° C for the 4.5-5.5, 8.0-13.5 and 9.3-11.7 μm bands), may be represented by an equation of the following form,

$$T = pE_{\Delta\lambda} \qquad \text{Eq. 3.2}$$

where,

$E_{\Delta\lambda}$ = is the energy emitted by a blackbody over the 4.5-5.5, 8.0-13.5 and 9.3-11.7 μm bands

p = a proportionality constant

T = temperature

However, if a more rigorous representation of the actual behavior of the relationship between $E_{\Delta\lambda}$ and T is desired, and the functional form is unknown, it is possible to describe it by means of a polynomial equation of degree 'k',

$$T = a_0 + a_1 E_{\Delta\lambda} + a_2 E_{\Delta\lambda}^2 + \ldots\ldots + a_k E_{\Delta\lambda}^k \qquad \text{Eq. 3.3}$$

The coefficients a_i (i = 0, 1, 2, ..., k) can be calculated by a regression analysis, assuming that the underlying relationship is "well behaved" to the extent that it has a Taylor series expansion and that the first few terms of this expression will yield a fairly good approximation. Therefore, if more accurate temperatures are required, the LARSYS Calibration Function has to be changed from its present linear form, Equation 3.1 to a polynomial equation of degree 'k' similar to Equation 3.3.

In order to compute the polynomial regression that would best describe the curve in Figure 3.6, a computer

program originated at the University of California Biomedical Center was used. The program is documented at LARS as a LARSYS program abstract, number 0510.

The calculated regression coefficients for a second degree polynomial that would best represent (in mathematical terms) the curve in Figure 3.6 are,

$$a_0 = -0.259$$

$$a_1 = 2.433$$

$$a_2 = -1.815$$

If one substitutes the values of a_0, a_1 and a_2 in Equation 3.3, one obtains the non-linear calibration function that would yield the most accurate results when measuring radiant temperatures between -20 and 60° C and using the 4.5-5.5 μm band. This non-linear calibration function can be described as follows:

$$T = -0.259 + 2.433E_{\Delta\lambda} - 1.815E_{\Delta\lambda}^2 \qquad \text{Eq. 3.3.a}$$

Polynomials similar to Equation 3.3.a may be computed for different temperature intervals and for the 8.0-13.5 and 9.3-11.7 μm bands.

Before proceeding further, it should also be noted that the total amount of energy radiated by a blackbody over the entire electromagnetic spectrum at a temperature of 20° C (293° K) as given by the Stefan-Boltzmann Law, is:

$$E_{0\rightarrow\infty} = \sigma T = 0.041813 \text{ Watts/cm}^2\text{-hemisphere}$$

Whereas calculations of the total amount of energy emitted by a blackbody at the same temperature (293° K) and over the 4.5-5.5, 8.0-13.5 and 9.3-11.7 μm wavelength bands, yielded the following results:

$E_{4.5-5.5}$ = 0.001354 Watts/cm^2-hemisphere

$E_{9.3-11.7}$ = 0.009670 Watts/cm^2-hemisphere

$E_{8.0-13.5}$ = 0.026012 Watts/cm^2-hemisphere

A comparison of the above results with the total amount of energy emitted by the same blackbody over the entire spectrum gives an idea of the percent of energy radiated in the different wavelength bands. Table 3.7 and Figure 3.12 illustrate this comparison.

Table 3.7. Percent radiant energy emitted by a blackbody at 293° K in different portions of the spectrum.

Band (μm)	Percentage
0 → ∞	100%
8.0-13.5	62%
9.3-11.7	23%
4.5-5.5	3%

For temperatures higher than 293° K, such as the temperature of forest fires (approximately 600° K), the blackbody peak emission shifts toward the five micrometer region of the spectrum as predicted by Wien's displacement law. Consequently, the percent energy available for detection in the 4.5-5.5 μm band increases considerably.

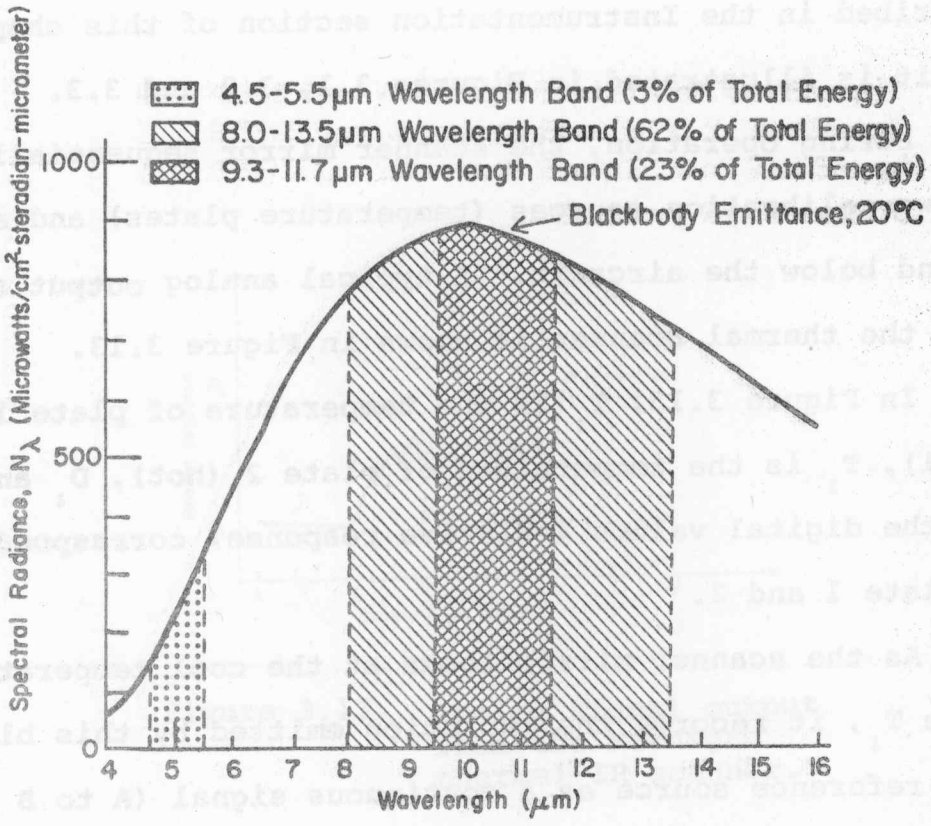

Figure 3.12. Percent radiant energy emitted by a blackbody in the 4.5-5.5, 8.0-13.5 and 9.3-11.7 micrometer spectral bands.

Therefore, this band may be satisfactorily used for measurements of temperatures higher than the ones commonly encountered on the surface of the earth.

Reference Sources and Calibration Signals. The configuration of the Michigan scanner has already been described in the Instrumentation section of this chapter and it is illustrated in Figures 3.1, 3.2 and 3.3.

During operation, the scanner mirror sequentially looks at two calibration sources (temperature plates) and at the ground below the aircraft. A typical analog output signal from the thermal scanner is shown in Figure 3.13.

In Figure 3.13, T_1 is the temperature of plate 1 (cool), T_2 is the temperature of plate 2 (hot), D_1 and D_2 are the digital values (relative response) corresponding to plate 1 and 2.

As the scanner mirror looks at the cool temperature plate T_1, it records the radiation emitted by this blackbody reference source as a continuous signal (A to B in Figure 3.13). Then, it sweeps the ground and records the radiation emitted by the different ground cover types (B to C in Figure 3.13). Finally, the scanner looks at the hot temperature plate T_2 and records its radiance as shown by the segment C-D of Figure 3.13.

In order to make the continuous signal of Figure 3.13 compatible with the LARSYS hardware (digital computer) and related software, it is necessary to perform an A/D (analog

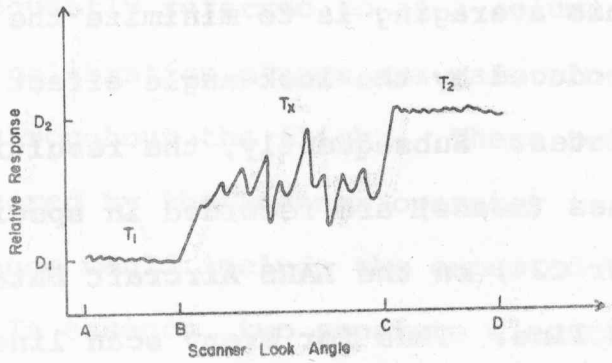

Figure 3.13. Analog signal output from the Michigan thermal IR scanner.

to digital) conversion of multispectral scanner data. The A/D conversion of multispectral scanner data has been described by Anuta (1970). In the particular case of quantizing the thermal scanner data, the analog signal for every scan line is divided into a number of discrete (digital) values corresponding to the thermal radiances of the two calibration sources and of the scene on the ground. Twenty digital radiance values are randomly selected for each of the temperature plates and then averaged. The purpose of this averaging is to minimize the errors that could be introduced by the look-angle effect and nonuniformity of the plates. Subsequently, the resulting averaged radiance values (means) are recorded in specific locations (as C0, C1, or C2*) on the LARS Aircraft Data Storage tapes for each scan line. Thus for every scan line, there exists a pair of mean thermal radiance values (D_1 and D_2) which are related to the two reference-plate temperatures T_1 and T_2. Until 1971, the radiance values corresponding to the temperature plates T_1 and T_2 were written on the LARS Aircraft Data Storage tapes in locations C1 and C2 respectively, in other words, the calibration code

---

*Phillips (1969) states that, "In the digitization process at LARS, several samples of each calibration source are recorded on the Bulk Digital tape. When the Bulk Digital tape is reformatted, the means and variances of these several samples for each calibration source are recorded on the Aircraft Data Storage Tape as the last six samples in each line scan". C0, C1, and C2 define the location of these different calibration values on the LARS Aircraft Data Storage Tape.

describing the combination of C1 and C2 was 6. From 1971 to date, the thermal calibration digital values for T_1 and T_2 are recorded as C0 and C1 (calibration code 4). See Appendix A for calibration codes.

During the reformatting of the data, identification information is written on the LARS Data Storage tapes and an X-Y grid reference system is developed. This is accomplished by assigning each scan line a line number, and each resolution element along each line is denoted by a number (which is frequently referred to as a column number).

The two calibration plates are maintained at a constant temperature throughout the flight. These temperatures are set and monitored by the scanner operator in such a way that their range would include the expected temperatures of the ground. In essence, two separate electrical circuits are used for setting and monitoring the temperature of each of the two reference plates. The "control circuit" includes a thermoelectric module coupled to a water-cooled heat sink and a thermistor embedded in the plate as a sensor. The "monitor circuit" utilizes a thermistor that is physically located within the plate, thus allowing the plate temperature to be determined very accurately (Hasell and Larsen, 1968). In practice, a computer program PLATEMP (Simmons, 1970) is used to determine the temperature of the reference plates. The input to the program are the reference and monitored voltages which are recorded in the scanner

operator's log. The output is, of course the two reference temperatures required for the thermal calibration of the scanner data.

Automatic Calibration. From the known temperatures of the reference plates (T_1 and T_2) and their corresponding digitized output (D_1 and D_2), it is possible to write a linear equation (assuming that $[T_2 - T_1]$ is not greater than 10° C) for each one of the reference plates.

$$T_1 = aD_1 + b \qquad \text{Eq. 3.4.a}$$

$$T_2 = aD_2 + b \qquad \text{Eq. 3.4.b}$$

Solving simultaneously the system of linear Equations 3.4.a and 3.4.b, one obtains,

$$a = \frac{T_1 - T_2}{D_1 - D_2} \qquad \text{Eq. 3.5.a}$$

$$b = \frac{T_2 D_1 - T_1 D_2}{D_1 - D_2} \qquad \text{Eq. 3.5.b}$$

which are the two parameters required by the LARSYS linear calibration function described by Equation 3.1. Hence, substituting Equations 3.5.a and 3.5.b into Equation 3.1,

$$T = \left[\frac{T_1 - T_2}{D_1 - D_2}\right] D + \frac{T_2 D_1 - T_1 D_2}{D_1 - D_2} \qquad \text{Eq. 3.6}$$

one obtains a linear equation (Equation 3.6) relating temperature and digitized scanner output in terms of known constants T_1, T_2, D_1 and D_2.

The above operations are performed automatically by the LARSYS hardware and software, and the final output consists of "calibrated thermal data." In this study, calibrated thermal data refers to radiant temperatures.

In practice, the known values D_1 and D_2 are already in the LARS Data Storage tapes, and the values of T_1 and T_2 may be input into the LARSYS calibration function by means of the LARSYS CHANNELS card (Phillips, 1969). The CHANNEL card, for thermal calibration purposes, has the following format:

CHANNEL A(C/T_1, T_2/)

where,

A = calibration code (See Appendix A)

C = channel number

T_1 and T_2 = the temperature of the two calibration plates

Data Analysis

LARS Hardware

At the present time, the computer facility at LARS consists of an IBM 360 Model 67 digital computer, capable of handling a number of remote terminals on a time sharing basis (LARS Computer Users' Guide, 1971), and a digital

display unit for data editing purposes (IBM, 1970). This type of arrangement has the advantage of allowing the user or researcher to have easy access to the system, thus offering an extremely functional means of man-machine interaction.

LARSYS Software

Once the multispectral scanner data is available in a form compatible with the LARS hardware and software, it may be displayed in a number of ways in imaging or non-imaging formats. It may be further analyzed using "Pattern Recognition Algorithms" (Cardillo and Landgrebe, 1966; Landgrebe et al., 1968; Swain and Fu, 1972).

The LARSYS software is composed of a series of programs written for two purposes: (a) to display the remotely sensed multispectral data (LARSPLAY) and (b) to allow quantitative analysis of the data (LARSYSAA). Figure 3.14 illustrates, in block diagram form, the major steps of the LARS data processing system.

LARSPLAY. The kinds of data display capabilities available in the LARSYS system are indicated in Table 3.8.

The first two types of data display shown in Table 3.8, that is, the Pictorial Printout and the Digital Display picture enable the researcher to work with multispectral data presented in a picture-like or image format. Thus, the researcher is provided with spatial information, such

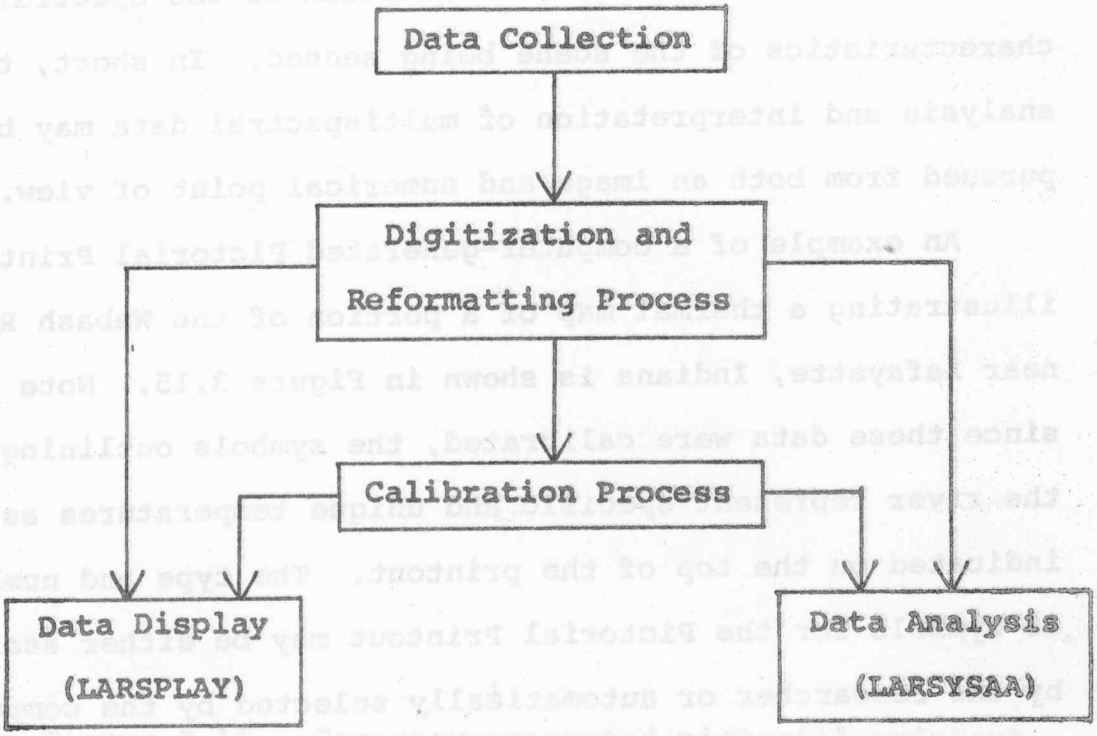

Figure 3.14. LARS data flow chart

Table 3.8. LARS multispectral data display processors.

LARSPLAY	
Pictorial Printout	$PIC
Digital Display Picture	$EDIT
Graph Individual Line of Data	$GLINE
Graph Individual Column of Data	$GCOL
Graph of Calculated Histograms	$GHIS

as size, shape and texture, in addition to the spectral characteristics of the scene being sensed. In short, the analysis and interpretation of multispectral data may be pursued from both an image and numerical point of view.

An example of a computer-generated Pictorial Printout illustrating a thermal map of a portion of the Wabash River near Lafayette, Indiana is shown in Figure 3.15. Note that since these data were calibrated, the symbols outlining the river represent specific and unique temperatures as indicated on the top of the printout. The type and number of symbols for the Pictorial Printout may be either assigned by the researcher or automatically selected by the computer on the basis of previously calculated histograms. Figure 3.16.a shows a photograph taken from the Digital Display screen. The rectangular outline in the center of the photo shows the same area displayed in the pictorial printout of Figure 3.15. The LARS Digital Display unit has also the capability of enlarging the imagery. An enlargement of the area outlined in Figure 3.16.a is shown in Figure 3.16.b. The light tones in the image represent high temperatures, the dark tones stand for cool temperatures and the intermediate gray levels are designated automatically by the computer on the basis of statistical calculations. Even though these data are calibrated, since a person has difficulty in accurately assessing differences in gray tones, this type of data display provides only a relative

Figure 3.15. Computer-generated pictorial printout (thermal map) of a segment of the Wabash river near Lafayette, Indiana. The symbols represent temperatures in degrees centigrade.

LABORATORY FOR APPLICATIONS OF REMOTE SENSING
PURDUE UNIVERSITY

MAR 12,1973
5 09 30 AM

WABASH RIVER ISLAND

RUN NUMBER..... 70002522
FLIGHT LINE.. PURDUE FLT LN 36
DATA TAPE..... 76
REFORMATTING DATE.JAN 10,1972

DATE..... 6/30/70
TIME..... 1045
ALTITUDE..... 3000
GROUND HEADING.... 225 DEGREES

CHANNEL 2 SPECTRAL BAND 8.00 TO 14.00 MICROMETERS CALIBRATION CODE = 4 C0 = 25.84 C1 = 33.82

THE CHARACTER SET USED FOR DISPLAY IS

FROM******* TO 24.7 DISPLAYED AS M
FROM 24.7 TO 24.9 DISPLAYED AS $
FROM 24.9 TO 25.1 DISPLAYED AS X
FROM 25.1 TO 25.3 DISPLAYED AS Z
FROM 25.3 TO 25.5 DISPLAYED AS =
FROM 25.5 TO 25.7 DISPLAYED AS -
FROM 25.7 TO 27.0 DISPLAYED AS .
FROM 27.0 TO 33.0 DISPLAYED AS
(Degrees Centigrade)

Figure 3.15.

Figure 3.16a. Thermal imagery from the LARS digital display. Light tones represent warmer areas and dark tones represent cooler areas.

Figure 3.16b. Thermal imagery from the LARS dogital diaplay showing enlargement of outlined area in Figure 3.16a.

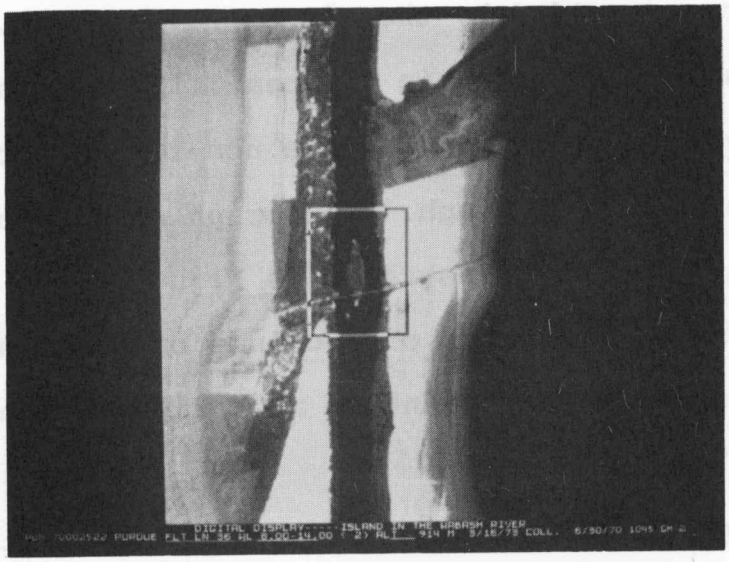

Figure 3.16.a.

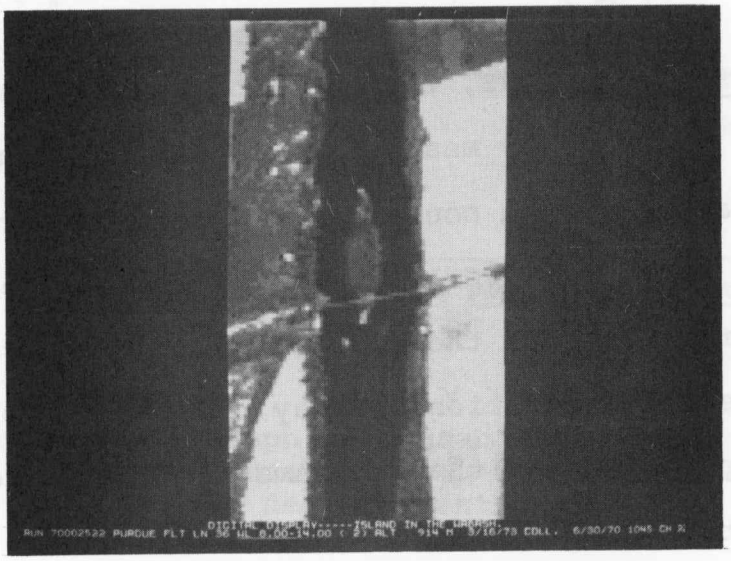

Figure 3.16.b.

indication of the radiant temperatures on the ground, in contrast to the more quantitative display of radiant temperatures provided by the Pictorial Printout.

The same data shown in Figures 3.15, 3.16.a and 3.16.b may also be displayed in a non-imaging format, that is, in the form of a graph. The graph of a data line across the Wabash River is illustrated in Figure 3.17. In a similar manner, the graph of a column of data may be displayed, resulting in a printout much like the one shown in Figure 3.17.

Histograms of selected areas of data may also be displayed. A typical histogram graph of an area in the river is shown in Figure 3.18. It should be noted that the data displayed in Figures 3.17 and 3.18 have been calibrated in such a way that one of the axes of these graphs represents temperatures in degrees Centigrade.

LARSYSAA. At LARS, the multispectral scanner data may be further analyzed by means of the LARSYSAA computer software package which contains four major programs, (1) the statistics processor ($STAT), (2) the feature selection ($DIVERG or $SEP), (3) the classification processor ($CLASS), and (4) the classification display processor ($DISPLAY). The description of all the programs has been extensively discussed by the LARS staff (LARS, 1970).

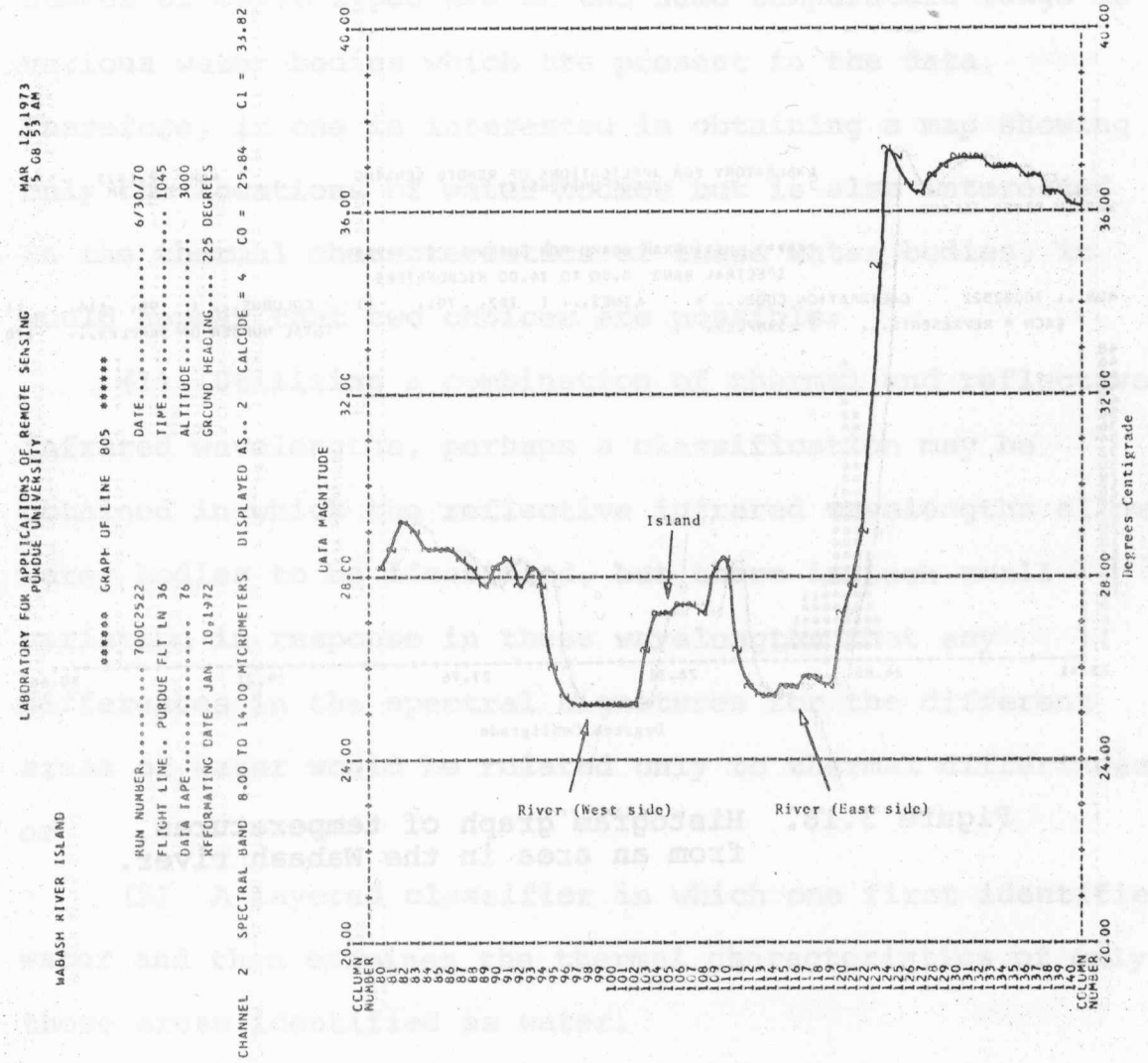

Figure 3.17. Graph of a scan line across the Wabash river. Calibrated data in degrees centigrade.

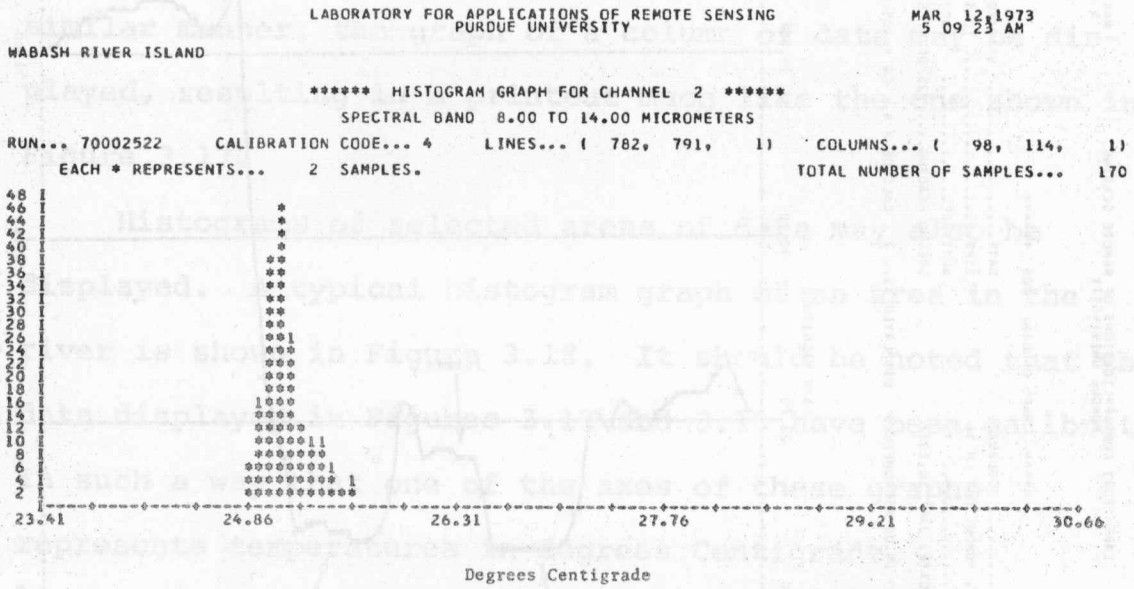

Figure 3.18. Histogram graph of temperatures from an area in the Wabash river.

Layered Classifier

Background. Analysis of the August 1970 thermal scanner data has indicated that at many times of the day and the year thermal scanner data are obtained in which a number of cover types are in the same temperature range as various water bodies which are present in the data. Therefore, if one is interested in obtaining a map showing only the locations of water bodies but is also interested in the thermal characteristics of these water bodies, it would appear that two choices are possible:

(1) Utilizing a combination of thermal and reflective infrared wavelengths, perhaps a classification may be obtained in which the reflective infrared wavelengths allow water bodies to be identified, but there is such small variation in response in these wavelengths that any differences in the spectral signatures for the different areas of water would be related only to thermal differences, or

(2) A layered classifier in which one first identifies water and then examines the thermal characteristics of only those areas identified as water.

Since the thermal characteristics of water bodies and the ability to map such thermal characteristics is an extremely important application in water resource problems, determining the methodology required to obtain maps of the thermal characteristics of water only is important in defining future programming needs.

Procedures. In order to test the first possibility, it was thought that a classification might be feasible using the existing LARSYS software and procedures, in which one could identify water bodies and also obtain information concerning the thermal characteristics of the water. However, it was found that the spectral response of water changed considerably in the visible (as it was expected) and also in the near infrared. Thus, the resulting classification gave no indication of the thermal characteristics of the water bodies, but only revealed the differences in water turbidity (suspended solids). Therefore, a "layered classifier" had to be developed. The layered classifier essentially combines a pattern recognition algorithm with the existing LARSYS linear calibration function in order to produce a temperature map of one cover type (class) only. In this particular case, the Layered Classifier generates a thermal map of only water. Swain and Wu (1973) have described in detail the layered classification processor. Furthermore, Wu and Bartolucci (1973) have reported on the implementation of the linear calibration function into the layered classifier, and its immediate and potential applications to water resources studies.

CHAPTER IV

RESULTS AND DISCUSSION

Absolute Water Temperature Determination From Airborne Thermal IR Scanner Data

In this section, the results of determining absolute water surface temperatures from calibrated, airborne, thermal infrared scanner data will be shown and discussed.

Accuracy and Reliability of the Internal Calibration Technique

One of the advantages of the internal calibration technique is in its ability to determine absolute water surface temperatures directly from the remotely sensed thermal infrared radiation. Stated more simply, this calibration method does not require surface observation data, commonly referred to as "ground truth." However, in order to check the accuracy and reliability of the internal calibration technique, a number of water temperature measurements--using a conventional contact thermometer--were conducted at approximately the same time as the overflight.

After being put in digital form, the data were calibrated using the calculated reference temperatures T_1 = 25.8°C, and T_2 = 33.8°C and following the calibration procedures outlined in Chapter III. The result was a thermal map showing all the different features or cover types "seen" by the scanner. Because the temperature of the water was lower than the temperature of all the other cover types (soils, vegetation and cultural features) at this time of the year, it was possible to assign gray scale symbols to the temperature range that corresponded to water only, and a blank or no-symbol was assigned for temperatures higher than 26.5°C. Thus, a computer-generated thermal map showing water only was produced. Figure 4.1 shows a thermal map of the River Junction (Tippecanoe and Wabash Rivers) near Lafayette, Indiana. A different symbol was assigned for every 0.2°C as illustrated on the top of the printout. The outlined areas (3 x 3 resolution elements), correspond to approximately the same sites where ground measurements were conducted. The variations in symbols, indicating a significant variation in temperature, for the lower test area tends to point out one of the difficulties of relating the location where surface measurements were obtained to the same location in the scanner data. At an altitude of approximately 900 meters (3,000 feet) the instantaneous field of view of the scanner covers an area on the ground

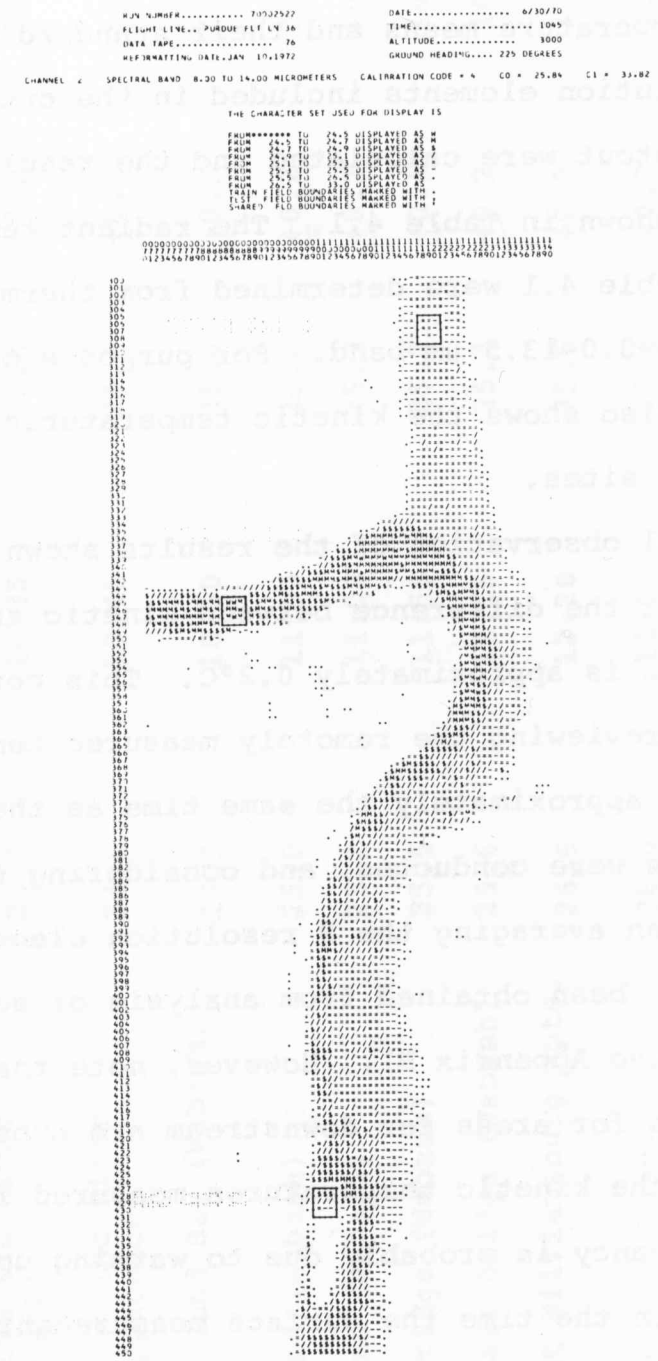

Figure 4.1. Computer-generated thermal map of the Wabash and Tippecanoe river junction near Lafayette, Indiana. Every symbol represents a temperature interval of 0.2° C.

that is approximately 1 meter (9 feet) in diameter. The radiant-temperature means and their standard deviation for the 9 resolution elements included in the outlined areas of the printout were calculated and the results for 12 test sites are shown in Table 4.1. The radiant temperatures shown in Table 4.1 were determined from thermal radiation data in the 8.0-13.5 μm band. For purposes of comparison, Table 4.1 also shows the kinetic temperatures measured at the same 12 sites.

Careful observation of the results shown in Table 4.1 suggest that the difference between kinetic and radiant temperatures is approximately 0.2°C. This conclusion is reached by reviewing the remotely measured temperatures, gathered at approximately the same time as the ground observations were conducted, and considering the variances obtained when averaging the 9 resolution elements. Similar results have been obtained from analysis of several other data sets (See Appendix B). However, note that the radiant temperatures for areas far downstream are substantially lower than the kinetic temperatures measured from the boat. This discrepancy is probably due to warming up of the water between the time the surface measurements started and the time the last measurements were taken, approximately 3 hours later. On the other hand, it took the airplane only 8 minutes to cover the same distance.

Table 4.1. Comparison of Kinetic and Radiant Temperatures

Location	Kinetic Temp. (°C)	Time (EST)	Radiant Temp.* (°C) Mean	Std. Dev.	Time (EST)
300 yards above the River Junction (Wabash)	25.4	10:35	25.4	±0.1	10:45
300 yards above the River Junction (Tippecanoe)	24.2	10:45	24.4	±0.3	10:45
North end of Sand Bar (Wabash)	25.3	10:50	25.0	±0.2	10:46
West of Island (Wabash)	25.0	11:00	25.0	±0.2	10:46
East of Island (Wabash)	25.3	11:08	25.3	±0.2	10:47
9th Street Bridge (Wabash)	25.5	11:56	25.2	±0.1	10:47
U.S. 52 By-Pass Bridge (Wabash)	25.6	12:15	25.4	±0.2	10:48
North Pond at Williamsburg Apts. (Wabash)	26.6	12:20	25.6	±0.2	10:49
Main St. Bridge (Wabash)	26.0	12:27	25.4	±0.2	10:50
Stiney's Tavern (Wabash)	26.0	12:54	25.3	±0.3	10:51
Boes Creek (Wabash)	26.0	13:45	25.4	±0.2	10:52
Granville Bridge (Wabash)	26.1	13:55	25.4	±0.4	10:53

*Radiant temperatures were determined from the 8.0-13.5μm thermal scanner data by averaging 9 resolution elements. Data gathered on June 30, 1970.

Radiant temperatures were also determined from thermal radiation detected and recorded in the 4.5-5.5 μm band, for those same locations shown in Table 4.1. The resulting temperature means were consistently lower than the kinetic temperatures (surface measurements) by approximately one degree centigrade. Such large errors may be accounted for by: (a) the non-linearity between temperature and emitted energy in the 4.5-5.5 μm band, (b) the lower emissivity of water in this portion of the spectrum, and (c) the partial transparency of the atmosphere in this wavelength band. Furthermore, all water surface temperature determinations achieved through thermal IR radiation measurements (regardless of wavelength band), will appear lower than the bulk kinetic temperature of the water body because of "top surface" cooling by evaporative effects. In reality, water radiant temperatures are indicative of the thermal state of only the top 0.02 mm thickness of water (McAlister, 1964). Consequently, unless the meteorological conditions near the water surface are such that the water vapor pressure in the atmosphere is high enough to compensate for the evaporation pressure of the water surface, radiant temperatures will always be biased in such a way that it would appear that the water body is at a temperature lower than in reality.

It is noteworthy to point out that the calibration of scanner data, particularly the calibration of thermal data,

besides yielding physically meaningful quantities such as "temperatures," also provides a means to remove the effects of system drift and gain changes, and thereby improve overall quality of the data. Figure 4.2 demonstrates how the calibration has improved the quality of the scanner data by revealing additional information that otherwise would have been lost because of long term system drift. Note that at the end of the flightline--approximately 40 km. (25 miles)--the calibrated printout shows information that is not present in the uncalibrated pictorial printout.

Flight Altitude Effects on Remotely Measured Temperatures

As indicated in Table 3.1, two overflights of the Cayuga test site were made on July 1, 1970 at 3,040 m. (10,000 feet), and at 608 m. (2,000 feet) of altitude. The time of the flights over the test site were from 09:44 to 09:47 EST at 3,040 m. (10,000 feet), and from 09:56 to 09:58 EST at 608 m. (2,000 feet). Note that the time between the two overpasses was less than 10 minutes. Therefore, no appreciable changes in the thermal regime of the river should be expected. An aerial photograph of the power plant and Wabash River at the Cayuga test site is shown in Figure 4.3. Figures 4.4 and 4.5 show the thermal imagery from the Cayuga test site in channels 14 and 15, at 608 and 3,040 meters of flight altitude respectively. This imagery was produced by the LARS Digital Display unit. Note the

Figure 4.2. Calibration effects on system drift. The map indicates the location where the data for segment A was collected at the begining of the data collection run, and segment B data was collected over a portion of the river 40 km. downstream.

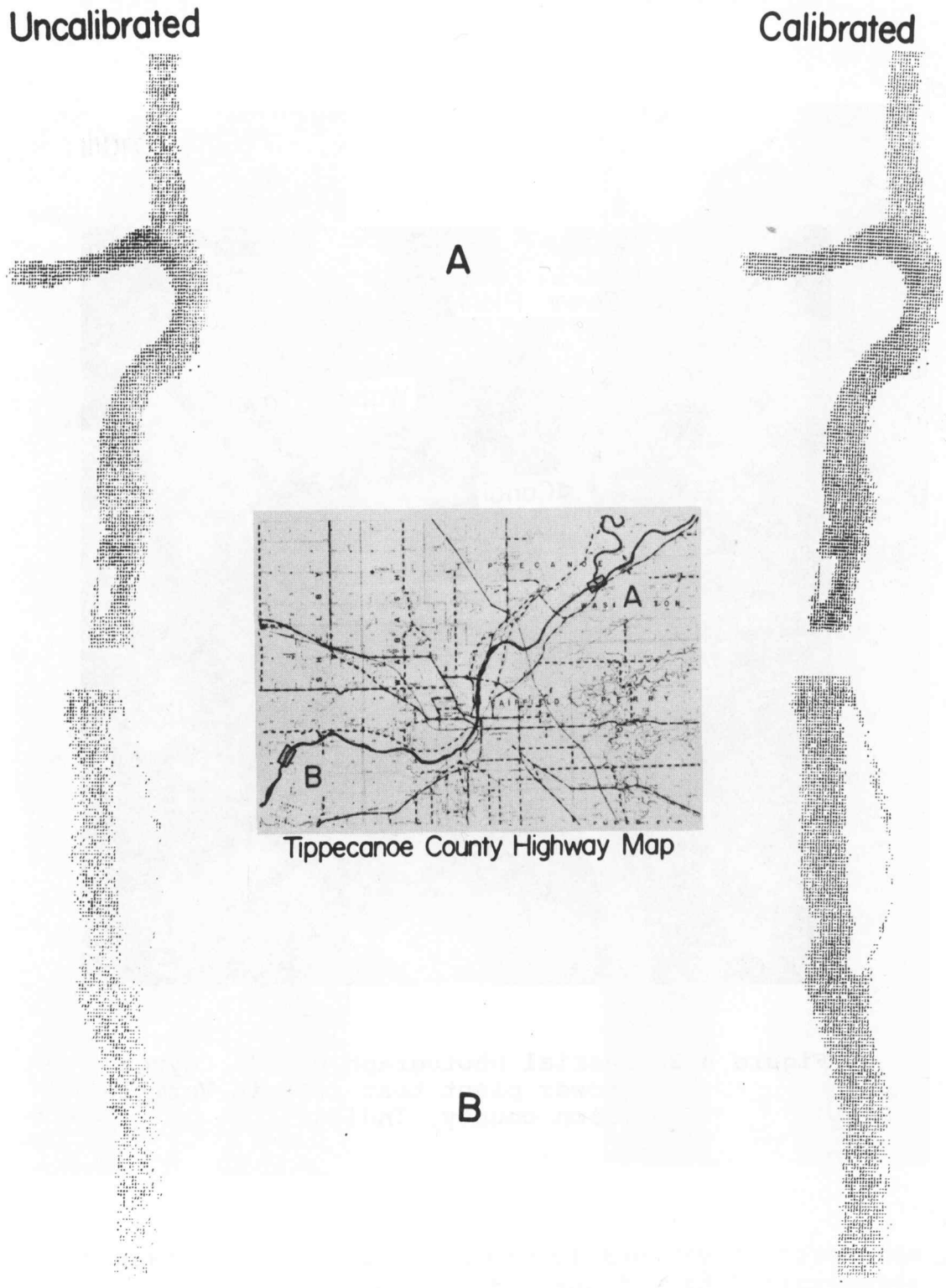
Uncalibrated
Calibrated
A
B
A
B
Tippecanoe County Highway Map

Figure 4.2.

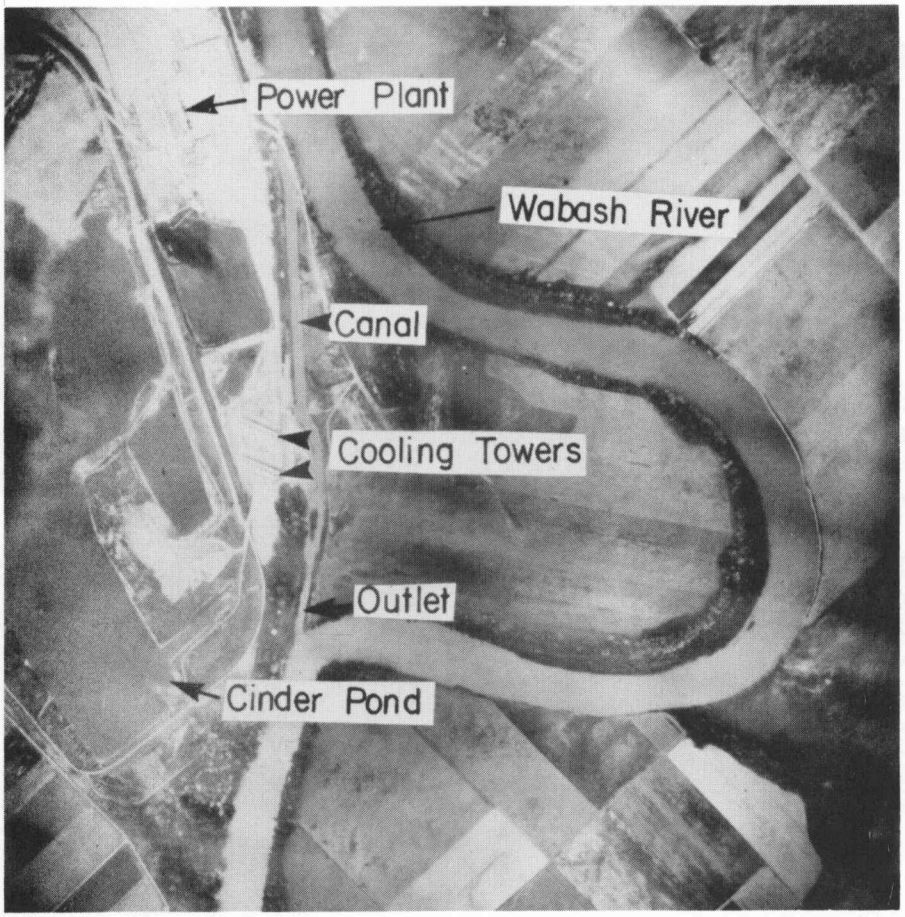

Figure 4.3. Aerial photograph of the Cayuga power plant test site in Vermillion county, Indiana.

4.5-5.5 μm

8.0-13.5 μm

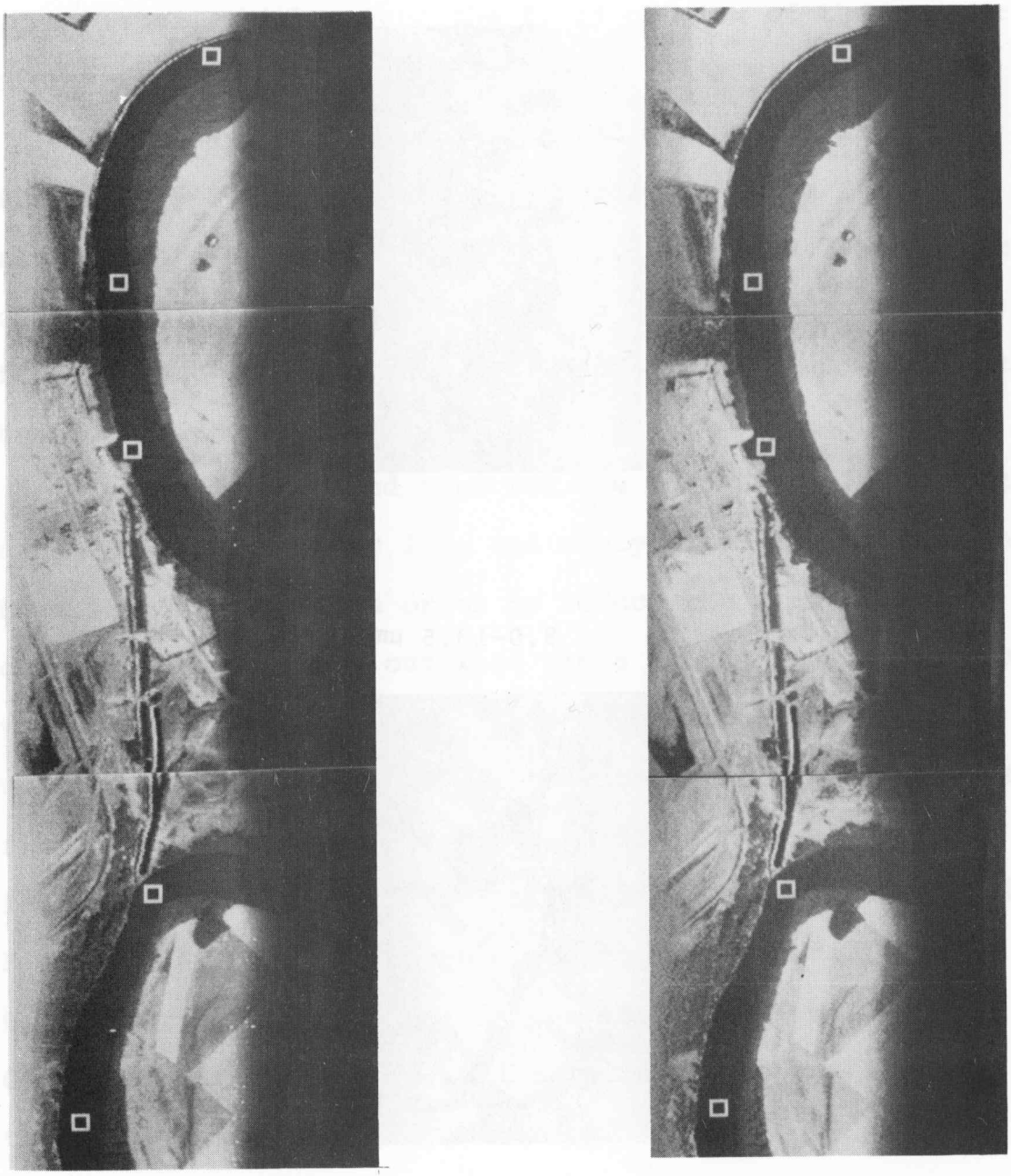

Figure 4.4. Thermal imagery of the Cayuga test site for the 4.5-5.5 and 8.0-13.5 micrometer spectral bands, from 600m. (2000 ft.) altitude, and displayed on the LARS digital display unit.

4.5-5.5 μm

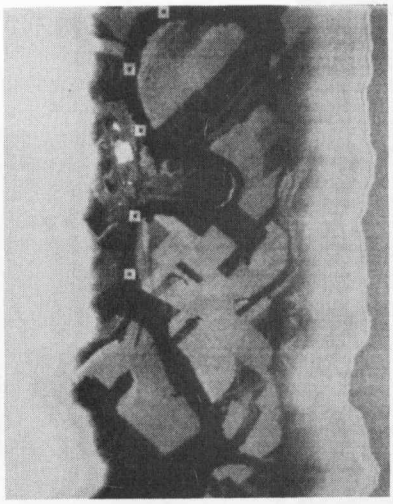

8.0-13.5 μm

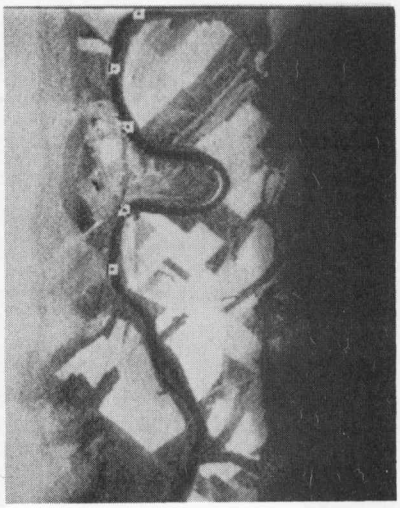

Figure 4.5. Thermal imagery of the Cayuga test site for the 4.5-5.5 and 8.0-13.5 micrometer spectral bands, from 3040m. (10,000 ft.) altitude, and displayed on the LARS digital display unit.

light and dark tone bands appearing on both sides of the thermal imagery. They are caused by the reference temperature-plates, which reduce the field of view of the scanner mirror from the original 80° to only 37° FOV.

Figure 4.6 shows the calibrated grayscale printouts for the 4.5-5.5 and 8.0-13.5 μm bands and for a flight altitude of 608 meters (2,000 feet). Figure 4.7 shows the calibrated pictorial printout for a 3,040 meters (10,000 feet) flight and for the 4.5-5.5 and 8.0-13.5 μm wavelength bands.

It should be noted that for the 608 meter (2,000 foot) data, only every other line and every other column of data have been displayed in order to reduce the size of the computer output. The outlined areas in the river illustrate the locations where kinetic (ground control) temperatures were measured. Each one of the symbols that delineate the river represent a certain range of temperatures, as indicated on the top of the printouts. The symbols used in Figures 4.6 and 4.7 were selected to indicate different temperatures as variations in grayscale tonal values. Cooler areas appear dark, while warmer areas are illustrated by "light tone" symbols.

Several resolution elements of calibrated data were averaged, corresponding to locations in the river where ground measurements were made. The areas where radiant temperatures were averaged are outlined in Figures 4.6 and 4.7.

608 meters
(2,000 feet)

4.5-5.5 µm

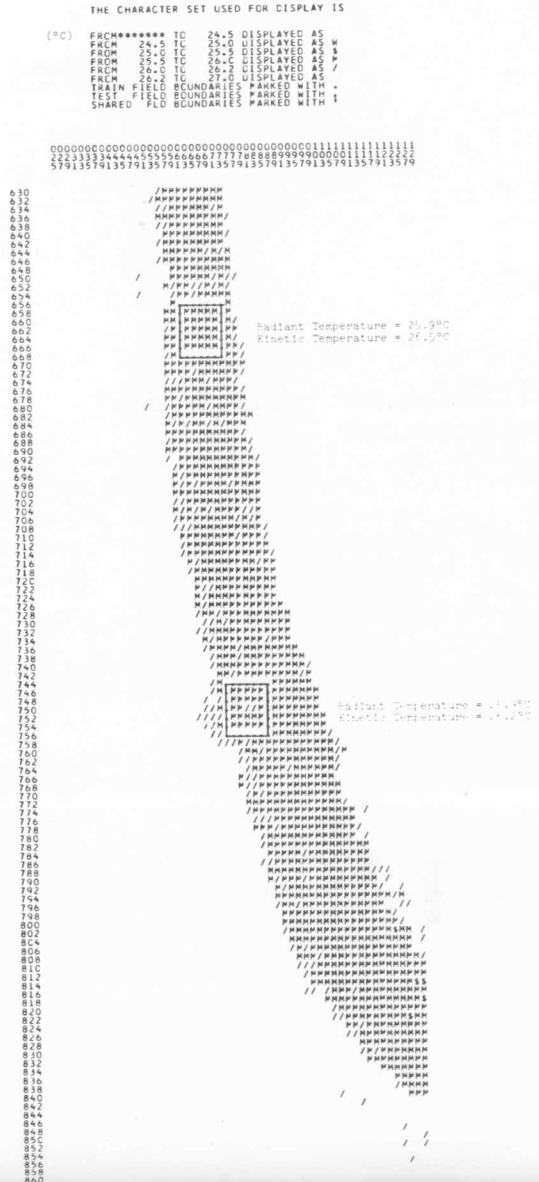

8.0-13.5 µm

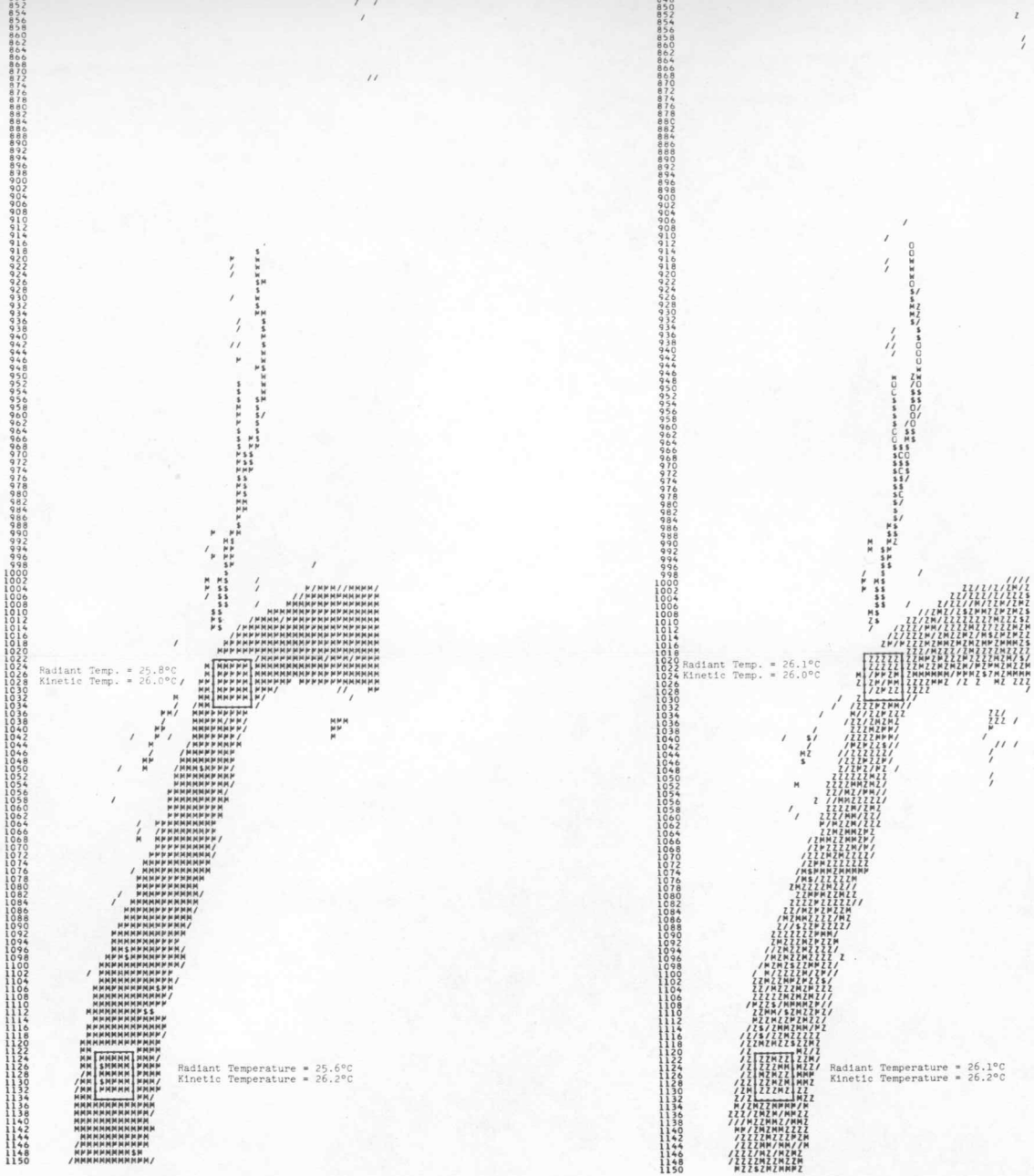

Figure 4.6. Temperature Maps of a Portion of the Wabash River near Cayuga, Indiana.

3,040 meters
(10,000 feet)

4.5-5.5 µm

THE CHARACTER SET USED FOR DISPLAY IS

(°C) FROM******* TO 18.5 DISPLAYED AS
FROM 18.5 TO 19.0 DISPLAYED AS M
FROM 19.0 TO 19.5 DISPLAYED AS X
FROM 19.5 TO 22.0 DISPLAYED AS .
TRAIN FIELD BOUNDARIES MARKED WITH .
TEST FIELD BOUNDARIES MARKED WITH ;
SHARED FLD BOUNDARIES MARKED WITH :

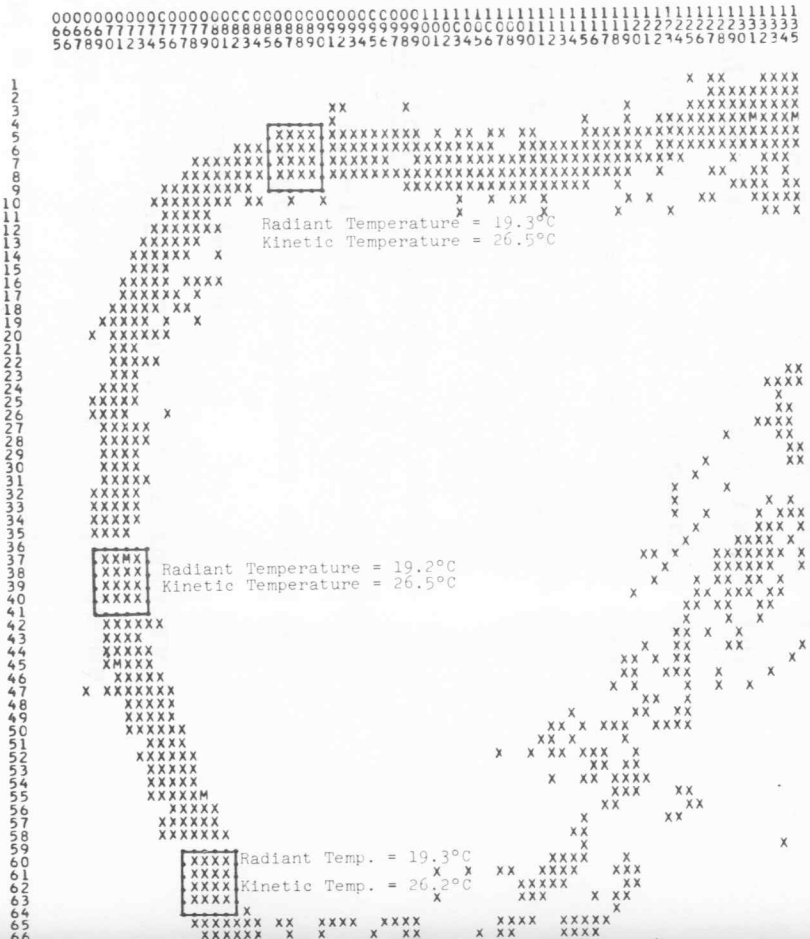

8.0-13.5 µm

THE CHARACTER SET USED FOR DISPLAY IS

(°C) FROM******* TO 23.3 DISPLAYED AS
FROM 23.3 TO 24.0 DISPLAYED AS M
FROM 24.0 TO 24.5 DISPLAYED AS X
FROM 24.5 TO 25.2 DISPLAYED AS Z
FROM 25.2 TO 30.0 DISPLAYED AS
TRAIN FIELD BOUNDARIES MARKED WITH .
TEST FIELD BOUNDARIES MARKED WITH ;
SHARED FLD BOUNDARIES MARKED WITH :

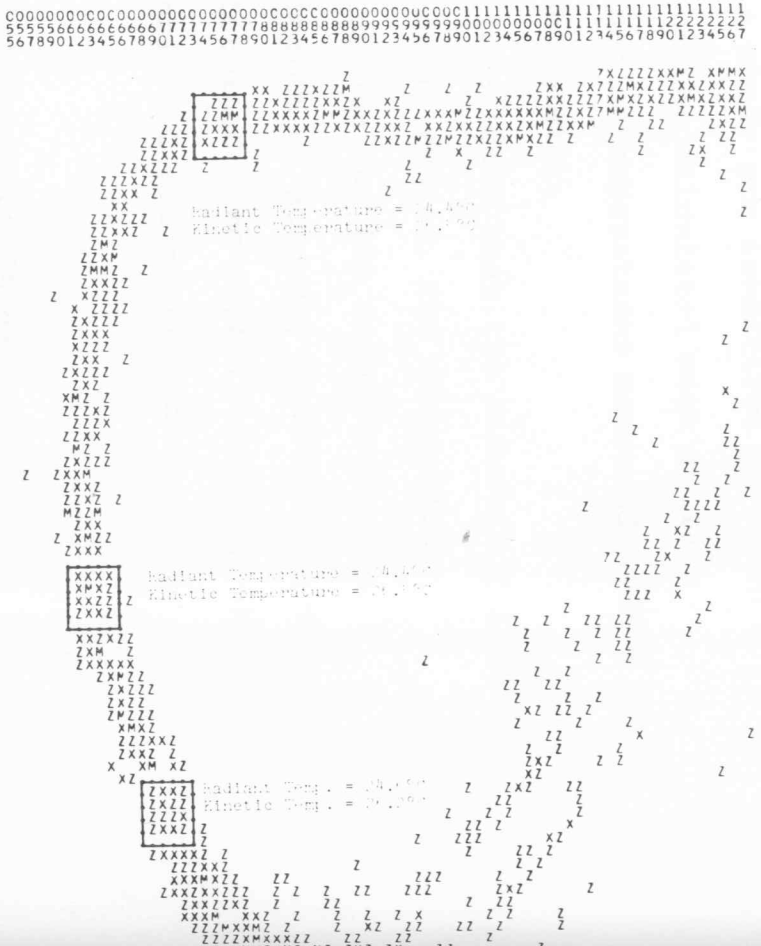

Figure 4.7. Temperature Maps of a Portion of the Wabash River near Cayuga, Indiana.

The results of this study are summarized in Table 4.2. This table indicates both the calculated mean radiant temperatures and the kinetic temperatures measured with a conventional contact thermometer.

From Table 4.2 it is evident that the aircraft flight altitude, or, more correctly stated, the atmospheric pathlength between the sensor and the target, plays an important role on the degree of accuracy with which radiant temperatures may be determined from airborne scanner data. The results shown in Table 4.2 are discussed in the following section.

Optimum Emissive IR Spectral Band for Water Surface Temperature Mapping

The evaluation of the advantages and disadvantages offered by the 4.5-5.5 and 8.0-14.0 μm spectral bands for thermal mapping of earth surface features, in particular for mapping thermal patterns in water bodies, may be done from an image oriented point of view or from a numerical oriented standpoint.

Image Oriented Evaluation. Two types of thermal imagery for the 4.5-5.5 and 8.0-14.0 μm bands have been analyzed, the CRT (cathode ray tube) continuous strip and the LARS Digital Display thermal imagery.

The author has analyzed several CRT thermal imagery sets of 4.5-5.5 and 8.0-13.5 μm data, and it always seems to be the case that the 8.0-13.5 μm band yields more

Table 4.2. Effects of altitude and wavelength band selection on remotely measured temperatures.

Measurement Site	Radiant Temperatures[1] (°C) 3,040 m. Alt. (10,000 Ft. Alt.) 4.5-5.5 μm	3,040 m. Alt. (10,000 Ft. Alt.) 8.0-13.5 μm	608 m. Alt. (2,000 Ft. Alt.) 4.5-5.5 μm	608 m. Alt. (2,000 Ft. Alt.) 8.0-13.5 μm	Kinetic Temp.[2] (°C) (Contact Thermometer)
1st River Bend	19.3	24.6	25.8	26.2	26.5
Above Intake	19.2	24.4	25.9	26.2	26.5
Intake	19.3	24.6	25.9	26.1	26.2
Outlet	19.2	24.4	25.8	26.1	26.0
1/2 Mile Below	19.3	24.4	25.6	26.1	26.2

[1] The Standard Deviation for the Radiant Temperatures is ± 0.2° C

[2] All the Ground Measurements of Temperatures Listed Above were Conducted Within Half an Hour from the Time the Aircraft Passed Overhead.

information on the thermal characteristics of water bodies than does the 4.5-5.5 μm band. In the 8.0-13.5 μm data, all water bodies (even very small areas) are easy to locate on the imagery because of their dark (black) appearance, as compared to the adjacent soils and vegetation that are shown as a series of gray and light tones. In the 4.5-5.5 μm data, water bodies usually appear as gray features that can easily be confused with other types of ground cover. However, the 4.5-5.5 μm band seems to be more useful than the 8.0-13.5 μm band for thermal studies of warm ground targets, such as bare soils. The cathod ray tube imagery used for this study was taken at 13:00 EST, that is, daytime data. Night time thermal data has also been qualitatively analyzed. The result of the analysis also shows that the 8.0-13.5 μm band provides the researcher with better contrasts between ground features than does the 4.5-5.5 μm imagery.

Analysis of the LARS Digital Display thermal IR imagery (Figures 4.4 and 4.5) shows that the data recorded in the 8.0-13.5 μm band seems to be more sensitive to small temperature differences than the 4.5-5.5 μm data. Also the thermal infrared imagery collected at 3,040 meters (10,000 feet) and recorded on the 8.0-13.5 μm spectral band appears to be more useful than the 4.5-5.5 μm imagery for descriminating water bodies (streams) from the adjacent vegetation.

At this point, it is noteworthy to point out that the thermal response of water bodies shows diurnal changes in the thermal infrared imagery. Daytime thermal imagery shows water as dark (cooler) areas as compared to the surrounding soils and vegetation which appear as light-toned (warmer) areas. On the other hand, nightime thermal infrared imagery shows a reversal in relative response. Water appears light in tone (warmer) as compared to the darker tones (cooler) associated with adjacent soils and vegetations.

Numerical-Oriented Evaluation. It should also be noted that the atmospheric effects influence to a greater extent, the remote determinations of temperature when using the 4.5-5.5 rather than the 8.0-13.5 μm waveband. As shown in Table 4.2, water surface temperatures may be accurately determined in the 8.0-13.5 μm band within 0.2 of a degree Centigrade for an altitude of 608 meters (2,000 feet). However, when going from a 608 meter (2,000 foot) to a 3,040 meter (10,000 foot) flight, the radiant temperatures, as determined by the 8.0-13.5 μm band, appear to be lower by approximately 2° C. Moreover, the atmospheric effects are so pronounced in the 4.5-5.5 μm band that the radiant temperatures as measured through this spectral band are approximately 7° C lower than the surface control temperatures for a flight altitude of 3,040 meters (10,000 feet) above terrain.

The major reason why radiant temperatures usually appear to be lower than kinetic temperatures is that the so called "atmospheric windows" are not completely transparent to thermal infrared radiation. Figure 2.2 in Chapter II illustrates the transmittance characteristics of the atmosphere in the 4.5-5.5 and 8.0-13.5 μm wavelength bands, for a 304 meter (1,000 foot) airpath at sea level. From this figure it is obvious that the 4.5-5.5 μm atmospheric window is far less transparent than the 8.0-13.5 μm window. In addition, the "non-linearity effect" discussed in Chapter III also affects the accuracy with which radiant temperatures can be determined by introducing errors of the order of several tenths of a degree Centigrade. These errors, in fact, always tend to produce lower radiant temperatures than expected.

In addition to the above effects, the emissivity of natural materials is generally lower in the 4.5-5.5 μm band than in the 8.0-13.5 μm band. For instance, the average emissivity of soils and vegetation in the 4.5-5.5 μm region are from 5 to 10% lower than in the 8.0-13.5 μm band (Kronstein, 1955). Likewise, the emissivity of water in the 4.5-5.5 μm spectral band is lower than in the 8.0-13.5 μm band as reported by Wolfe (1965)*.

---

*Viskanta and Toor (1972) have shown that the absorption of water in the 4.5-5.5 μm portion of the spectrum is smaller than it is in the 8.0-10.0 μm region. Since Kirchhoff's law is valid for water (practically a perfect radiator in the thermal IR), it can be deduced that water has a smaller emissivity in the 4.5-5.5 than in the 8.0-10.0 μm band.

Finally, for typical terrestrial temperatures, the amount of radiant energy available for remote sensing of temperatures in the 4.5-5.5 μm band is only 3% as compared with 62% in the 8.0-13.5 μm waveband. The small quantity of available energy requires a substantial amplification of the signal through which considerable noise might be introduced by the system. This will decrease the S/N (signal to noise ratio) and therefore degrade the quality of the data.

Scan Line Averaging

Utilization of additional information contained in over-scanned thermal infrared data by means of the scan line averaging procedure has proved to be a desirable processing option for accurate measurement of water temperatures. The results of applying the scan line averaging to thermal IR data for temperature mapping of the Wabash River near Lafayette, Indiana are shown and discussed in the following section.

Smoothing Effects of LINAVE on Pictorial Printouts

Figures 4.8 and 4.9 show the results of averaging 8 overlapping scan lines over the Wabash and Tippecanoe River junction. These two figures illustrate the obvious smoothing effect that line averaging has on thermal scanner data. Figure 4.8 shows a scan line graph ($GLINE) across

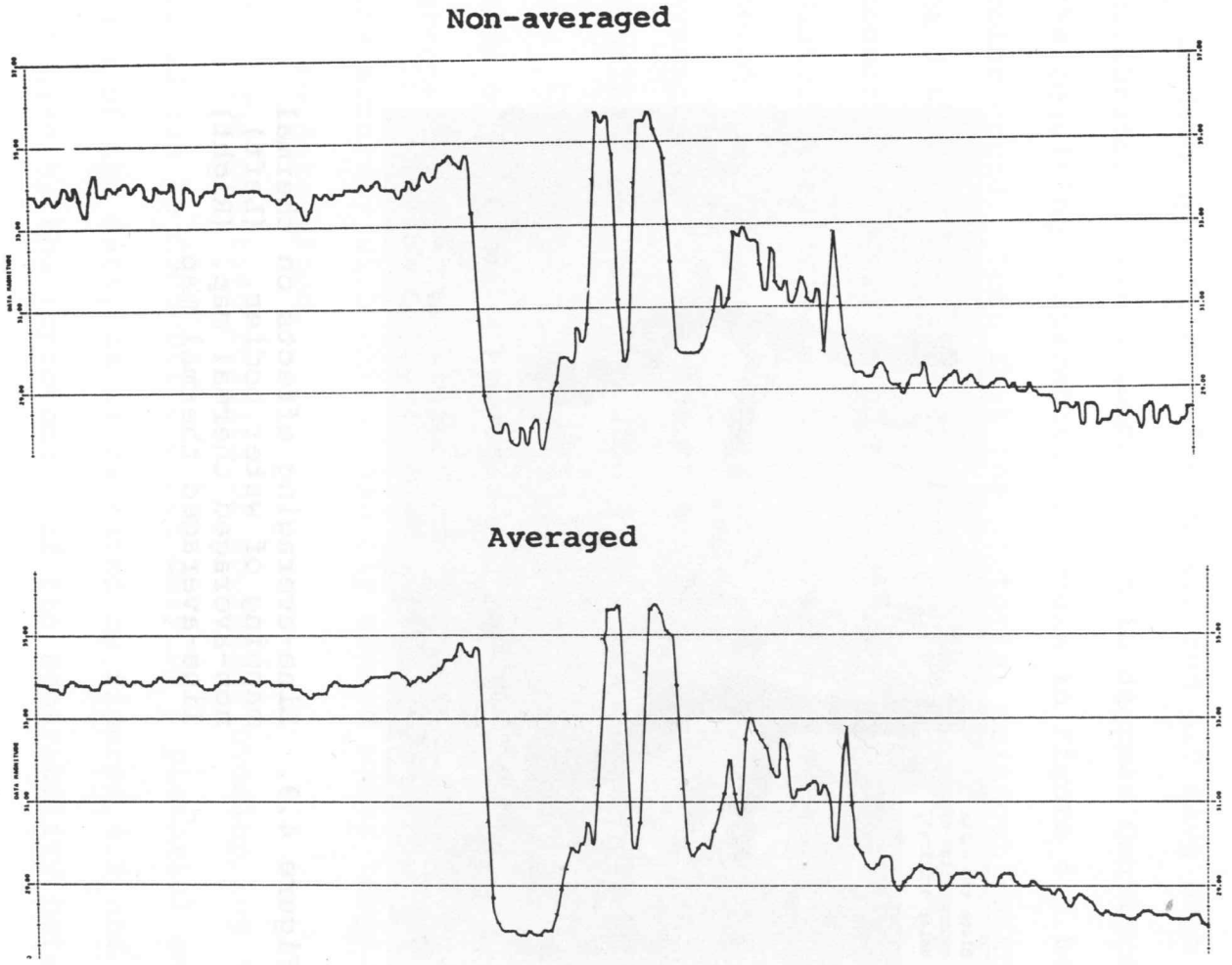

Figure 4.8. Graph of a scan line before and after scan-line averaging.

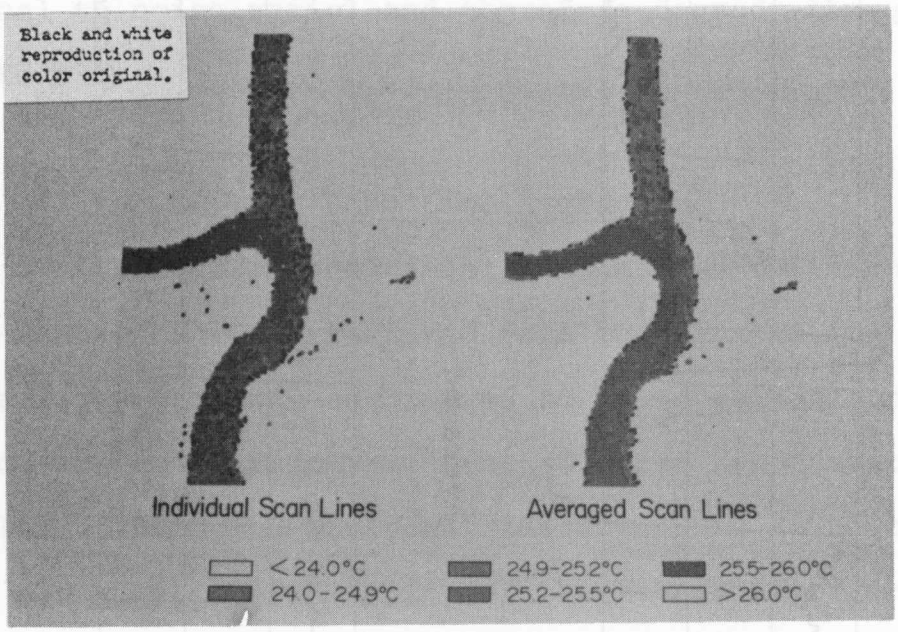

Figure 4.9. Line-averaging effects on thermal mapping of water bodies. (Left) non-averaged thermal map. (Right) line-averaged thermal map.

the river junction before and after applying the scan line averaging processor. Figure 4.9 illustrates the effects of line averaging on a computer-generated pictorial printout ($PIC) of the same area, the river junction. The thermal data displayed in both Figure 4.8 and 4.9 have been calibrated to yield temperatures in degrees Centigrade. The resulting temperature intervals in Figure 4.9 have been color coded. Note that the pictorial printout on the right hand side of Figure 4.9, which is the result of averaging 8 consecutive overlapping scan lines, shows a more homogeneous distribution of water temperatures. It should also be noted that there is no apparent spatial distortion in the averaged data, as compared to the non-averaged data displayed on the left hand side of Figure 4.9.

Comparison of the mean radiant temperatures of the two sets of data (line averaged and non-averaged data) demonstrate that the line averaging operation does not change the accuracy with which remotely sensed water temperatures can be determined.

The positive results of averaging overlapping scan lines can be demonstrated not only by a pictorial amelioration of the data, as illustrated by Figures 4.8 and 4.9, but also by the improvement of the separability between spectral classes.

Separability Effects of LINAVE on Spectral Classes

The results of calculating the divergence between pairs of three different spectral classes of water for (a) non-averaged data, (b) average of 4 lines skipping 4, and (c) for average of all 8 available overlapping scan lines are summurized in Table 4.3.

Table 4.3. $DIVERG ($SEP) values for non-averaged and line-averaged scanner data.

	Non-averaged Data	Average of 4 Lines	Average of 8 Lines
D(MIN)[1]	194	513	620
D(AVE)[2]	370	804	991

[1] D(MIN) is the minimum divergence found between any pair of spectral classes.

[2] D(AVE) is the average divergence calculated for all pairs of spectral classes.

Note how the average divergence value for line averaged data are approximately 2.8 times larger than the corresponding values for non-averaged data. In other words, the divergence between pairs of spectral classes has increased from a value of 370 for non-averaged data to a value of 991 for line averaged data. This is precisely the result predicted by statistical considerations.

One of the fundamental theorems of statistical analysis concerning the sample means and sample variances of a number n of random variables states that, assuming

that the n random variables have the same mean and variance or that,

$$E\{x_i\} = M \qquad \text{Eq. 4.1}$$

$$\sigma^2_{x_i} = \sigma^2 \qquad \text{Eq. 4.2}$$

where n = random variables

$i = 1, 2, 3, \ldots\ldots, n$

it can be shown (Papoulis, 1965) that,

$$E\{\bar{x}_i\} = M \qquad \text{Eq. 4.3}$$

$$\sigma^2_{\bar{x}_i} = \frac{\sigma^2}{n} \qquad \text{Eq. 4.4.a}$$

or

$$\sigma_{\bar{x}_i} = \frac{\sigma}{\sqrt{n}} \qquad \text{Eq. 4.4.b}$$

where, $\bar{x}_i$ is the average of the n random variables.

In other words, the above results proved that the mean of the average of n random variables, or more specifically n overlapping scan lines, is the same as the mean of the individual variables (scan lines) as shown by Equations 4.1 and 4.3. However, the variance, σ^2, of the average of n variables has decreased n times. The standard deviation, σ, has decreased by a factor of $\sqrt{n}$, as shown by Equations 4.2, 4.4.a and 4.4.b.

Because in this particular case it is safe to assume that adjacent overlapping scan lines have approximately the

same mean and standard deviation and that their noise is uncorrelated, random noise, the above statistical theorem may be adequately used to describe the behavior of the means and standard deviation of averaged scan lines.

Therefore, the expected means of non-averaged and 8-line averaged data should be the same. However, the standard deviation for 8-line averaged data should be $\sqrt{8}$ times smaller than the standard deviation for non-averaged data, that is, smaller by a factor of approximately 2.8.

Furthermore, if the separability between spectral classes of non-averaged data is expressed (in simple terms) by the following approximate relationship:

$$D_0 \propto \frac{d_{1-2}}{\sigma_1 + \sigma_2} \qquad \text{Eq. 4.5}$$

where, D_0 = divergence value for non-averaged data

d_{1-2} = distance between the means of class 1 and 2

σ_1 and σ_2 = the standard deviations of class 1 and 2,

the corresponding separability ($DIVERG values) for the 8-line averaged data may be represented by the following approximate expression:

$$D_8 \propto \frac{d_{1-2}}{\frac{\sigma_1}{\sqrt{8}} + \frac{\sigma_2}{\sqrt{8}}} = \frac{d_{1-2}}{\sigma_1 + \sigma_2} (\sqrt{8}) \qquad \text{Eq. 4.6}$$

which means that the separability between spectral classes for 8-line averaged data (D_8) would be larger than the

divergence between the same classes in non-averaged data by a factor of $\sqrt{8}$ or approximately 2.8. This result coincides exactly with the empirical results shown in Table 4.3.

Recent work done by Swain (1973) predicts that for one through six spectral features (wavelength bands), if the divergence value between spectral classes is increased from approximately 300 to 900 (relative units of transformed divergence), the expected percent correct classification would increase approximately 10 percent. (See Figure 3.5). This seems to be the case with the results shown in Table 4.3.

Layered Classifer

The need for a data processing program that would calibrate thermal scanner data of water only, is shown in Figure 4.10. Note that the temperature map or pictorial printout obtained by means of the existing LARSYS software, (left hand side of Figure 4.10) shows that several other ground cover types adjacent to the rivers (Wabash and Tippecanoe) appear to be at the same radiant temperatures as the water. This phenomenom may be explained by the fact that at certain times of the day and during certain seasons, for example during early afternoons of the summer months, the kinetic temperatures of soils and vegetation are higher than the kinetic temperatures of water in rivers and reservoirs. However, the emissivity of water is

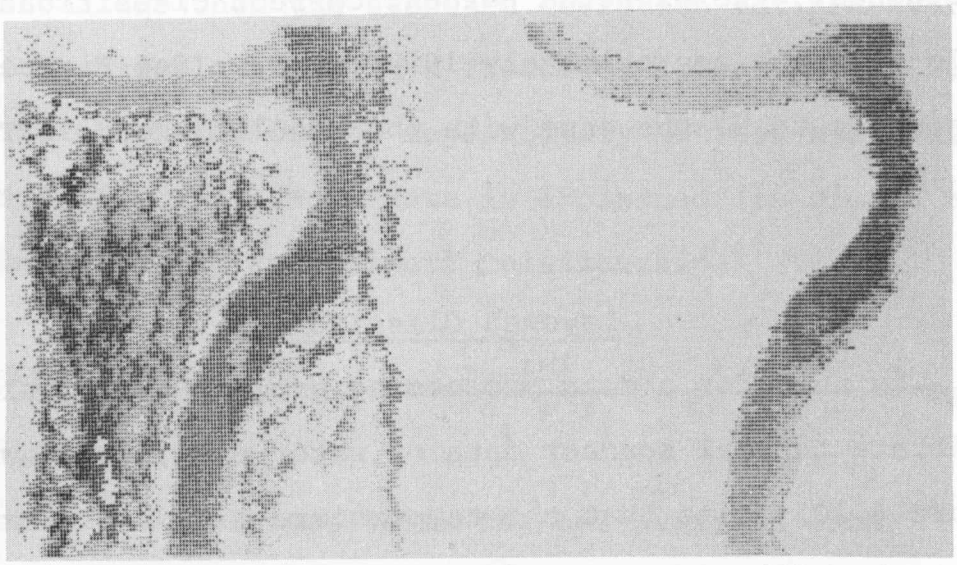

Figure 4.10. Thermal map and classification map of the River Junction near Lafayette, Indiana. Data collected from an altitude of 608 meters (2,000 feet) on August 13th, 1970.

higher than the emissivities of either vegetation or soils, so the radiant temperatures, which are a function of both the kinetic temperature and the emissivity of the materials, appear to be the same for the three types of ground cover even though their actual (kinetic) temperatures may be different. This behavior should be expected because of a compensation effect between emissivity and kinetic temperature.

As illustrated in Figure 4.10, utilization of the existing "standard" LARSYS software does not permit the acquisition of a temperature map of water only. Nevertheless, it is possible to do so by means of a special layered classifier which first identifies only areas of surface water, using one or more spectral features (wavelength bands) in the reflective portion of the spectrum, especially in the near infrared,* then calibrates the thermal data of only these surface water areas. Thus, a temperature map of water only is obtained. This capability is demonstrated by Figure 4.11, where the thermal characteristics of the Wabash river near Cayuga, Indiana are displayed. Figure 4.12 illustrated a method of displaying the radiant temperatures corresponding to the test areas

---

*The 0.8-1.0 μm band appears to be the best spectral feature for descriminating water from every other type of ground cover.

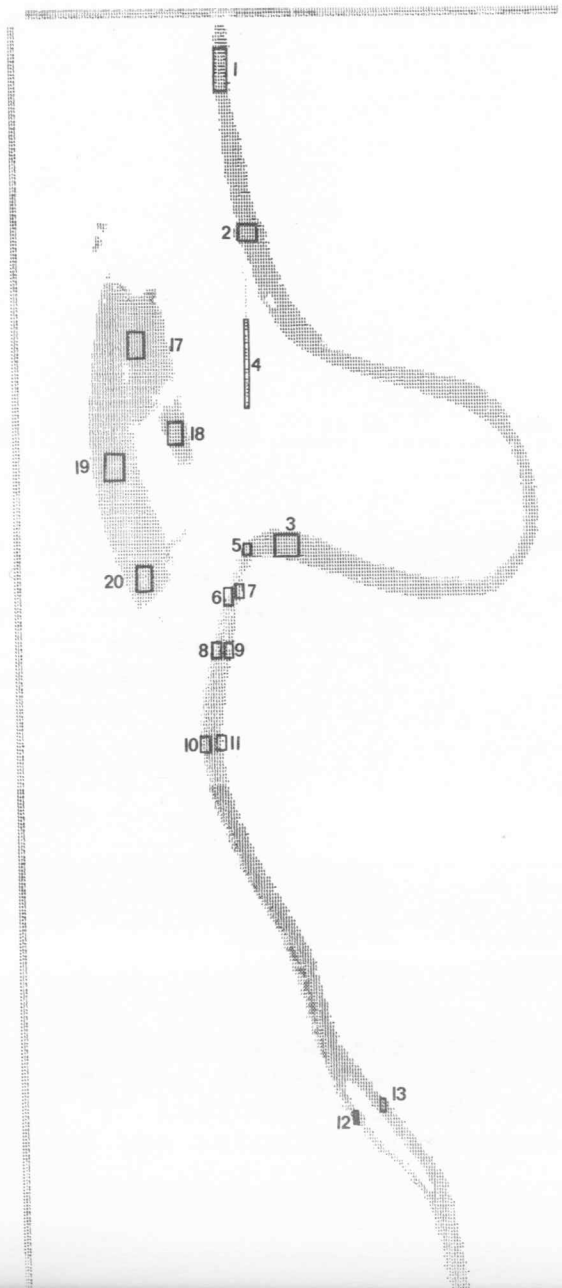
1
2
17
4
18
19
3
5
20
6
7
8
9
10
11
13
12

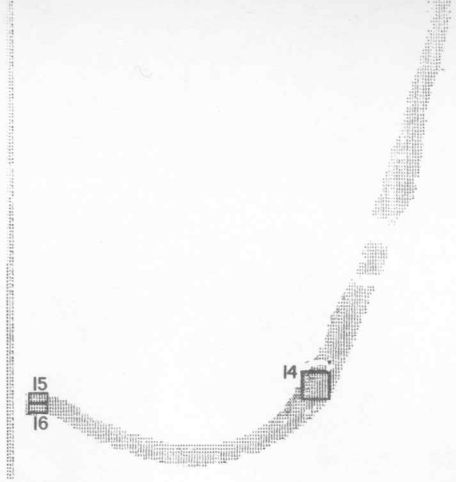

Test Areas		Mean Radiant Temp. (°C)
Above Intake	(1)	20.6
	(2)	21.0
	(3)	20.9
Canal	(4)	25.8
Below Outlet	(5)	24.9
	(6)	24.1 West Bank
	(7)	21.1 East Bank
	(8)	24.2 West Bank
	(9)	21.1 East Bank
	(10)	23.6 West Bank
	(11)	20.6 East Bank
	(12)	22.7 West Bank
	(13)	21.3 East Bank
	(14)	22.5
	(15)	21.3
	(16)	20.8
Cinder Pond	(17)	22.5
	(18)	20.8
	(19)	22.5
	(20)	22.7

Figure 4.11. Thermal map of water only, obtained from the "layered classifier." Data collected in the 9.3-11.7 μm band from an altitude of 1,500 meters (5,000 ft.).

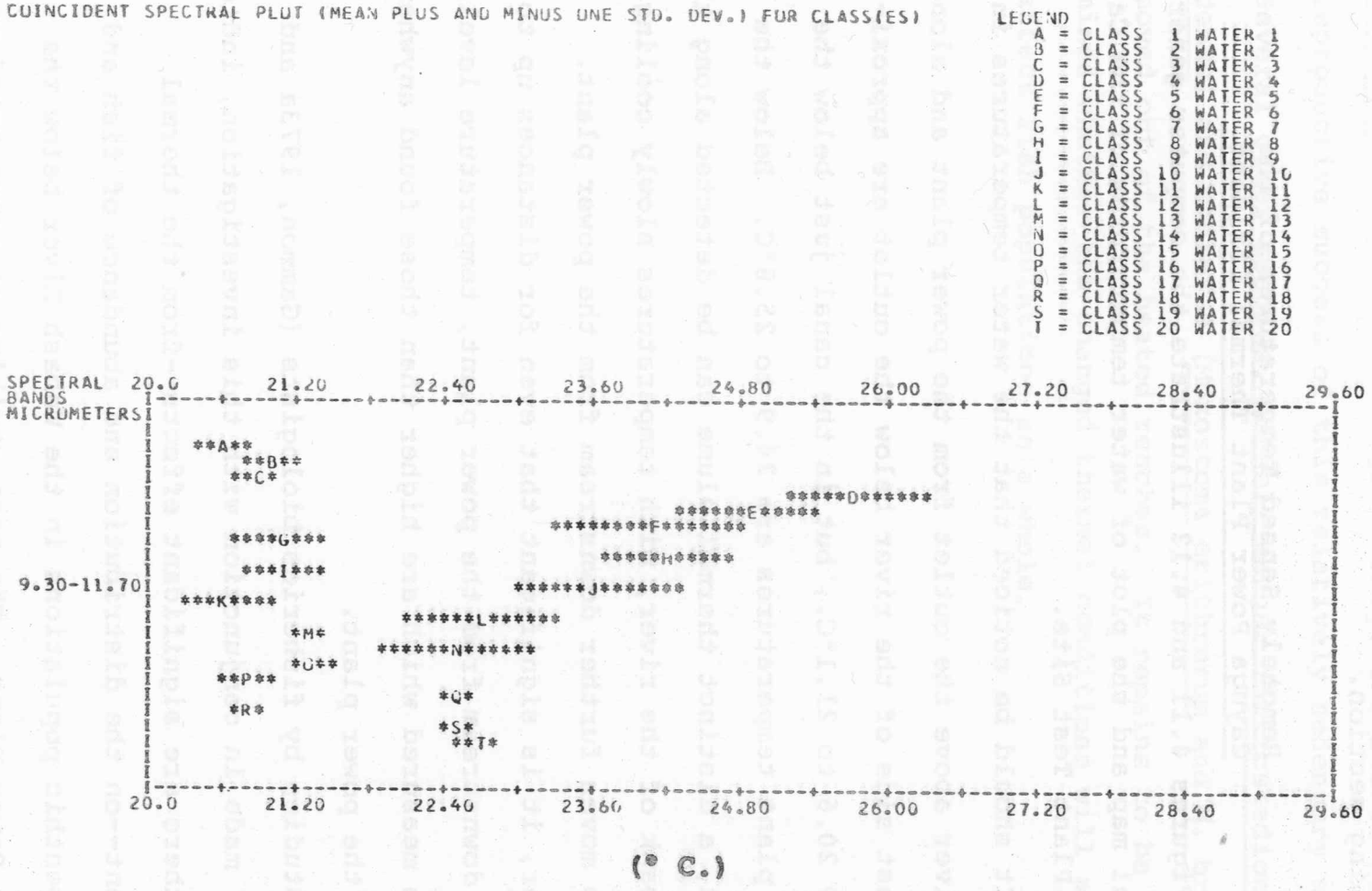

Figure 4.12. Plot of radiant temperatures corresponding to the areas outlined in Figure 4.11. The characters "A" through "T" indicate the mean temperatures and the length of the asterisks represent $\pm$ 1 σ .

outlined in Figure 4.11. The significance of the results shown in these two illustrations is discussed in the following section.

Remotely Sensed Temperatures of the Cayuga Power Plant Thermal Effluent

Figures 4.11 and 4.12 illustrate the computer generated thermal map and the plot of water temperatures of the Cayuga Power Plant Test Site.

It should be noticed that the water temperatures in the river above the outlet from the power plant and along the east side of the river below the outlet are approximately 20.6 to 21.1°C., but in the canal just below the power plant temperatures are 24.9 to 25.8°C. Below the outlet, a distinct thermal plume can be detected along the west bank of the river, with temperatures slowly cooling as one moves further downstream from the power plant. However, it is significant that even for distances up to 6 km. downstream from the power plant, temperature levels can be measured which are higher than those found anywhere above the power plant.

Studies by fisheries biologists (Gammon, 1973a and 1973b) made in conjunction with this investigation, indicate that there are significant effects--from the thermal effluent--on the distribution and abundance of fish and microbenthic populations in the Wabash River below the Cayuga Power Plant. The most striking response noted was

the increase in density of young flathead catfish (Pilodictis Olivaris) in the heated regions only, the result of increased reproductive success of this relatively sedentary species. Several other species, notably sauger (Stizostedion canadense) and redhorse (Moxostoma erithrurum and M. breviceps) moved out of the heated reaches. It remains to be determined whether the changed thermal conditions will adversely affect fish populations as a whole.

CHAPTER V

SUMMARY, CONCLUSIONS AND RECOMMENDATIONS

Summary and Conclusions

The Internal Calibration Technique

The internal calibration technique and automatic data processing of remotely sensed thermal infrared radiation provide a suitable means for accurately and reliably determining the temperature of surface water from aircraft altitudes. It should be emphasized that this technique does not require surface measurements of water temperatures for purposes of achieving absolute calibration of the data.

The assumption that the amount of radiation emitted from a blackbody over selected wavelength bands (4.5-5.5, 8.0-13.5 and 9.3-11.7 μm) is linearly related to its kinetic temperature is valid, provided the range of temperatures being sensed is not greater than approximately 10° C. However, the validity of the "linearity assumption" may be extended for larger temperature ranges if the wavelength band being used falls near the peak of the blackbody

maximum emission, such as, the 8.0-13.5 and 9.3-11.7 μm bands for temperatures close to 20° C. Furthermore, if more accurate temperatures are required, the linear calibration function of the LARSYS program package may be substituted by a non-linear polynomial function that better approximates the relationship between emitted energy and temperature.

Effects of Flight Altitude and Wavelength Band Selection on Remotely Sensed Temperatures

Qualitative and quantitative analysis of thermal infrared data collected at different altitudes and employing different portions of the spectrum has indicated that choice of the spectral band and altitude of flight are critical factors influencing the accuracy with which remotely sensed temperatures can be determined.

Of the two available thermal infrared atmospheric windows (3.0-5.5 and 8.0-14.0 μm), the 8.0-14.0 μm band offers the best potential for accurate determinations of water surface temperatures from remote locations.

Water surface temperatures may be determined from remotely sensed thermal IR data using the 8.0-13.5 μm band with an accuracy of 0.2° C from an altitude of approximately 900 meters (3,000 feet). This same accuracy may be achieved when using the 9.3-11.7 μm band for altitudes of up to 3,000 meters (10,000 feet). However, when using the 4.5-5.5 μm band for these same two altitudes the radiant

temperatures as determined from remotely sensed radiation may be biased by as much as 7° C. These errors are primarily caused by atmospheric attenuation of the thermal radiation passing through the partially transparent atmospheric windows.

Other factors that might significantly influence the accuracy of remotely sensed temperatures are: (a) the "non-linearity" effect, (b) the differences in emissive behavior of natural materials as a function of wavelength, for example, the emissivity of natural cover types is usually lower in the 4.5-5.5 μm band than it is in the 8.0-13.5 μm band, and (c) the amount of energy available for remote sensing purposes in the 4.5-5.5 μm band is only 3% of the total as compared to 23% for the 9.3-11.7 μm band and 62% for the 8.0-13.5 μm band, at typical terrestrial temperatures. Therefore, taking into account all the factors that might affect radiant temperatures, the 8.0-14.0 μm region of the spectrum and especially the 9.3-11.7 μm band offer the best potential for accurate determinations of water surface temperatures from airborne thermal infrared data.

Scan-Line Averaging

In the preceeding chapter it has been demonstrated that the scan-line averaging of thermal scanner data improves the quality of the data from a pictorial point of view as well

as from a numerical standpoint. Figures 4.8 and 4.9 show (pictorially) the smoothing effect of line-averaging on thermal mapping of water bodies. Table 4.3 indicates also that utilization of the scan-line overlap redundancy increases considerably the separability between spectral classes, thus implying that scan-line averaged data would yield a higher percent correct recognition (classification). In short, the scan-line averaging technique is a desirable processing feature for multispectral scanner data enhancement, provided the right number of scan lines to be averaged and the optimum values for the weighting coefficients are selected.

In the present investigation, the optimum number of scan lines for averaging was found to be the total number of overlapping lines (8), and the weighting coefficients that yielded the best results of compromising the loss of spatial resolution and the gain in signal to noise ratio seem to be those that more heavily weight the center lines. The utilization of these averaging parameters has produced accurate water surface temperature measurements.

The Layered Classifier

The need for a pattern recognition algorithm to be used in conjunction with the internal calibration technique for absolute temperature mapping of water only was demonstrated in Chapter IV. The layered classifier offers

an adequate means to produce thermal maps of water only (Figure 4.11), particularly in situations involving several cover types that are at the same radiant temperature as the water bodies. Thus, the layered classifier has been shown to be a desirable feature to be implemented as a pre-calibration processor for operational thermal mapping of one cover type only.

Recommendations and Future Work

During the progress of this study it became apparent that further work is needed in other areas of thermal mapping of surface water using remotely sensed data. The author feels that additional research should be pursued in the following specific areas:

1. Study of atmospheric effects caused by differences in flight altitude on thermal infrared scanner data, especially for data collected in the 9.3-11.7 μm band. In addition, development of atmospheric-correction models are needed to account for these effects.
2. Implementation of the "Layered Classifier" into the LARS software package as a standard capability for thermal mapping of one cover type only. Further development of this program is needed to include an option that would permit the setting of temperature levels as desired by the researcher.

3. To study the effects of "scan-line averaging" on the percent correct recognition (classification) in order to determine if line-averaged data indeed improves the classification accuracy as it would be expected from the increased spectral class separability (divergence) shown in this research.

It is also recognized that the temperature of thermal effluent from power plants, which affect the ecological balance of surface waters, is not the sole water-quality parameter that can be determined and monitored from aircraft scanner data. As reported in Chapter III of this study, the existing scanner systems have the capability of gathering data in a wide range of spectral bands including the visible and near infrared wavelengths (reflective portion of the spectrum). The author believes that multispectral reflective scanner data can contribute a great quantity of useful information on water quality of streams and larger water bodies. Some important water-quality parameters, such as turbidity, may be directly identified from remotely sensed data. Concentrations of dissolved oxygen, B.O.D. (Biological Oxygen Demand) and pH might be inferred from remote detection (sensing) of algal concentrations. However, more research is needed to determine the feasibility of utilizing multispectral scanner systems and computer-aided data processing techniques for rapid and reliable analysis of water quality from remote platforms.

Specifically, a better understanding of the energy-matter interactions (for example, radiation depth-penetration and scattering by suspended solids) is needed.

Finally, as the overall objective of this investigation was to develop further and to test the capability of using computer-processed remotely sensed data for thermal mapping of surface water on an operational basis the author would recommend the procedural sequence shown in Figure 5.1. Through the application of this sequence, accurate temperature maps can be obtained on an operational basis.

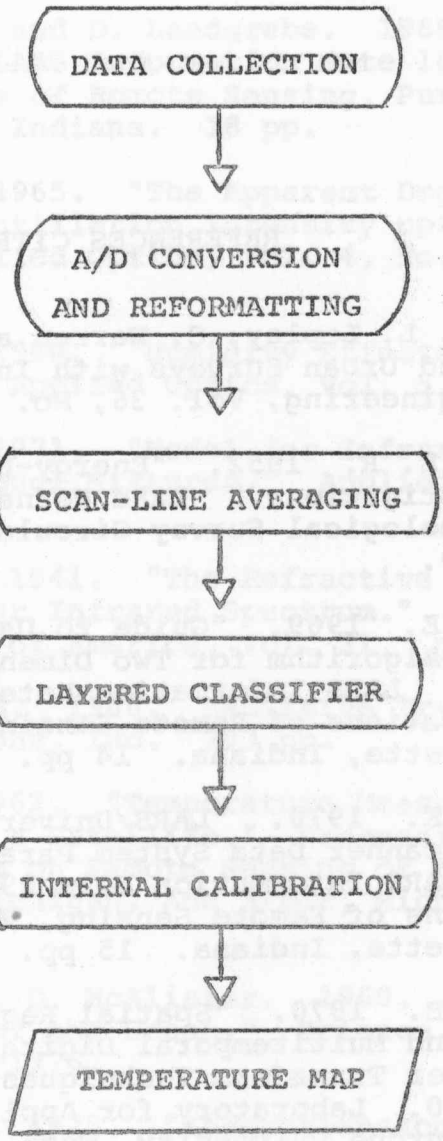

Figure 5.1. Recommended procedure-sequence for operational thermal mapping.

REFERENCES CITED

1. Adams, W., L. Lepley, C. Warren and S. Chang. 1970. "Costal and Urban Surveys with Infrared." Photogrammetric Engineering, Vol. 36, No. 2. pp. 173-180.

2. Anderson, E. R. 1952. "Energy-Budget Studies in Water-Loss Investigations." Lake Hefner Studies Technical Report, Geological Survey Circular 229. Vol. 1. pp. 71-119.

3. Anuta, P. E. 1969. "Guide to Use of the Fast Fourier Transform Algorithm for Two Dimensional Imagery Correlation." LARS Information Note 121069. Laboratory for Applications of Remote Sensing, Purdue University, West Lafayette, Indiana. 14 pp.

4. Anuta, P. E. 1970. "LARS/University of Michigan Aircraft Scanner Data System Parameter Identification Study." LARS Information Note 091470. Laboratory for Applications of Remote Sensing, Purdue University, West Lafayette, Indiana. 15 pp.

5. Anuta, P. E. 1970. "Spatial Registration of Multispectral and Multitemporal Digital Imagery Using Fast Fourier Transform Techniques." LARS Information Note 052270. Laboratory for Applications of Remote Sensing, Purdue University, West Lafayette, Indiana. 33 pp.

6. Atwell, B. H., R. B. MacDonald and L. A. Bartolucci. 1971. "Thermal Mapping of Streams from Airborne Radiometric Scanning." Water Resources Bulletin, Vol. 7, No. 2, Urbana, Illinois. pp. 228-242.

7. Buettner, K. J. K., C. D. Kern and J. F. Cromin. "The Consequences of Terrestrial Surface Infrared Emissivity." Proceedings of the Third Symposium on Remote Sensing, University of Michigan, Ann Arbor, Michigan. pp. 549-561.

8. Buettner, K. J. K. and C. D. Kern. 1965. "The Determination of Infrared Emissivities of Terrestrial Surfaces." Journal of Geophysical Research, Vol. 70. pp. 1329-1337.

9. Cardillo, G. P. and D. Landgrebe. 1966. "On Pattern Recognition." LARS Information Note 101866. Laboratory for Applications of Remote Sensing, Purdue University, West Lafayette, Indiana. 18 pp.

10. Carlon, H. R. 1965. "The Apparent Dependence of Terrestrial Scintillation Intensity upon Atmospheric Humidity." Applied Optics, Vol. 4, No. 9. pp. 1089-1098.

11. Carlon, H. R. 1966. "Humidity Effects in the 8.0-13.0 μm IR Window." Applied Optics, Vol. 5, No. 5. p. 879.

12. Carlon, H. R. 1971. "Model for Infrared Emission of Water Vapor/Aerosol Mixtures." Applied Optics, Vol. 10, No. 10. pp.

13. Centeno V., M. 1941. "The Refractive Index of Liquid Water in the Near Infrared Spectrum." Journal of the Optical Society of America, Vol. 31. pp. 244-247.

14. Chandrasekhar, S. 1960. Radiative Transfer. New York: Dover Publications, Inc. 393 pp.

15. Ehler, D. E. 1962. "Temperature Measurements of Earth and Clouds from a Satellite." Proceedings of the Second Symposium on Remote Sensing of Environment, University of Michigan, Ann Arbor, Michigan. pp. 235-265.

16. Ewing, G. and E. D. McAlister. 1960. "On the Thermal Boundary Layer of the Ocean." Science, Vol. 131, No. 3409. pp. 1374-1376.

17. Falckenberg, G. 1928. "Absorptianskontanten Einiger Meteorologisch Wichtiger Köper für Infrarote Wellen." Meteorologische Z., 45. pp. 334-337.

18. Fleagle, R. G. and J. A. Bussinger. 1963. Atmospheric Physics. New York: Academic Press. 346 pp.

19. Friedman, J. D. 1968. "Thermal Anomalies and Geologic Features of the Mono Lake Area, California, as Revealed by Infrared Imagery." NASA Interagency Report, Technical Letter NASA-82. 84 pp.

20. Gammon, J. R. 1973a. "The Effects of Thermal Inputs on the Populations of Fish and Microinvertebrates in the Wabash River." Purdue University, Water Resources Research Center, Lafayette, Indiana, Technical Report No. 32 (In Press).

21. Gammon, J. R. 1973b. "The Response of Fish Populations in the Wabash River to Heated Effluents." Proceedings of the Third (3rd) National Symposium on Radioecology. (In Press).

22. Goldberg, I. L., L. Foshee, W. Lordberg, and C. E. Catoe. 1964. "Nimbus High Resolution Infrared Measurements." Proceedings of the Third Symposium on Remote Sensing of Environment, University of Michigan, Ann Arbor, Michigan. pp. 141-151.

23. Greaves, J. R. 1966. "Sea Surface Temperature Determination from TIROS Satellite Data." Proceedings of the Fourth Symposium on Remote Sensing of Environment, University of Michigan, Ann Arbor, Michigan. pp. 447-455.

24. Hasell, P. G., Jr. and L. M. Larsen. 1968. "Calibration of an Airborne Multispectral Optical Sensor." Technical Report Ecom-00013-137, Willow Run Laboratory, Ann Arbor, Michigan. 87 pp.

25. Hasse, L. 1963. "On the Cooling of the Sea Surface by Evaporation and Head Exchange." Tallus, Vol. 15, No. 4. pp. 363-366.

26. Heerema, C. E. and Graboske, H. C. 1959. "Interpretation of Infrared Images." Proceedings IRIS, IV, 4, pp. 393-403. (Referenced by Wolfe, W. L. 1965).

27. Hirsch, S. H. 1962. "Applications of Remote Sensing to Forest Fire Detection and Suppression." Proceedings of the Second Dymposium on Remote Sensing of Environment, University of Michigan, Ann Arbor, Michigan. pp. 295-308.

28. Hirsch, S. H. 1964. "Preliminary Experimental Results with Infrared Line Scanner for Forest Fire Surveillance." Proceedings of the Third Symposium on Remote Sensing of Environment, University of Michigan, Ann Arbor, Michigan. pp. 623-648.

29. Hirsch, S. H. 1968. "Project Fire-Scan--Summary of Five Years' Progress in Airborne Infrared Fire Detection." Proceedings of the Fifth Symposium on Remote Sensing of Environment, University of Michigan, Ann Arbor, Michigan. pp. 447-452.

30. Hoffer, R. M. 1971. "Remote Sensing--A Tool for Resource Management." Proceedings of the Third International Symposium of Hydrology Professors, Purdue University, West Lafayette, Indiana. (In Press).

31. Hoffer, R. M. and L. A. Bartolucci. 1972. "Remote Sensing Techniques for Measurement of Water Temperatures." Proceedings of the Indiana Academy of Science for 1971, Vol. 81. pp. 150-153.

32. Hoffer, R. M. 1972. "Class Notes for Remote Sensing Course, FORESTRY 558." Purdue University, West Lafayette, Indiana.

33. Holter, M. R., S. Nudelman, G. H. Suits, W. L. Wolfe and G. J. Zissis. 1962. Fundamentals of Infrared Technology. New York: MacMillan Company. 442 pp.

34. Holter, M. R. and W. L. Wolfe. 1959. "Optical-Mechanical Scanning Techniques." Proceedings of the Institute of Radio Engineering (I.R.E.), Vol. 47, No. 9. pp. 1546-1550.

35. Hood, P. and S. H. Ward. 1969. "Airborne Geophysical Methods." Advances in Geophysics, Vol. 13, Academic Press, New York. pp. 2-112.

36. IBM 4507 Digital Image Display System. 1970. IBM Federal Systems Division, Gaithersburg, Maryland.

37. Kondratyev, K. Ya. 1969. Radiation in the Atmosphere. New York: Academic Press. 912 pp.

38. Kronstein, M. 1955. "Research Studies and Investigations on Spectral Reflectance and Absorption Characteristics of Camouflage Paint Materials and Natural Objects." Final Report, New York University, AD-100-058. (Referenced by Wolfe, W. L. 1965).

39. Kumar, R. 1973. "Radiation from Healthy and Stressed Natural Targets with Spectroradiometeric and Multispectral Line Scanner Data." PhD. Thesis, Aereonautical Engineering, Purdue University, West Lafayette, Indiana.

40. Laboratory for Agricultural Remote Sensing (LARS). 1967. "Remote Multispectral Sensing in Agriculture." Vol. II (Annual Report). Purdue University Agricultural Experiment Station Research Bulletin 832. 75 pp.

41. Laboratory for Agricultural Remote Sensing (LARS). 1968. "Remote Multispectral Sensing in Agriculture." Vol. III (Annual Report). Purdue University Agricultural Experiment Station Research Bulletin 844. 175 pp.

42. Laboratory for Agricultural Remote Sensing (LARS). 1970. "Remote Multispectral Sensing in Agriculture." Vol. IV (Annual Report). Purdue University Agricultural Experiment Station Research Bulletin 873. 112 pp.

43. Landgrebe, D. A., P. J. Min, P. H. Swain and K. S. Fu. 1968. "The Application of Pattern Recognition Techniques to a Remote Sensing Problem." LARS Information Note 080568. Laboratory for Applications of Remote Sensing, Purdue University, West Lafayette, Indiana. 17 pp.

44. Lee, K. 1969. "Infrared Exploration for Shoreline Springs at Meno Lake, California, Test Site." Stanford University, Stanford, California. pp. 100-103.

45. Lindenlaub, J. C. and J. Keat. 1971. "Use of Scan Overlap Redundancy to Multispectral Aircraft Scanner Data." LARS Information Note 120271. Laboratory for Applications of Remote Sensing, Purdue University, West Lafayette, Indiana. 24 pp.

46. Lyon, R. J. P. and K. Lee. 1968. "Infrared Exploration for Coastal and Shoreline Springs." Stanford RSL Technical Report 68-1, Stanford University, Stanford, California. 68 pp.

47. Marlatt, W. E. and R. L. Grossman. 1968. "An Investigation of Water Surface Temperature by an Airborne Infrared Radiometer: Lake Hefner, Oklahoma." Atmospheric Science Paper No. 119, Colorado State University. 118 pp.

48. Martin, T. A. and L. A. Bartolucci. 1973. "Computer Integration of Planck's Equation over Selected Wavelength Bands." LARS Technical Memorandum. Laboratory for Applications of Remote Sensing, Purdue University, West Lafayette, Indiana. (In Press).

49. Moore, D. G., V. I. Myers and W. H. Giles. 1972. "Location of Flowing Artesian Wells Using Thermal Infrared Scanner Imagery." Interim Technical Report RSI-72-04. Remote Sensing Institute, South Dakota State University, Brookings, South Dakota. 6 pp.

50. Morse, P. M. 1965. Thermal Physics. New York: W. A. Bengamin, Inc. 455 pp.

51. Morse, P. M. and H. Feshback. 1953. Methods of Theoretical Physics, Part I. New York: McGraw-Hill Book Company, Inc. 997 pp.

52. Myers, V. I., F. A. Waltz and J. R. Smith. 1972. "Remote Sensing for Evaluating Flood Damage Conditions." SDSU-RSI-72-11. Remote Sensing Institute, South Dakota State University, Brookings, South Dakota. 29 pp.

53. McAlister, E. D. 1964. "Infrared-Optical Techniques Applied to Oceanography 1. Measurement of Total Heat Flow from the Sea Surface." Applied Optics, Vol. 3, No. 5. pp. 609-612.

54. McDonald, R. K. 1960. "Techniques for Measuring Emissivity." Proceedings IRIS, Vol. 3, 153, July 1960. (Referenced by Wolfe, W. L. 1965).

55. McLeish, W. 1964. "The Use of Infrared Maps in the Study of Small-Scale Ocean Circulations." Proceedings of the Third Symposium on Remote Sensing of Environment, University of Michigan, Ann Arbor, Michigan. pp. 717-735.

56. McLerran, J. H. 1964. "Airborne Crevasse Detection." Proceedings of the Third Symposium on Remote Sensing of Environment, University of Michigan, Ann Arbor, Michigan. pp. 801-802.

57. McLerran, J. H. 1964. "Infrared Sea Ice Reconnaissance." Proceedings of the Third Symposium on Remote Sensing of Environment, University of Michigan, Ann Arbor, Michigan. pp. 789-799.

58. McLerran, J. H. and J. O. Morgan. 1966. "Thermal Mapping of Yellowstone National Park." Selected Papers on Remote Sensing of Environment. Reprinted by the American Society of Photogrammetry in Cooperation with Willow Run Laboratories, The University of Michigan, Ann Arbor, Michigan. pp. 119-132.

59. Office of Naval Research, Department of the Navy. 1965. Handbook of Military Infrared Technology. Washington, D. C. pp. 74-75.

60. Papoulis, Anthanasios. 1965. Probability, Random Variables, and Stochastic Processes. New York: McGraw-Hill Book Company. Chapter 8, pp. 245-246.

61. Parker, D. C. and M. F. Wolff. 1966. "Remote Sensing." Selected Papers on Remote Sensing of Environment, Reprinted by the American Society of Photogrammetry, in Cooperation with Willow Run Laboratories, University of Michigan, Ann Arbor, Michigan. pp. v-xvi.

62. Phillips, T. L. 1969. "Calibration of Scanner Data for Operation Processing at LARS." LARS Information Note 071069. Laboratory for Applications of Remote Sensing, Purdue University, West Lafayette, Indiana. 7 pp.

63. Pickett, R. L. 1966. "Environmental Corrections for an Airborne Radiation Thermometer." Proceedings of the Fourth Symposium on Remote Sensing of Environment, University of Michigan, Ann Arbor, Michigan. pp. 259-262.

64. Pierce, K. L. 1968. "Evaluation of Infrared Imagery Applications to Studies of Surficial Geology-Yellowstone Park." Technical Letter NASA-93. Manned Spacecraft Center, Houston, Texas. 20 pp.

65. Planck, M. 1932. Theory of Heat. London: MacMillan and Company, Limited. 301 pp.

66. Rib, H. T. and R. D. Miles. 1969. "Multisensor Analysis of Soils Mapping in Remote Sensing and its Applications to Highway Engineering." Highway Research Board Special Report-102. 56 pp.

67. Robinson, B. F. and L. F. Silva. 1970. "Portable Precision Thermistor Thermometer." LARS Information Note 072470 (Revised). Laboratory for Applications of Remote Sensing, Purdue University, West Lafayette, Indiana. 9 pp.

68. Rossi, B. 1957. Optics. Reading, Massachusetts: Addison-Wesley Publishing Company, Inc. 510 pp.

69. Rovinove, C. J. 1966. "Remote-Sensor Applications in Hydrology." Proceedings of the Fourth Symposium on Remote Sensing of Environment, University of Michigan, Ann Arbor, Michigan. pp. 25-32.

70. Saunders, P. M. 1967. "Aerial Measurement of Sea Surface Temperature in the Infrared." Journal of Geophysical Research, American Geophysical Union, Vol. 72, No. 16. pp. 4109-4117.

71. Saunders, P. M. and C. H. Wilkins. 1966. "Precise Airborne Radiation Thermometry." Proceedings of the Fourth Symposium on Remote Sensing of Environment University of Michigan, Ann Arbor, Michigan. pp. 815-826.

72. Shaw, R. W. 1966. "Environmental Errors in the Use of the Airborne Radiation Thermometer." M. A. Thesis, Department of Physics, University of Toronto. 58 pp.

73. Shaw, R. W. and J. G. Irbe. 1972. "Environmental Adjustments for the Airborne Radiation Thermometer Measuring Water Surface Temperature." Water Resources Research, Vol. 8, No. 5. pp. 1214-1225.

74. Siegel, R. and J. R. Howell. 1968. "Thermal Radiation Head Transfer. The Blackbody, Electromagnetic Theory and Material Properties." NASA Scientific and Technical Information Division, Vol. 1, NASA SP-164, Washington, D. C. 190 pp.

75. Simmons, W. R. 1970. "PLATEMP." LARS Program Abstract-LARSYS 1021. Laboratory for Applications of Remote Sensing, Purdue University, West Lafayette, Indiana.

76. Simmons, W. R. 1971. "Average Data Storage Tape Lines." (LINAVE). LARS Program Abstract-LARSYS 1133. Laboratory for Applications of Remote Sensing, Purdue University, West Lafayette, Indiana. 3 pp.

77. Skiles, J. J., T. A. Grzelak, R. S. Dixon, R. A. Ragotzkie and J. D. McFadden. 1962. "An Airborne Instrumentation System for Microwave and Infrared Radiometry." Proceedings of the Second Symposium on Remote Sensing of Environment, University of Michigan, Ann Arbor, Michigan. pp. 175-185.

78. Slavecki, R. J. 1964. "Detection and Location of Subsurface Coal Fires." Proceedings of the Third Symposium of Remote Sensing of Environment, University of Michigan, Ann Arbor, Michigan. pp. 537-547.

79. Smedes, H. W. 1968. "Geologic Evaluation of Infrared Imagery, Eastern Part of Yellowstone National Park, Wyoming and Montana." Technical Letter NASA-83, Manned Spacecraft Center, Houston, Texas. 27 pp.

80. Standberg, C. H. 1963. "Analysis of Thermal Pollution from the Air." Photogrammetric Engineering, Vol. 29, No. 4. pp. 656-671.

81. Swain, P. H. 1973. "A Result from Studies of Transformed Divergence." LARS Technical Memorandum T-8, 050173. Laboratory for Applications of Remote Sensing, Purdue University, West Lafayette, Indiana. 3 pp.

82. Swain, P. H., T. V. Robertson and A. G. Walker. 1971. "Comparison of the Divergence and B-Distance in Future Selection." LARS Information Note 020871. Laboratory for Applications of Remote Sensing, Purdue University, West Lafayette, Indiana. 12 pp.

83. Swain, P. H. and K. S. Fu. 1972. "Stochastic Programmed Grammars for Syntactic Pattern Recognition." Pattern Recognition. Pergamon Press, Vol. 4. Great Britain. pp. 83-100.

84. Swain, P. H. and C. L. Wu, 1973. Personal Communication on the Development of the Layered Classifier. Laboratory for Applications of Remote Sensing, Purdue University, West Lafayette, Indiana.

85. Tanguay, M. C. and R. D. Miles. 1970. "Multispectral Data Interpretation for Engineering Soil Mapping." Highway Research Record No. 319. pp. 58-77.

86. Viskanta, R. and J. S. Toor. 1972. "Radiant Energy Transfer in Waters." Water Resources Research, Vol. 8, No. 3. Washington, D. C. pp. 595-608.

87. Weiss, M. 1962. "Earth and Sea Surface Temperature Measurement Using Infrared." Selected Papers on Remote Sensing of Environment, Reprinted by the American Society of Photogrammetry, 1962. Proceedings of the Second Symposium on Remote Sensing of Environment, University of Michigan, Ann Arbor, Michigan. pp. 343-357.

88. Wolfe, W. L. 1965. Handbook of Military Infrared Technology. Washington, D. C.: Office of Naval Research. Department of the Navy. 906 pp.

89. Wood, C. R. 1972. "Ground-Water Flow." Photogrammetric Engineering, Vol. 38, No. 4. pp. 347-352.

90. Worthing, A. G. 1940. "The Temperature Concept." American Journal of Physics, Vol. 8, No. 1. pp. 28-30.

91. Wu, C. L. and L. A. Bartolucci. 1973. "Selective Radiant Temperature Mapping Through a Layered Classifier." LARS Information Note 042973. Laboratory for Applications of Remote Sensing, Purdue University, West Lafayette, Indiana. (In Press).

APPENDIX A

Table 1A. LARSYS calibration codes.

1	C0 (Column 223)
2	C1 (Column 225)
3	C2 (Column 227)
4	C0 and C1
5	C0 and C2
6	C1 and C2
7	no calibration

APPENDIX B

Table 1B. Multispectral Scanner Data Available at LARS for Water Resources Studies.

DATE	LARS RUN#	FLT.LN.#	FLT.Time (Local Time)	# of CHAN.	Alt. (ft)
05/13/69	--------	36			5200
05/27/69	69001400	36	14:42	1(8-14μm)	2000
08/06/69	--------	36			
11/06/69	--------	36			3000
12/17/69	69009000	36	14:41	1	3000
	69009001	36	14:41	12	3000
05/06/70	70001400	50	14:05	1	6000
	70002100	36	15:51	10	2000
	70002101	36	15:51	2	2000
06/30/70	70002500	36	10:45	2 IR	3000
	70002501	36	10:45	13	3000
	70002503	36	10:45	11+2(VisIR)	3000
	70002504	36	10:45	13	3000
	70002505	36	10:45	13	3000
	70002520	36	10:45	2 IR	3000
	70002521	36	10:45	2 IR	3000
	70002522	36	10:45	2 IR	3000
	70002523	36	10:45	13	3000
	70002524	36	10:45	13	3000
	70002525	36	10:45	13	3000
	70002526	36	10:45	13	3000
07/01/70	70003100	50	09:44	2 IR	10000
	70003101	50	09:44	13	10000
	70003200	50	09:46	2 IR	2000
	70003201	50	09:46	13	2000
08/12/70	--------	36			

Table 1B, cont.

DATE	LARS RUN#	FLT.LN.#	FLT.Time (Local Time)	# of CHAN.	Alt. (ft)
08/13/70	70006800	36	15:47	13	2000
	70006801	36	15:47	3	2000
	70006802	36	15:47	13+2 (VisIR)	2000
	70007200	50-A	16:38	13	2000
	70007201	50-A	16:38	3 IR	2000
	70007300	50-B	16:44	13	2000
	70007301	50-B	16:44	3 IR	2000
	70007400	50-C	16:47	13	2000
	70007401	50-C	16:47	3 IR	2000
08/09/72	72001800	4A	09:31	12	5000
08/10/72	72002700	4	10:53	12	5000
	72002900	1	11:19	12	10000
	72001900	3	09:52	12	10000
10/17/72	72046500	5	11:46	12	10000
	72046600	4A	12:22	12	5000
	72046700	4	12:47	12	5000
05/04/73	73015300	4	09:54	12	10000
	73015400	4A	10:20	12	5000
	73015500	3	10:45	12	10000